EARTHQUAKE ENGINEERING RESEARCH LABORATORY

THE RESPONSE OF STICK-SLIP SYSTEMS TO RANDOM SEISMIC EXCITATION

Thesis by

Michael Anthony Moser

Report No. EERL 86-03

A Report on Research Supported by a
Grant from the National Science Foundation,
an IBM Fellowship,
and the Earthquake Research Affiliates Program
of the California Institute of Technology

Pasadena, California

1986

The Response of Stick-Slip Systems to Random Seismic Excitation

Thesis by

Michael Anthony Moser

In Partial Fulfillment of the Requirements

for the Degree of

Doctor of Philosophy

California Institute of Technology

Pasadena, California

1987

(Submitted September 29, 1986)

Acknowledgements

The author wishes to express his deep gratitude to his advisor, Professor W. D. Iwan, for his guidance and insightful suggestions. His encouragement and optimistic viewpoint have been sources of inspiration throughout this investigation.

The financial assistance from the IBM Corporation and the California Institute of Technology is greatly appreciated.

To his wife, Caryn, the author is very thankful for her understanding and sacrifices throughout his years of graduate study. The companionship of the SOPS, especially Nick Jones, Harri Kytomaa, Janet Blume, Garrett Jeong, and Bill Donlon will be sorely missed.

Finally, the author thanks his parents, to whom this thesis is dedicated, for their encouragement and support in all his educational endeavors.

Abstract

This thesis examines the response of stick-slip, or frictional, systems to harmonic and random excitation. Two frictional models are considered: constant slip force, or Coulomb, friction, and displacement dependent slip force, used to model a caster, or pivoting wheel. The response to harmonic excitation of systems exhibiting both frictional models is determined using the method of slowly varying parameters. Changes in the response amplitude of both systems caused by the addition of a linear centering mechanism are also examined.

The response of the system with displacement dependent slip force is examined under Gaussian mean zero white noise excitation using the generalized equivalent linearization method. It is shown that a lower bound is obtained from the Coulomb friction system's response.

For filtered random excitation, linearization methods are shown to predict erroneous displacement trends for the Coulomb system when the input has no spectral content at zero frequency. When the excitation is modeled as a Poisson pulse process, an approximate method exhibiting the proper displacement trends can be constructed. The method is shown to be accurate over a broad range of input parameters if overlaps in the input pulses are considered. A set of excitation parameters consistent with seismic events is then used to estimate final rms displacements as a function of coefficient of friction.

Contents

Acknowledgements i

Abstract ii

List of Figures iv

List of Tables v

1 Introduction 1

2 Response of Stick-Slip Systems to Harmonic Excitation 6

2.1 Introduction 6

2.2 The Method of Slowly Varying Parameters 7

2.3 Application of Slowly Varying Parameters to Stick-Slip Systems 10

2.3.1 Systems Without Centering Devices 10

2.3.1.1 Constant Slip Force Systems 10

2.3.1.2 A System With Displacement Dependent Slip Force—The Caster 14

2.3.2 Systems With Centering Devices 22

2.3.2.1 Constant Slip Force Systems 22

2.3.2.2 Effect of Centering Mechanism on Caster System 26

2.4 Conclusions 29

3 Response of Stick-Slip Systems to White Noise Excitation **30**

3.1 Introduction 30

3.2 Previous Work 31

3.3 The Generalized Equivalent Linearization Method 32

3.3.1 Determination of the Equivalent Linear Parameters . . 32

3.3.2 Transient Response of the Linearized System 35

3.4 Application of Generalized Equivalent Linearization to the Caster-Mounted System 36

3.4.1 Derivation of Covariance Equation for Caster System . 36

3.4.2 Numerical Solution of Covariance Equations 38

3.4.3 Discussion of Results 41

3.5 Conclusions 48

4 Response of the Coulomb System to Filtered Random Excitation — Equivalent Linearization Approach **50**

4.1 Introduction 50

4.2 Previous Work 52

4.3 Stationary Equivalent Linearization Applied to a Coulomb Element 53

4.3.1 The Method of Stationary Equivalent Linearization for Random Excitation 54

4.3.1.1 Determination of the Stationary Linear Parameters 54

4.3.1.2 Stationary Response of the Linearized System 55

4.3.2 Application of Stationary Equivalent Linearization to the Coulomb Element 57

4.3.3 Response of a Coulomb Element to Band-Pass Filtered Random Excitation 60

4.4 Simulation studies 69

4.5 Comparison of Stationary Equivalent Linearization and Simulation Results for Ideal Band-Pass Filtered Input 77

5 Response of the Coulomb System to Filtered Random Excitation — Poisson Process Approximate Approach **88**

5.1 Introduction 88

5.2 An Illustration of Differences in Response for Coulomb and Linear Systems 89

5.3 A Poisson Process Approximate Method 96

5.4 Simulation Techniques 106

5.5 Comparison of Poisson Pulse Process and Simulation Results . 109

5.6 Response of Stick-Slip System to Earthquake-Like Motions . . 113

6 Summary and Conclusions **124**

References **131**

A Equations of Motion for a Caster **132**

A.1 Resisting Force as a Function of Angle 133

A.2 Kinematics of the Caster Motion 138

A.3 Force-Displacement Relation for Rectilinear Caster Motion . . 139

List of Figures

2.1 Response amplitude as a function of frequency for a Coulomb block. 13

2.2 Response amplitudes for caster system with harmonic input. . 18

2.3 Caster response amplitude curves plotted to the parameters used for Coulomb block. 21

2.4 Stability boundaries for the caster as a function of $a/3\ell$. 23

2.5 Response amplitude as a function of frequency for a Coulomb block with a centering spring. 25

2.6 Response amplitudes for caster system with a centering device and harmonic input. 28

3.1 Transient velocity variance for caster-mounted system subjected to white noise excitation. 42

3.2 Transient velocity-displacement covariance for caster-mounted system subjected to white noise excitation. 43

3.3 Transient displacement variance for caster-mounted system subjected to white noise excitation. 44

4.1 Stationary rms Coulomb block velocity as a function of low-pass frequency and input bandwidth 66

4.2 Stationary rms velocity of the caster as a function of low-pass frequency 67

4.3 Amplitude modulation of the input spectrum caused by linear interpolation. 74

4.4 Comparison of response velocity standard deviation for simulations of Coulomb element and equivalent linear systems, along with stationary equivalent linearization results. 79

4.5 Stationary velocity spectral densities from simulations of Coulomb and equivalent linear systems, and analytical stationary equivalent linearization. 81

4.6 Comparison of displacement variance for simulations of Coulomb element and equivalent linear systems. 83

4.7 Comparison of rms velocities using equivalent linearization and simulations for fixed $\Delta\Omega$. 85

4.8 Comparison of rms velocities using equivalent linearization and simulations for fixed Ω_1. 86

5.1 Input acceleration pulse used to illustrate differences in responses of linear and Coulomb systems. 93

5.2 Fourier amplitude for the pulse used in the example. 94

5.3 Response relative velocity and relative displacement for Coulomb and linear systems subjected to single input pulse. 95

5.4 Comparison of simulation and approximate method results for the rms velocity and the displacement rate for Poisson pulse input. Rms acceleration pulse amplitude to slip level ratio is 1:3. 111

5.5 Comparison of simulation and approximate method results for the rms velocity and the displacement rate for Poisson pulse input. Rms acceleration pulse amplitude to slip level ratio is 1:1. 112

5.6 Comparison of simulation and approximate method results for the rms velocity and the displacement rate for Poisson pulse input. Rms acceleration pulse amplitude to slip level ratio is 5:1. 114

5.7 Final rms displacement as a function of Coulomb element coefficient of friction using the overlap series method. 120

A.1 Caster configuration used in the equations of motion. 134

A.2 Normalized lateral caster force as a function of caster geometry 137

List of Tables

5.1 Event parameters used in study of response of stick-slip systems to seismic excitation. 118

Chapter 1

Introduction

A problem that has been of interest for some time, but that is receiving increased attention recently, is the response of freestanding objects to earthquake motions. When the center of gravity of these objects is not high compared with their width, the predominant mode of motion is sliding, with the forces restricting the motion being frictional. The size of the objects extends from the small, such as merchandise on a market shelf, through the moderate, which includes data-processing, hospital and industrial equipment, to the large, with buildings on base-isolation foundations or soft first stories as prime examples. The damage or loss of these systems, in addition to endangering human life, can have large economic consequences. It has been estimated that the loss of a major banking institution's computing facilities could adversely affect the world economy. Additionally, lifeline systems in hospitals and some utilities could be imperilled if proper precautions are not taken. Thus, it is important that the behavior of these systems during seismic events be understood, and that estimates of the magnitudes of the motions be obtained.

The advantages of leaving objects freestanding are twofold. First, in applications such as computer or hospital equipment, mobility is important, and anchoring these systems makes their use impractical. A second benefit,

due to the frictional interface between the object and the seismic excitation, is that the largest acceleration to which the system is subjected is the frictional slip level. It is this feature that is exploited in the base-isolation of some structures in an attempt to minimize damage. If the seismic accelerations are below the frictional threshold, the system "sticks" and there is no relative motion between the system and the surface on which it rests. For higher forces, the system slips, and the maximum force to which it is subjected is the frictional one. This slippage produces relative displacement between the object and its support, introducing a source of potential damage if provisions are not made to account for the motion.

The damage can take on various forms, depending on the object involved. In supermarkets and warehouses where the inventory is kept on shelves, substantial losses occur from breakage of containers sliding off the shelving. Delicate hospital equipment can injure patients or be damaged from rolling or sliding into stationary objects, possibly compromising the effectiveness of the medical facilities during a time of great need. Computer equipment may crush operators or be destroyed if provisions are not made for seismically induced motion. Even large machinery that is often anchored, such as machine tools, respond principally by sliding when their restraints fail. If sufficient space is not left between a base-isolated building and its abutment, the collision of these during an earthquake could lead to structural damage and injury. Thus, to minimize the risk from sliding objects, it is important to estimate their seismic motions.

Previous work on sliding systems [1,2,3,4,5,6] has concentrated on systems restrained by Coulomb friction, where the frictional force is dependent

only on the sign of the system's relative velocity. However, many freestanding objects have a frictional force, which is dependent on the magnitude of the relative motion. Specifically, a system mounted on casters, or swiveling wheels, such as those on which hospital and computer equipment are routinely set, exhibits such a behavior. To determine the seismic response of these systems, a model for the frictional force-relative displacement relationship is developed herein and examined under both deterministic and random excitation. This response is compared to that obtained from the constant frictional force system, and it is shown that the constant force system provides a lower bound to the caster-mounted system's response for various types of excitation.

In Chapter 2, both the constant force and the displacement-dependent frictional systems' response to deterministic, harmonic excitation is examined. The effect of centering mechanisms, intended to reduce the amplitude of the motions, is also studied in this chapter and is shown to actually increase the displacements in many cases. Additionally, the constant frictional force, or Coulomb, system's behavior is a lower bound to the caster-mounted response for configurations both with and without centering devices.

The response of the Coulomb and caster-mounted systems to random excitation with a white-noise spectrum is examined in Chapter 3. Although the white noise excitation is not representative of a typical earthquake, many of the existing methods in the theory of random vibrations are most easily applied when a white spectrum is used. Previous studies on the Coulomb system have used this excitation [1,2,3,6], and in this thesis the work is extended to cover systems with decreasing frictional force. The Coulomb system is again shown to be a lower bound to the response of the caster-mounted system by means of

the generalized equivalent linearization.

A study of the response to more general excitation spectra is undertaken in the fourth chapter, where filtered stationary excitation is taken as an input. The equivalent linearization method is used and is shown by simulation to be accurate in predicting velocity response for the majority of the cases considered, but the displacement response trends computed by linearization are erroneous when the input spectrum has no content at zero frequency. It is also shown that the greatest sensitivity in the velocity response is to the spectral content at low frequencies. Consequently, a model of the seismic spectrum should be accurate in this range. Unfortunately, stationary seismic spectra with correct large-time velocity and displacement behavior have negligible content at zero frequency. Thus, the equivalent linearization method cannot be used to predict displacements for realistic seismic spectra. Previous equivalent linearization studies of the response of a Coulomb block to filtered excitation [4] used the Kanai-Tajimi input spectrum [7,8], which has a non-zero component at zero frequency, thus avoiding the an error in the displacement trend. However, for the reasons outlined previously, this spectrum does not correctly characterize the seismic input in the case of stick-slip systems.

To correctly predict the displacement response of the Coulomb system excited by spectra with no zero frequency content, a different method is developed. In Chapter 5, a Poisson process model of the input is used, and the overall mean-squared response is computed using a superposition of the responses to the individual pulses. This procedure is similar to the one developed by Lin [5] to estimate the mean response for a block on an inclined plane. If the overlapping of pulses in the input process is included in the analysis, then the

agreement between the Poisson process method and simulations is improved. Final rms displacements are computed for parameters representative of seismic events, and displayed as a function of the coefficient of friction. Lower and upper response bounds for a caster-mounted system are obtained from the Coulomb system and frictionless systems, respectively.

Chapter 2

Response of Stick-Slip Systems to Harmonic Excitation

2.1 Introduction

To understand some features of the stick-slip systems that play a role in their response to random excitation, these systems are first studied under harmonic excitation. Two types of stick-slip systems are considered: a constant slip force system, also known as a Coulomb friction system, and a system whose resisting force is dependent on its relative displacement. It is shown that the Coulomb system, for which the analysis is algebraically more straightforward, can be used, through a judicious choice of parameters, as both a lower and an upper bound to the response of the latter system. The effect of centering mechanisms such as springs or caster cups is investigated and shown in many cases to increase, rather than decrease, the amplitude of the system response.

The technique used in this investigation is the method of slowly varying parameters. In addition to predicting approximate values for the amplitude and phase of the periodic response, the method presents information about the stability of these solutions. A derivation of the method is presented in Section 2.2, and is used in the following section to determine response estimates

for the various systems.

2.2 The Method of Slowly Varying Parameters

The method of slowly varying parameters, also known as the Krylov-Bogoliubov method, is a widely used averaging method for determining approximate periodic solutions to nonlinear equations with harmonic excitation [9, pp.165–168] [10]. As the notation to be used in this chapter differs from that in the references, a brief derivation of the method is presented.

The general second-order equation of motion with harmonic input is given by

$$\ddot{x} + f(x, \dot{x}) = B \cos \omega t, \tag{2.1}$$

where dots denote derivatives with respect to time. The periodic solution of interest is of the form

$$x(t) = A(t) \cos \theta(t) \qquad \theta(t) = \omega t + \phi(t), \tag{2.2}$$

where $A(t)$ and $\phi(t)$ are the amplitude and phase, respectively. If $f(x, \dot{x})$ is linear and time invariant, then the solution is exact once the initial conditions decay, and $A(t)$ and $\phi(t)$ are constants. For nonlinear $f(x, \dot{x})$, an approximate solution is obtained for $A(t)$ and $\phi(t)$ being slowly varying functions of time. Differentiating $x(t)$ with respect to time results in

$$\dot{x}(t) = -\omega A \sin \theta + \dot{A} \cos \theta - A\dot{\phi} \sin \theta. \tag{2.3}$$

At this point, an auxiliary equation is added, akin to that used in the method of variation of parameters for linear differential equations. It is

$$\dot{A} \cos \theta - A\dot{\phi} \sin \theta = 0. \tag{2.4}$$

Thus,

$$\dot{x} = -\omega A \sin\theta, \tag{2.5}$$

$$\ddot{x} = -\omega^2 A \cos\theta - \omega[\dot{A}\sin\theta + A\dot{\phi}\cos\theta]. \tag{2.6}$$

Substituting these expressions for x, $\dot{x}$, and $\ddot{x}$ into the equation of motion (2.1), results in

$$-\omega^2 A\cos\theta - \omega[\dot{A}\sin\theta + A\dot{\phi}\cos\theta] + f(A\cos\theta, -\omega A\sin\theta) = B\cos(\theta-\phi). \tag{2.7}$$

Multiplication of (2.7) by $\sin\theta$, (2.4) by $\omega\cos\theta$, and subtraction yields

$$-\omega^2 A\cos\theta\,\sin\theta - \omega\dot{A} + f(\cdot)\sin\theta = B\,\cos(\theta-\phi)\,\sin\theta, \tag{2.8}$$

while multiplying (2.7) by $\cos\theta$, (2.4) by $\omega\sin\theta$ and adding results in

$$-\omega^2 A\cos^2\theta - \omega A\dot{\phi} + f(\cdot)\cos\theta = B\,\cos(\theta-\phi)\,\cos\theta. \tag{2.9}$$

When the previous equations are integrated over one cycle of the input the resulting formulae represent the average value and change in value for both the amplitude and phase, if these vary slowly over a cycle. These are

$$-2\omega\dot{A} + S(A) = -B\,\sin\phi, \tag{2.10}$$

$$-2\omega A\dot{\phi} - \omega^2 A + C(A) = B\,\cos\phi, \tag{2.11}$$

where

$$S(A) = \frac{1}{\pi}\int_0^{2\pi} f(A\,\cos\theta, -\omega A\,\sin\theta)\sin\theta\,d\theta, \tag{2.12}$$

$$C(A) = \frac{1}{\pi}\int_0^{2\pi} f(A\,\cos\theta, -\omega A\,\sin\theta)\cos\theta\,d\theta. \tag{2.13}$$

$S(A)$ is the average force out of phase with the response, while $C(A)$ is the average in-phase portion.

The approximate steady-state periodic solutions are obtained by setting $\dot{A}$ and $\dot{\phi}$ to zero. Letting the steady-state values be A_0 and ϕ_0, respectively, Equations (2.10) and (2.11) become

$$S(A_0) = -B \sin \phi_0, \tag{2.14}$$

$$-\omega^2 A_0 + C(A_0) = B \cos \phi_0. \tag{2.15}$$

By squaring and adding the previous equations the following expression in the amplitude variable A_0 is obtained:

$$S^2(A_0) + [C(A_0) - \omega^2 A_0]^2 = B^2. \tag{2.16}$$

An equation for the phase

$$\phi_0 = \arctan \left[\frac{-S(A_0)}{-\omega^2 A_0 + C(A_0)} \right] \tag{2.17}$$

is found by dividing Equation (2.14) by (2.15).

From a perturbation expansion on (2.10) it can be shown that there are two conditions for the stability of the approximate solutions. These are

$$0 \leq \left. \frac{\partial S(A)}{\partial A} \right|_{A_0} + \frac{S(A_0)}{A_0}, \tag{2.18}$$

$$0 \leq \left[-\omega^2 + \frac{C(A_0)}{A_0} \right] \left[-\omega^2 + \left. \frac{\partial C(A)}{\partial A} \right|_{A_0} \right] + \frac{S(A_0)}{A_0} \left. \frac{\partial S(A)}{\partial A} \right|_{A_0}. \tag{2.19}$$

The equality in Equation (2.19) corresponds to the condition that $\frac{d\omega(A)}{dA} = 0$, the point of vertical tangency of the curve $A(\omega)$. For this reason, this line is known as the "locus of vertical tangencies."

2.3 Application of Slowly Varying Parameters to Stick-Slip Systems

Two stick-slip systems are examined in this section: a constant slip force system, and a system whose slip force is dependent on its position. The former is important because it is commonly used in models of nonlinear systems. The latter is examined since many physical devices, such as a caster, or pivoting wheel, can be shown to exhibit a displacement dependence in the slip force. In fact, a model of a caster-mounted system is used in this analysis with the expectation that many of the features illustrated by this particular model are typical of systems with varying slip.

The use of centering devices has been proposed for systems mounted on casters [11] in the expectation that the magnitude of the motions is reduced. The effect of these devices is modeled, to first order, as a linear restoring force and is examined in connection with the response of both the constant and non-constant slip force systems.

2.3.1 Systems Without Centering Devices

2.3.1.1 Constant Slip Force Systems

As was mentioned in the introduction, constant slip force systems, also known as Coulomb systems or Coulomb elements because of the frictional resisting force, are used in various models of physical systems. In some applications, a rigid mass with a Coulomb friction interface has been used as a model for studying the response of buildings with "soft first stories," or base isolation systems, to seismic forces [2,3,4]. It can be equally well employed to examine the

behavior of freestanding rigid equipment such as computer cabinets or hospital equipment during an earthquake. Elements exhibiting Coulomb friction are also used as components in more complex systems such as bilinear systems [12], generalized yielding systems [13], and even deteriorating systems [14]. It is felt that the insights gained through this work are useful in both sets of applications.

When the relative velocity is non-zero, the resisting force of the Coulomb element is dependent only on the sense of the relative velocity, with an amplitude equal to the so-called "slip level." For zero relative velocity, the force equilibrates any applied force whose magnitude is less than the slip level; for larger applied forces, the element slips and the first statement applies. In the notation of Equation (2.1) in the previous subsection, the nonlinear system function is given by

$$f(\dot{x}) = a\,\mathrm{sgn}(\dot{x}), \tag{2.20}$$

where $a = \mu g$, μ is the coefficient of friction, g is the gravitational acceleration, and

$$\mathrm{sgn}(\dot{x}) = \begin{cases} +1, & \dot{x} > 0; \\ -1, & \dot{x} < 0; \\ 0, & \dot{x} = 0. \end{cases} \tag{2.21}$$

The functions $S(A)$ and $C(A)$ are found by substituting the above expression for $f(\dot{x})$ into (2.12) and (2.13), resulting in

$$S(A) = -\frac{4a}{\pi}, \tag{2.22}$$

$$C(A) = 0. \tag{2.23}$$

Since $C(A) = 0$, and $S(A)$ is negative, the resisting forces lag the response by 90°. The approximate amplitude for the periodic response is obtained by

substituting $S(A)$ and $C(A)$ into (2.16), yielding

$$\left(\frac{4a}{\pi}\right)^2 + \omega^4 A_0^2 = B^2. \tag{2.24}$$

Solving this equation to find an explicit expression for frequency in terms of the other system parameters results in

$$\omega = \left[\frac{B^2 - \left(\frac{4a}{\pi}\right)^2}{A_0^2}\right]^{1/4}. \tag{2.25}$$

This function is plotted in Figure 2.1. A dimensionless form of the equation is not used, as (2.25) is more useful for comparisons with the response of a caster-mounted system. Although in this particular example it is possible to explicitly determine $A(\omega)$, for most problems it is difficult to obtain this functional form. Note that (2.25) indicates that there is no response solution for $|B/a| < 4/\pi$. For this range, the only solution admitted by the equations of motion is $A_0 = 0$. An exact solution to the equation of motion would show there is a non-zero response for $1 < |B/a| < 4/\pi$, while slowly varying parameters admits only the zero solution. This is because for sufficiently large input, the slip force is a mean zero square wave with amplitude a. The first term in a Fourier series expansion of this wave, equal to $S(A)$, has amplitude $4a/\pi$. Thus, the input harmonic excitation must exceed this level for the system to move.

The amplitude of the absolute ground displacement input to the system is

$$A = \frac{B}{\omega^2}, \tag{2.26}$$

where A is the displacement corresponding to a sinusoidal acceleration with amplitude B. This expression can be obtained from either of two methods. The first is by direct calculation from the harmonic acceleration input. The

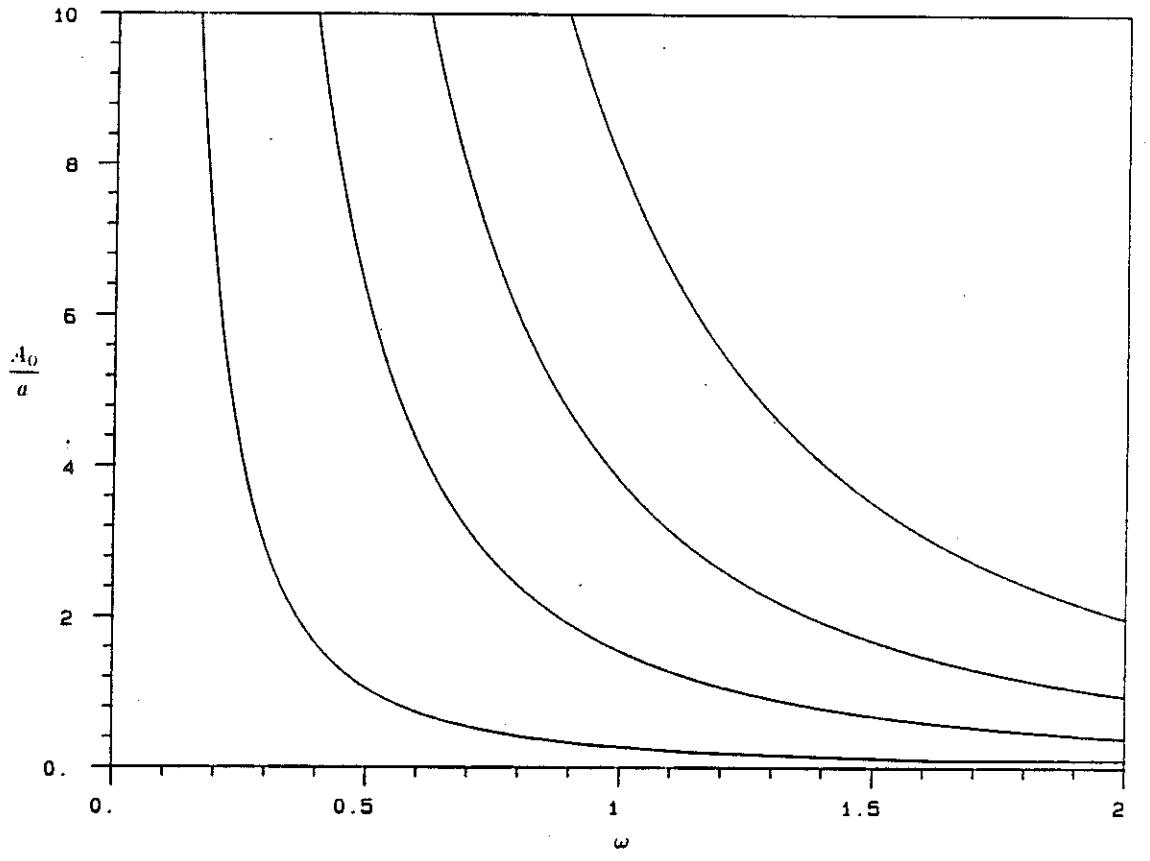

Figure 2.1: Response amplitude as a function of frequency for a Coulomb block. The different curves correspond to, from left to right, B/a equal to 1.3, 2, 4, and 8.

second method, which will prove useful for calculations in later chapters, is by allowing the slip level of the Coulomb system to go to zero. When this is done the mass remains fixed in the absolute coordinate frame, and its relative displacement is equal in magnitude to the absolute displacement but opposite in sign. As can be seen by the form of Equation (2.25), this displacement is an upper bound to the system response. This contrasts with the Coulomb element with a centering spring that is examined in a later subsection, for which the relative displacements can exceed the magnitude of the input displacements. The peak displacements of the system without a spring occur as the frequency goes to zero, due to the input displacements becoming unbounded in this range. For large B/a, the relative displacement amplitude of the system approaches the ground displacement, and the absolute displacement of the system is small compared to the other displacements. In other words, the system remains practically stationary, while the ground slides beneath it. For smaller B/a, the relative displacement is a fraction of the ground motion.

2.3.1.2 A System With Displacement Dependent Slip Force—The Caster

To examine the response of systems with varying slip force, a particular system with this characteristic is investigated in this subsection. The caster-mounted system is an idealization of objects such as computer cabinets or hospital equipment that are routinely mounted on these pivoting wheels. The model consists of a rigid mass with a low center of gravity, with weight evenly distributed among the wheels on which it rests. If a simple frictional law is assumed for the casters, then, as shown in Appendix A, the system equation for motion

along one dimension is given by

$$\ddot{x} + a\,\mathrm{sgn}(\dot{x})\mathrm{sech}\left(\frac{x}{3\ell}\right) = -n(t), \tag{2.27}$$

where the constants a and ℓ are determined from the caster properties discussed in the appendix, and $n(t)$ is the absolute ground acceleration. The problem of interest in this chapter is the response to the harmonic excitation

$$-n(t) = B\cos\omega t. \tag{2.28}$$

From (2.27), the system resisting force per unit mass is given by

$$f(x,\dot{x}) = a\,\mathrm{sgn}(\dot{x})\mathrm{sech}\left(\frac{x}{3\ell}\right). \tag{2.29}$$

The functions $S(A)$ and $C(A)$ used by the method of slowly varying parameters are found by substitution of the resisting force function into (2.12) and (2.13). This results in

$$\begin{aligned} S(A) &= -\frac{12a\ell}{\pi A}\arctan\left(\sinh\left(\frac{A}{3\ell}\right)\right) \\ &= -\frac{12a\ell}{\pi A}\arcsin\left(\tanh\left(\frac{A}{3\ell}\right)\right), \end{aligned} \tag{2.30}$$

where the last substitution of trigonometric and hyperbolic functions has been performed to avoid numerical overflow in computations. Additionally,

$$C(A) = 0. \tag{2.31}$$

As in the case of the Coulomb block, the system forces are 90° out of phase with the response displacement. Replacing (2.30) and (2.31) into (2.16), and solving to obtain frequency as an explicit function of the steady-state amplitude A_0, results in

$$\omega^4 = \frac{B^2 - \left[\frac{12a\ell}{\pi A_0}\arcsin\left(\tanh\left(\frac{A_0}{3\ell}\right)\right)\right]^2}{A_0^2}. \tag{2.32}$$

Ideally, one would prefer to obtain the amplitude as an explicit function of the frequency, but in this case it appears impossible to do so analytically.

Bounds for the relative displacement are obtained from the previous equation by observing that

$$0 \leq \arcsin\left(\tanh\left(\frac{A_0}{3\ell}\right)\right) \leq \frac{A_0}{3\ell}, \quad \text{for } \frac{A_0}{3\ell} \geq 0. \tag{2.33}$$

Using these inequalities in (2.32) results in

$$\frac{B^2 - \left(\frac{4a}{\pi}\right)^2}{A_0^2} \leq \frac{B^2 - \left[\frac{12a\ell}{\pi A_0}\arcsin\left(\tanh\left(\frac{A_0}{3\ell}\right)\right)\right]^2}{A_0^2} \leq \frac{B^2}{A_0^2}. \tag{2.34}$$

By comparing the left-hand side of this expression to Equation (2.25), it is seen that the lower bound to $\omega(A_0)$ for a caster is given by the response of a Coulomb block with slip level a. The right-hand bound is the amplitude of the absolute ground displacement. Since the function $\omega(A_0)$ is bounded both above and below by either single valued functions or constants, its inversion $A_0(\omega)$ is bounded by the inverses of bounding functions. Thus, the response amplitude for the caster motion is bounded from below by the response of a Coulomb system with a slip level a, and bounded above by the amplitude of the absolute ground displacement. These same limits should apply for any system whose resisting force is bounded, with velocity dependence of the form $\text{sgn}(\dot{x})$. For these systems, the Coulomb slip level should be set to the maximum resisting force to obtain a lower bound for the response amplitude.

To further understand the function $\omega(A_0)$, a non-dimensionalization is performed on (2.32) to obtain

$$\omega\sqrt{\frac{3\ell}{a}} = \left\{\left(\frac{3\ell}{A_0}\right)^2\left[\left(\frac{B}{a}\right)^2 - \left(\frac{12\ell}{\pi A_0}\arcsin\left(\tanh\left(\frac{A_0}{3\ell}\right)\right)\right)^2\right]\right\}^{1/4}, \tag{2.35}$$

where a frequency group $\omega\sqrt{3\ell/a}$ is presented as a function of an input amplitude group B/a and a response amplitude group $A_0/3\ell$. The results of substituting numerical values for these groups can be observed in Figure 2.2. In addition to the approximate solutions found in Equation (2.35), another solution to the equation of motion for the caster is $A_0 = 0$. Based on the response of a Coulomb system, the zero solution is always stable for $|B/a| < 4/\pi$ and unstable for larger input amplitudes. Immediately observable differences in Figure 2.2 between the caster response and that of a Coulomb block are the caster exhibiting non-zero response amplitude for $B/a < 4/\pi$, and the response diagram containing an unstable region. The remainder of this subsection is devoted to exploring these two subjects.

For a solution to (2.32) to exist,

$$\frac{B}{a} \geq \frac{12\ell}{\pi A_0} \arcsin\left(\tanh\left(\frac{A_0}{3\ell}\right)\right). \tag{2.36}$$

The minimum value of $A_0/3\ell$ for which a solution exists is found by iterating on $A_0/3\ell$ in the equation

$$\left(\frac{A_0}{3\ell}\right)_{n+1} = \frac{4a}{\pi B} \arcsin\left(\tanh\left(\frac{A_0}{3\ell}\right)_n\right). \tag{2.37}$$

This procedure converges to the correct limiting value independently of the initial value chosen for $A_0/3\ell$, with the convergence rate determined by the closeness of B/a to $4/\pi$. These minimum values for which the solution exists appear in Figure 2.2 at the intersections of the amplitude curves with the $A_0/3\ell$ axis.

Stability of the approximate solutions is determined by substituting the appropriate functions into the stability boundary Equations (2.18) and (2.19).

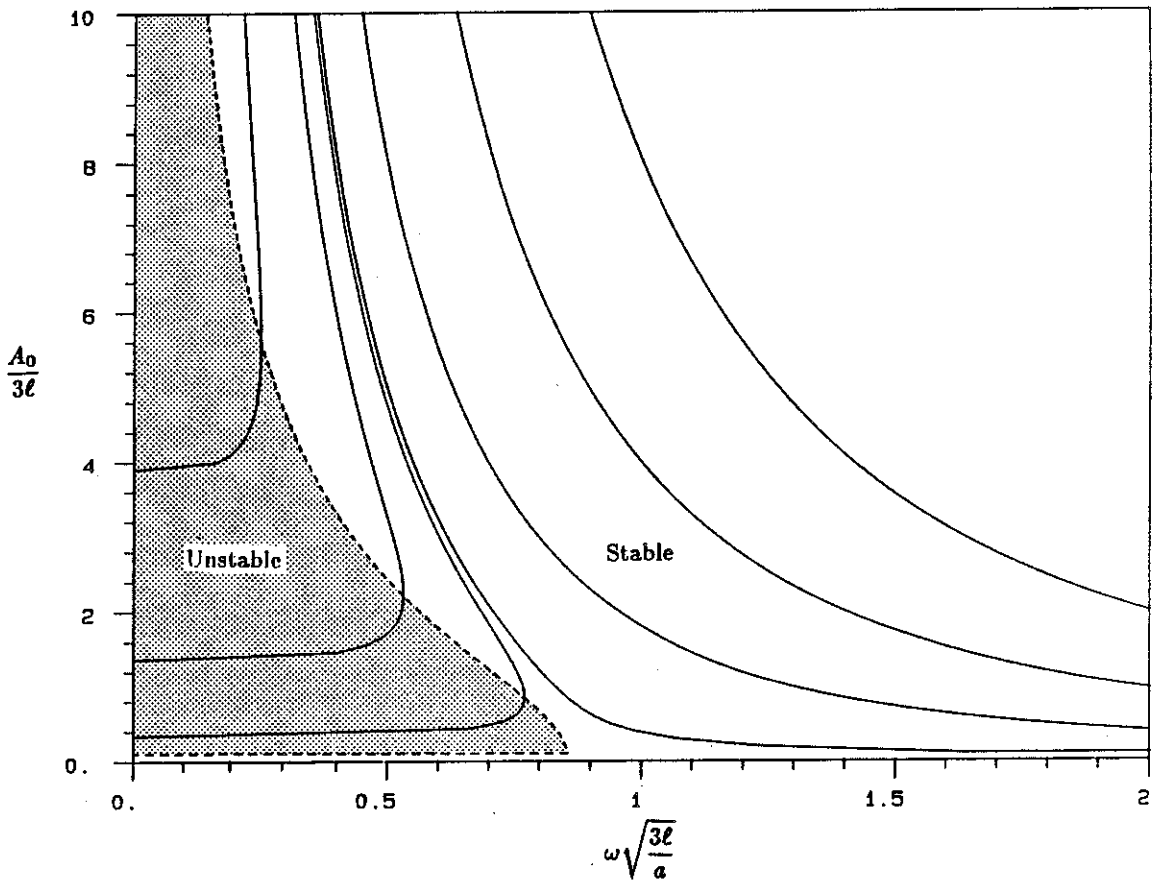

Figure 2.2: Response amplitudes for caster system with harmonic input. The curves represent from left to right, B/a= 0.5, 1.0, 1.25, 1.30, 2, 4, and 8.

From (2.30) and (2.31), the derivatives of $S(A)$ and $C(A)$ are

$$\left.\frac{\partial S(A)}{\partial A}\right|_{A_0} = \frac{12a\ell}{A_0^2\pi}\left[\arcsin\left(\tanh\left(\frac{A_0}{3\ell}\right)\right) - \frac{A}{3\ell}\mathrm{sech}\left(\frac{A}{3\ell}\right)\right], \tag{2.38}$$

$$\left.\frac{\partial C(A)}{\partial A}\right|_{A_0} = 0. \tag{2.39}$$

Thus, the solution is stable if

$$0 \leq \frac{4a}{\pi A_0}\mathrm{sech}\left(\frac{A_0}{3\ell}\right), \tag{2.40}$$

$$\frac{\omega^4(3\ell)^2}{a^2} \geq \left(\frac{4(3\ell)^2}{\pi A_0^2}\right)^2 \arcsin\left(\tanh\left(\frac{A_0}{3\ell}\right)\right) \times\left[\arcsin\left(\tanh\left(\frac{A_0}{3\ell}\right)\right) - \frac{A_0}{3\ell}\mathrm{sech}\left(\frac{A_0}{3\ell}\right)\right]. \tag{2.41}$$

The first of these inequalities is automatically satisfied for all realistic values of parameters. The range over which the second holds is determined numerically and displayed in Figure 2.2. The plot of the unstable region does not include the value $A_0/3\ell = 0$, because the stability of this solution is dependent on the input amplitude.

From an asymptotic expansion on the second stability condition for small $A_0/3\ell$ it is found that the stability boundary crosses the frequency axis at

$$\omega\sqrt{\frac{3\ell}{a}} = \sqrt{\frac{4}{\sqrt{3}\pi}}. \tag{2.42}$$

The minimum B/a for which the response amplitude curves cross into the unstable region is found by isolating those curves intersecting the $A_0/3\ell$ axis. Expanding (2.25) for small $A_0/3\ell$, one obtains

$$\omega^4 \geq \frac{B^2 - \left(\frac{4a}{\pi}\right)^2}{A_0^2}. \tag{2.43}$$

Substituting $\omega = 0$ into this relation shows that for $B/a < 4/\pi$, curves cross the unstable region. The frequency at which the response curve crosses the stability

boundary separates domains for which the system has different numbers of solutions. Above this frequency the only stable periodic solution is the zero solution, while below there are three amplitude solutions for a given frequency. The stable solutions are the zero solution and the upper branch of the solution to (2.35), while the intermediate solution given by the lower branch of (2.35) is unstable. The choice of which stable solution is exhibited by the system is determined by the initial conditions on the caster. For $B/a > 4/\pi$ the amplitude curves do not cross the locus of vertical tangencies and are single valued functions of frequency representing the stable periodic solution. The zero amplitude solution is unstable for these larger inputs.

For comparison with the amplitude response curves of the Coulomb block, the caster amplitude responses have been plotted as a function of the parameters used for the former system's response curves in Figure 2.3. The difference between the sets of curves shown is the value chosen for $a/3\ell$. Since the Coulomb element response is a lower bound to the caster responses, all curves lie above those for a Coulomb block with the same slip level. As $a/3\ell$ is decreased with all else held constant, the response amplitude decreases, making the values closer to those of a Coulomb element. In addition, the stability boundary shrinks horizontally and is elongated in the vertical direction. For $a/3\ell \to 0$, the caster behaves like a Coulomb block, and the stability boundary disappears. In Figure 2.4, the stability boundaries are plotted for various values of $a/3\ell$, and the dependence of the shape on the caster parameters is more easily discerned.

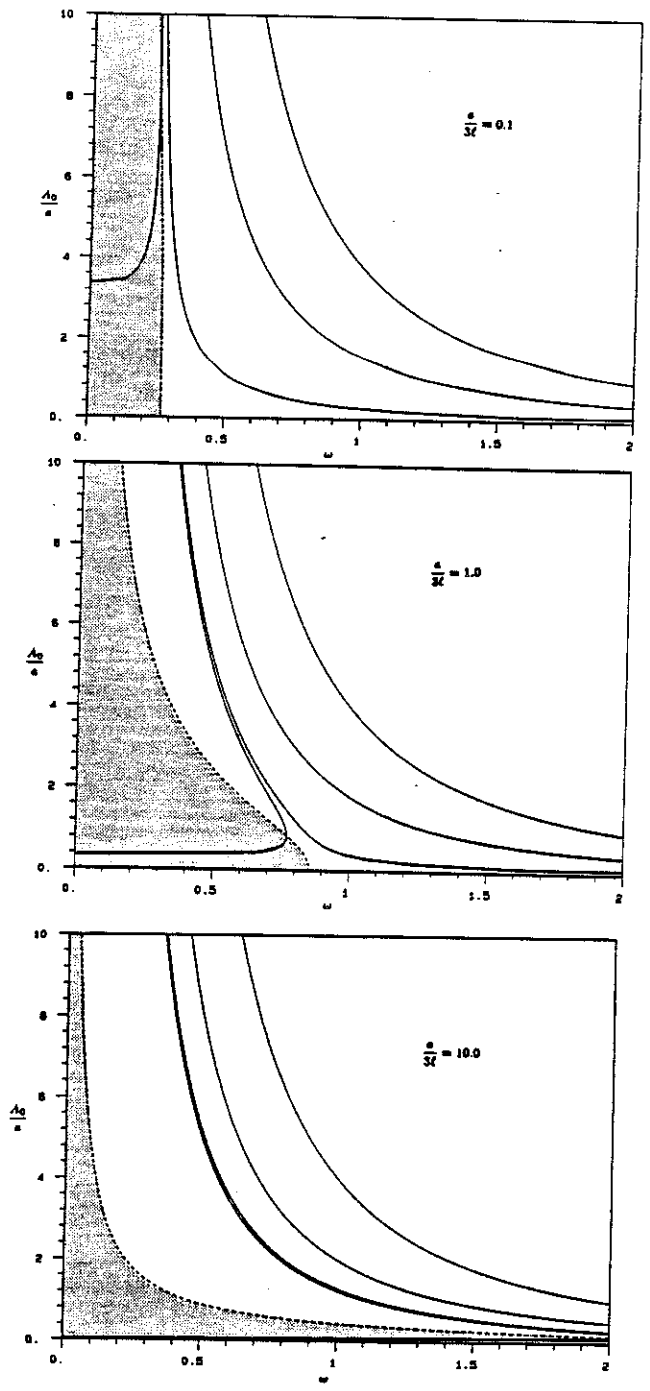

Figure 2.3: Caster response amplitude curves plotted to the parameters used for Coulomb block. Values of B/a used are, from left to right, 1.25, 1.3, 2, and 4. The shaded area of the plots are regions of unstable solutions.

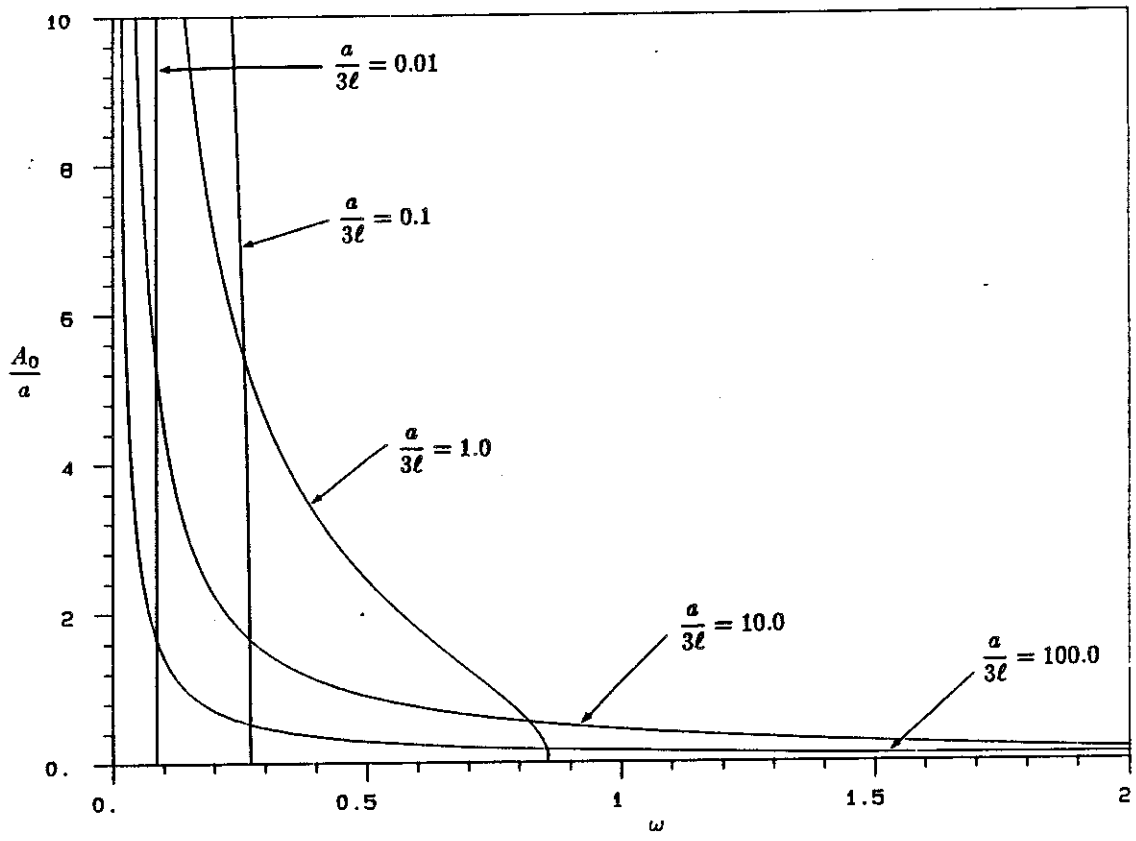

Figure 2.4: Stability boundaries for the caster as a function of $a/3\ell$.

2.3.2 Systems With Centering Devices

The effect of a centering device, represented herein by a linear restoring force, is studied in this section. It is shown that the addition of a centering device causes a shift in the frequency squared parameter of the response curves by an amount equal to the squared natural frequency system. The peak of the response curve is unbounded for all possible parameters of both the Coulomb and caster systems, and the centering system is more likely to result in an increase rather than a decrease in the amplitude of the response.

2.3.2.1 Constant Slip Force Systems

The equation of motion for the relative displacement of the Coulomb system with an attached spring is given by

$$\ddot{x} + a\,\mathrm{sgn}(\dot{x}) + \omega_n^2 x = B\cos\omega t, \tag{2.44}$$

with $\omega_n^2 = k/m$. The slowly varying parameter functions $S(A)$ and $C(A)$ are given by

$$S(A) = -\frac{4a}{\pi}, \tag{2.45}$$

$$C(A) = \omega_n^2 A. \tag{2.46}$$

Note that the only the $C(A)$ function is affected by the addition of the spring, and the component of the resisting force in-phase with the response is now non-zero. The response amplitude is found by substituting these functions into (2.16) to obtain

$$\left(\frac{4a}{\pi}\right)^2 + A_0^2(\omega_n^2 - \omega^2)^2 = B^2, \tag{2.47}$$

which, when solved for ω^2 results in

$$\omega^2 = \omega_n^2 \pm \sqrt{\frac{B^2 - \left(\frac{4a}{\pi}\right)^2}{A_0^2}}. \tag{2.48}$$

This function is plotted in Figure 2.5. When the preceding equation is compared with (2.25), it can be seen that the addition of a spring shifts the frequency squared axis by an amount ω_n^2, leaving the shape of the curves unchanged. All solutions can easily be shown to be stable through the use of Equations (2.18) and (2.19).

The response of the system with a centering device is no longer bounded from above by the amplitude of the absolute ground displacement. In fact, if the input frequency is above the system natural frequency, the response of the centering system is *larger* than that of the system without the spring, thereby defeating the purpose of the centering device. For frequencies between zero and the ω_n, the response may increase or decrease, depending on the precise location of the input frequency.

Although this analysis has been performed for a single harmonic input, the same type of behavior is to be expected for excitation with a moderate bandwidth. Many forms of random excitation occurring in engineering applications have negligible components at zero frequency, with the majority of their energy being in higher frequencies. Since the spring has shifted the unbounded response from the zero frequency to the system natural frequency, the response may well be larger than that without a centering device. Thus, although on an intuitive level it might seem that a centering device would reduce the size of the relative displacement, it appears that for some situations the effect may be the opposite.

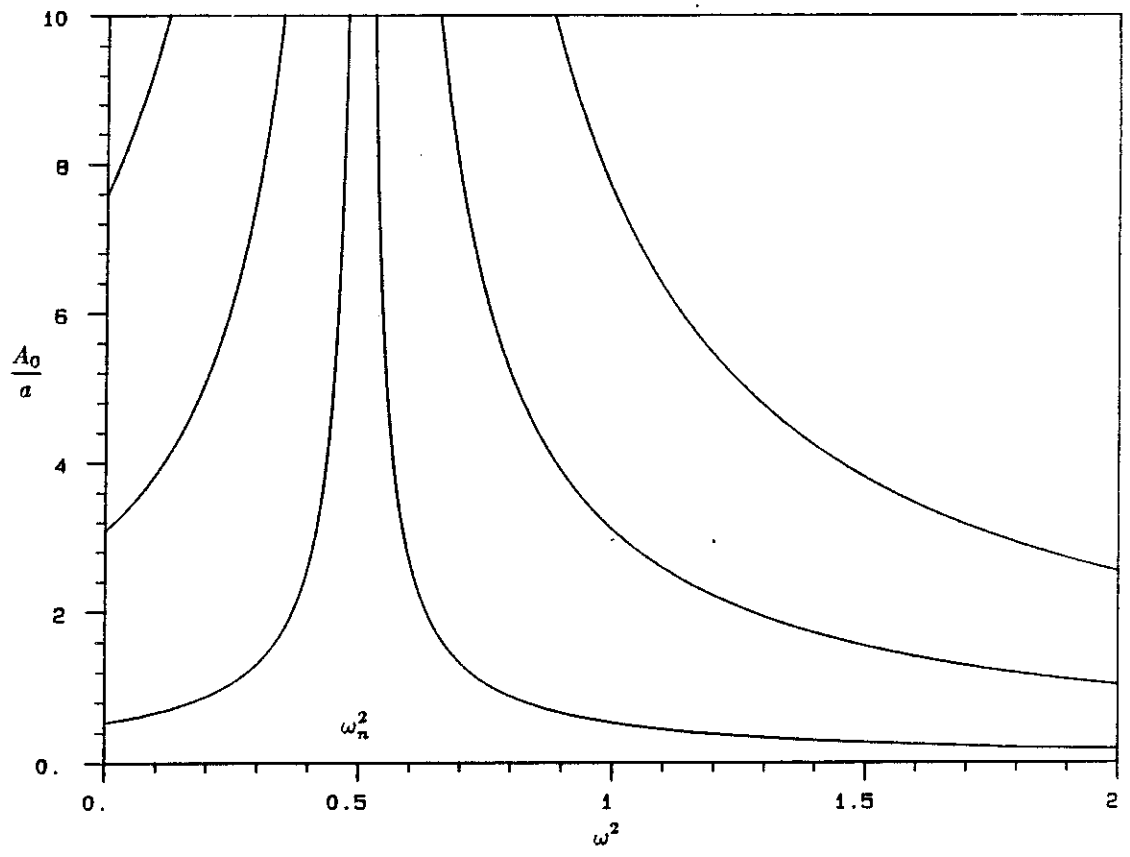

Figure 2.5: Response amplitude as a function of frequency for a Coulomb block with a centering spring. The spring-mass system's squared natural frequency has been set to 0.5 rad/sec. The different curves correspond to, from lowest to highest, B/a equal to 1.3, 2, and 4.

The steady-state displacement response becomes unbounded at the natural frequency of the spring-mass system, even though the input displacement is bounded. This behavior is independent of the slip level of the frictional element. For inputs at this frequency, the frictional element dissipates less energy per cycle than that stored in the spring. Since the energy in the spring is proportional to the square of its extension, the transient response grows as the square root of time and has no upper bound.

2.3.2.2 Effect of Centering Mechanism on Caster System

A proposed mechanism meant to restrict the motion of a caster-mounted system is a so-called "caster cup" [11]. It consists of a bowl-shaped piece of hard material affixed to the ground, with a concave surface onto which the caster is placed. This device is intended to decrease the amplitude of the motion since the caster must move up the side of the cup as the system displaces. Unfortunately, as is shown in this section, for many types of excitation the motion's amplitude actually increases.

If the shape of the caster cup is a conic section or hemispherical, then, to first order, the natural frequency introduced by the cup is

$$\omega_n = \sqrt{\frac{g}{r_c}}, \tag{2.49}$$

where g is the gravitational acceleration, and r_c is the radius of curvature of the cup. This frequency is the same as that of a pendulum of length r_c.

The equation of motion for the overall system is

$$\ddot{x} + a\,\mathrm{sgn}(\dot{x})\mathrm{sech}\left(\frac{x}{3\ell}\right) + \omega_n^2 x = B\cos\omega t. \tag{2.50}$$

For this system,

$$S(A) = -\frac{12a\ell}{\pi A}\arcsin\left(\tanh\left(\frac{A_0}{3\ell}\right)\right), \tag{2.51}$$

$$C(A) = \omega_n^2 A. \tag{2.52}$$

Using these relations in (2.16) and solving for $\omega(A_0)$ one obtains

$$\omega^2 = \omega_n^2 \pm \sqrt{\frac{B^2 - \left[\frac{12a\ell}{\pi A_0}\arcsin\left(\tanh\left(\frac{A_0}{3\ell}\right)\right)\right]^2}{A_0^2}}. \tag{2.53}$$

From a comparison with (2.32), it can be seen that, as in the Coulomb system, the centering device introduces a shift of ω_n^2 in the frequency squared axis. The response curves are displayed in Figure 2.6, where a non-dimensionalization has been performed to capture the overall nature of the response. The stability boundaries are the same as those for the caster without a centering mechanism, except for a shift of ω_n^2. It can be seen the peak response has been shifted to the natural frequency of the centering system, as occurred in the Coulomb system. For the most part, the nature of the solutions is the same as that of the caster without a centering force, except for the shift. One major difference in the response is that it is no longer bounded from above by the ground motion.

Recall that the Coulomb system without a centering device is a lower bound for the caster system without caster cups. Since the addition of centering mechanisms causes the same shift in the frequency for both systems, the Coulomb system attached to a spring is a lower bound for the corresponding caster system. Thus, all comments made in the previous subsection about the centering device's tendency to increase rather than decrease the response hold equally well for the caster-mounted system. Consequently, the caster cups appear to perform the opposite function for which they were designed.

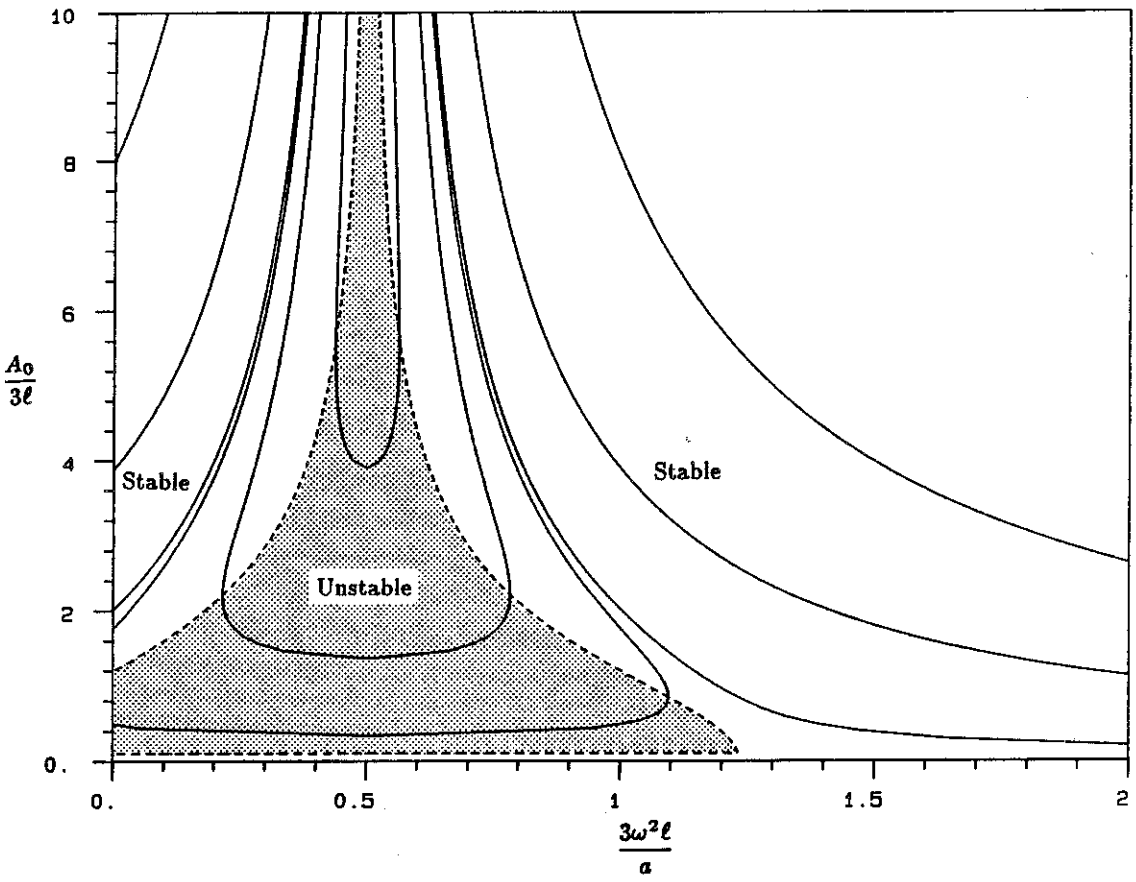

Figure 2.6: Response amplitudes for caster system with a centering device and harmonic input. The curves represent from innermost outward, B/a= 0.5, 1.0, 1.25, 1.30, 2, and 4. The non-dimensional squared natural frequency has been set to 0.5.

2.4 Conclusions

The method of slowly varying parameters has been used to examine the response to harmonic excitation of Coulomb and caster-mounted systems, both with and without centering mechanisms. The Coulomb system has been shown to be simpler to analyze than the caster system, as well as useful for determining both upper and lower bounds for the caster system response through the proper choice of slip level. The addition of a centering mechanism has been shown to shift the frequency axis of the amplitude vs frequency function. In terms of system response, this shift is likely to cause an increase in amplitude, the opposite effect from that sought. The response will also not be bounded by the amplitude of the ground motion, which can be a distinct disadvantage when the nature of the input is not known beforehand.

Chapter 3

Response of Stick-Slip Systems to White Noise Excitation

3.1 Introduction

In the previous chapter, the Coulomb system, whose resisting force is dependent only on the sign of the velocity, and the caster-mounted system, with a force dependent on the relative displacement and the sign of the velocity, were examined under deterministic harmonic excitation. To examine the response of these systems to random excitation, their behavior under white noise excitation is determined in this chapter. The method used is the generalized equivalent linearization method, an approximate technique useful for determining the transient response of nonlinear systems subjected to random excitation. It is shown that the response of a caster is non-stationary in both velocity and displacement. When a limiting case of the caster parameters is taken, the response is that of a Coulomb system, which is stationary in velocity and non-stationary in displacement. The Coulomb system is shown to be a lower bound to the response of the caster-mounted system. An upper bound is found in the frictionless system, for which exact solutions for the response statistics are easily found.

3.2 Previous Work

To the author's knowledge, this is the first examination of the response of a caster-mounted system to random excitation. However, a reasonable body of work exists pertaining to the response of a Coulomb block to stochastic excitation. As the Coulomb block's response is shown to be a lower bound to the caster system response when equivalent linearization is used, a short review of earlier work on this system is included.

The problem of a Coulomb system under white noise excitation was first examined by Caughey and Dienes [1]. Using the Fokker-Planck equation, they obtained the exact stationary probability density function and stationary spectral density of the velocity. In addition, they obtained equivalent linearization estimates of the stationary velocity spectral density using both the Gaussian and exact stationary probability density functions.

The problem was also investigated by Crandall, Lee, and Williams [2] using the stationary equivalent linearization method to obtain the transient velocity and displacement response to white noise. The probability density function used for the velocity was the exact stationary one found by Caughey and Dienes [1], instead of the Gaussian one commonly assumed in equivalent linearization. Simulations were used to check the approximate analytical results.

Ahmadi [3] solved the same problem using the generalized equivalent linearization method, explained in this chapter. He found that both stationary and generalized linearization predict identical values for both short and long time velocity and displacement standard deviation, but for moderate times, discrepancies up to 15% occur.

3.3 The Generalized Equivalent Linearization Method

As was mentioned in the introduction, the generalized equivalent linearization method is useful for determining the non-stationary response of nonlinear systems with random inputs. For reasons of expediency, the version presented in this chapter is restricted to stationary white noise input, although the general method can account for non-whiteness and non-stationarity in the excitation. The method presented here is based upon the work of Iwan and Mason [15], who extended the stationary equivalent linearization method of Caughey [16] and Booten [17] to cover the general non-stationary response of multi-degree-of-freedom systems. The technique consists of two parts. First, the "equivalent" linear system is determined and used as a replacement for the nonlinear system. The linear parameters of this system are generally time-varying. The next step is the determination of the transient mean-squared statistics of this linear system. This consists of solving a Liapaunov-type matrix differential equation for the covariance matrix. In this way, the nonlinear stochastic differential equation is approximated by a deterministic ordinary differential equation in terms of the covariance of the response variables.

3.3.1 Determination of the Equivalent Linear Parameters

The general nonlinear system of interest stated in first-order form, is given by

$$\dot{\boldsymbol{x}} = \boldsymbol{h}(\boldsymbol{x}) + \boldsymbol{D}\boldsymbol{n}(t), \tag{3.1}$$

where $\boldsymbol{x}$ is an n-dimensional state vector, $\boldsymbol{h}(\boldsymbol{x})$ is the nonlinear system restoring force, $\boldsymbol{D}$ is a diagonal matrix, and $\boldsymbol{n}(t)$ is a white noise process. It is not strictly proper to write the equation in the above form because the white noise

input causes $\dot{x}$ to exist almost nowhere. However, the notation is kept as it is simpler than the more rigorous integral equation formulations. Using the first-order form of the equation presents no loss of generality as higher-order equations can always be written in this form. The above nonlinear system is to be approximated by a linear system of the form

$$\dot{\boldsymbol{x}} = \boldsymbol{A}(t)\boldsymbol{x} + \boldsymbol{D}\boldsymbol{n}(t), \tag{3.2}$$

where the variation of the linear system is dependent on the response statistics. An equation deficiency ϵ can be defined by subtracting Equation (3.2) from (3.1) to obtain

$$\boldsymbol{\epsilon} = \boldsymbol{h}(\boldsymbol{x}) - \boldsymbol{A}(t)\boldsymbol{x}. \tag{3.3}$$

A suitable criterion on the equation deficiency must then be imposed. The usual approach is to minimize the expected value of the Euclidean, or mean-squared, norm of this deficiency with respect to the linear parameter values. Although different minimization criteria have been used in other studies [18], none appears to have significant advantages over this approach. From [15], minimization implies

$$\frac{\partial E[\boldsymbol{\epsilon}^T \boldsymbol{\epsilon}]}{\partial a_{ij}} = 0. \tag{3.4}$$

Substitution of (3.3) into the above expression and manipulation results in

$$a_{ij}(t) = \frac{E[h_i(\boldsymbol{x})x_j]}{E[x_i x_j]}. \tag{3.5}$$

To evaluate the expectation operators in the previous equation, a probability density function must be assigned to the random variable $\boldsymbol{x}$. The most common assumption is that the response process is described by an n-dimensional Gaussian distribution. The reason for this is twofold. First, a linear operation of

a Gaussian vector process results in another Gaussian process; thus, an equivalent linear system acted upon by a Gaussian process has Gaussian response statistics. Second, the Central Limit Theorem for random variables states that the probability distribution for the sum of random variables approaches the Gaussian distribution as the number of variables in the sum becomes large, making the Gaussian distribution a good estimate when little is known about the true distribution.

For some nonlinear systems, knowledge exists on the form of the response variable's distribution. In these cases, it is advantageous to use this information when one is determining the equivalent parameters [1,2]. However, no such knowledge exists for the caster system considered in this chapter.

Once the response is assumed to have a Gaussian distribution, a result of Atalik and Utku [19] can be used to simplify Equation (3.5), the expression for the equivalent linear parameters. This gives

$$a_{ij}(t) = E\left[\frac{\partial}{\partial x_j} h_i(\boldsymbol{x})\right]. \tag{3.6}$$

To evaluate this expression, one must compute

$$a_{ij}(t) - \int_{-\infty}^{\infty} \cdots \int_{-\infty}^{\infty} \frac{\partial h_i(\boldsymbol{x})}{\partial x_j} p(\boldsymbol{x})\, dx_1 \cdots dx_n. \tag{3.7}$$

The probability density function for a mean zero Gaussian response is given by

$$p(\boldsymbol{x}) = \frac{1}{[(2\pi)^n \det \boldsymbol{Q}(t)]^{1/2}} \exp[-\frac{1}{2}\boldsymbol{x}^T \boldsymbol{Q}^{-1}(t)\boldsymbol{x}], \tag{3.8}$$

where $\boldsymbol{Q}(t) = E[\boldsymbol{x}(t)\boldsymbol{x}^T(t)] = \boldsymbol{Q}^T(t)$ is the covariance matrix, and T denotes transpose. As the response is Gaussian, evaluation of the expression (3.6) for a given $\boldsymbol{h}(\boldsymbol{x})$ results in the linear coefficient matrix's being a function of the mean vector and covariance matrix of the response.

3.3.2 Transient Response of the Linearized System

The previous subsection described a method for determining the equivalent linear parameters. The transient response of this system is now found. Only mean zero processes, and "non-rectifying" functions $\boldsymbol{h}(\boldsymbol{x})$ are considered in the remainder of this study, so the response is taken to be mean zero.

An expression for the response covariance matrix for a linear system is given by the Liapaunov equation [15]

$$\dot{\boldsymbol{Q}}(t) = \boldsymbol{A}(t)\boldsymbol{Q}(t) + (\boldsymbol{A}(t)\boldsymbol{Q}(t))^T + 2\pi S_0 \boldsymbol{D}\boldsymbol{D}^T, \tag{3.9}$$

$$\boldsymbol{Q}(0) = 0, \tag{3.10}$$

where

$$\boldsymbol{Q}(t) = E[\boldsymbol{x}(t)\boldsymbol{x}^T(t)] = \boldsymbol{Q}^T(t), \tag{3.11}$$

$$E[n(t)] = 0, \tag{3.12}$$

$$E[n(t)n(s)] = 2\pi S_0 \delta(t-s), \tag{3.13}$$

and $\boldsymbol{A}(t)$ is found from (3.6). The problem has been converted from solving a stochastic differential equation to finding solutions to a deterministic matrix differential equation. Equation (3.9) is usually solved numerically with standard techniques.

3.4 Application of Generalized Equivalent Linearization to the Caster-Mounted System

3.4.1 Derivation of Covariance Equation for Caster System

The equation of motion for a caster-mounted system, as described in the previous chapter, is given by

$$\ddot{x} + a\,\mathrm{sgn}(\dot{x})\mathrm{sech}\left(\frac{x}{3\ell}\right) = -n(t). \tag{3.14}$$

To convert this equation to the first-order system notation use

$$x_1 = x, \tag{3.15}$$

$$x_2 = \dot{x}, \tag{3.16}$$

$$\boldsymbol{h}(\boldsymbol{x}) = \{x_2, -f(x_1, x_2)\}^T, \tag{3.17}$$

$$f(x_1, x_2) = a\,\mathrm{sgn}(x_2)\mathrm{sech}\left(\frac{x_1}{3\ell}\right), \tag{3.18}$$

$$\boldsymbol{D} = \begin{bmatrix} 0 & 0 \\ 0 & -1 \end{bmatrix}. \tag{3.19}$$

Substituting these expressions into (3.6), results in

$$a_{11} = 0, \tag{3.20}$$

$$a_{12} = 1, \tag{3.21}$$

$$a_{21} = E\left[\frac{a}{3\ell}\mathrm{sgn}(x_2)\mathrm{sech}\left(\frac{x_1}{3\ell}\right)\tanh\left(\frac{x_1}{3\ell}\right)\right], \tag{3.22}$$

$$a_{22} = E\left[-2a\,\delta(x_2)\mathrm{sech}\left(\frac{x_1}{3\ell}\right)\right]. \tag{3.23}$$

Note that the kernel of the expectation operator in (3.22) is odd in both x_1 and x_2. Thus,

$$a_{21} = 0. \tag{3.24}$$

Computing a_{22} by replacing Equation (3.23) in (3.7), yields

$$\begin{aligned} a_{22} &= \int_{-\infty}^{\infty}\int_{-\infty}^{\infty} -2a\,\delta(x_2)\mathrm{sech}\left(\frac{x_1}{3\ell}\right) p(x_1,x_2)\,dx_1dx_2 \\ &= -2a\int_{-\infty}^{\infty} \mathrm{sech}\left(\frac{x_1}{3\ell}\right) p(x_1,0)\,dx_1, \end{aligned} \tag{3.25}$$

where, from (3.8),

$$p(x_1,0) = \frac{1}{2\pi\sqrt{\det \boldsymbol{Q}}}\exp\left(\frac{-q_{22}x_1^2}{2\det \boldsymbol{Q}}\right), \tag{3.26}$$

$$\det \boldsymbol{Q} = q_{11}q_{22} - q_{12}^2. \tag{3.27}$$

The integral in (3.25) is difficult to determine in closed form, so an approximation is performed to sech(·). This is

$$\mathrm{sech}(y) \approx \frac{1}{1+y^2}. \tag{3.28}$$

This approximation has the correct asymptotic behavior for both small and large arguments, and integration of both functions from zero to infinity yields the same value. Hence, for large displacement excursions, both the exact and approximate relations account for equal expenditures of energy by the caster-mounted system. Substituting (3.28) into (3.25), and integrating, results in

$$a_{22}(q_{11},q_{12},q_{22}) = -a\sqrt{\frac{2}{q_{22}}}\,z\exp(z^2)\mathrm{erfc}(z), \tag{3.29}$$

where

$$z = \frac{3\ell\sqrt{q_{22}}}{\sqrt{2\det \boldsymbol{Q}}}, \tag{3.30}$$

$$\mathrm{erfc}(z) = 1-\mathrm{erf}(x) = \frac{2}{\sqrt{\pi}}\int_z^{\infty} e^{-t^2}\,dt, \tag{3.31}$$

The components of the covariance matrix are given by substituting the expressions for a_{ij} into the coupled differential equations

$$\dot{q}_{11} = 2q_{12}, \tag{3.32}$$

$$\dot{q}_{12} = a_{22}(q_{11}, q_{12}, q_{22})q_{12} + q_{22}, \tag{3.33}$$

$$\dot{q}_{22} = 2a_{22}(q_{11}, q_{12}, q_{22})q_{22} + 2\pi S_0, \tag{3.34}$$

where $a_{22}(\cdot)$ is found in (3.29) and initial conditions are $q_{ij}(0) = 0$. These equations are solved numerically, using the procedure described in the next subsection.

From (3.29) it can be seen that a_{22} is non-positive. Thus, the maximum rate of growth of the covariance equations is achieved when $a_{22} \to 0$. In a later subsection it is shown that this maximum growth rate is achieved when the rms displacement becomes much larger than 3ℓ.

3.4.2 Numerical Solution of Covariance Equations

Particular attention is paid to two topics in the numerical solution of the covariance equations (3.32), (3.33), and (3.34). The first is the selection of proper numerical values for the initial conditions, as the zero values introduce numerical problems. The second is the numerical integration technique used for efficiently solving the covariance equations.

The exact initial conditions for the covariance equations are $q_{ij} = 0$. Unfortunately, substitution of these values into the covariance equations results in numerical division by zero, although a carefully performed limiting process indicates that the equations are not singular. There are two ways to deal with this numerical anomaly. The first is to perform an expansion of the equations that does not become unbounded at zero, commence the solution with these equations, and later patch this solution with one to the complete equations. The second approach, the one adopted in this study, is to initiate the solution with small but non-zero values. The choice of these values is now examined.

Conditions that must be satisfied by any solution, including the starting values, are the following:

1. The covariance matrix must be positive semidefinite. Thus, $\det Q = q_{11}q_{22} - q_{12}^2 \geq 0$.

2. $q_{ii} = E[x_i^2] \geq 0$.

3. Using the previous condition in Equation (3.32) implies that $q_{12} \geq 0$ when q_{11} is small.

These conditions provide constraints used in determining the initial conditions.

Note that Equations (3.33) and (3.34) are closely coupled nonlinear equations, while (3.32) involves the integral of (3.33). Thus, the rate of change of q_{11} is slower than that of q_{12} and q_{22}. One of the methods for finding suitable initial conditions is to first set q_{11} to an arbitrary, but small, fixed value, and to then obtain equilibrium solutions of (3.33) and (3.34). Although fixing the value of q_{11} implies through the covariance equations that q_{12} and q_{22} are both zero, the interpretation used here is that q_{11} is slowly varying, and its value is frozen at a particular instant. Letting the equilibrium values be denoted by $q_{ij(e)}$, it is found that equilibrium solutions to (3.33) and (3.34) are

$$q_{12(e)} = \frac{\pi S_0}{a_{22}\left(q_{11(e)}, q_{12(e)}, \sqrt{\pi S_0 q_{12(e)}}\right)}, \tag{3.35}$$

$$q_{22(e)} = \sqrt{\pi S_0 q_{12(e)}}. \tag{3.36}$$

The conditions on the non-negative determinant of the covariance matrix and positiveness of $q_{12(e)}$ require that

$$0 \leq q_{12(e)} \leq \sqrt[3]{\pi S_0 q_{11(e)}}. \tag{3.37}$$

Equilibrium values are determined by first selecting an arbitrary $q_{12(e)}$ satisfying (3.37), and using this value as a seed for iteration on (3.35). This value is then used in (3.36) to find $q_{22(e)}$. The triplet of $q_{ij(e)}$ values found in this manner are suitable non-zero starting conditions for the covariance equations. After the covariance equations are solved numerically, a check is performed to determine whether the initial conditions are truly small in comparison with the characteristic dimensions of the transient solutions. This ensures that the character of the solutions has not been modified by the choice of non-zero initial values. The particular initial conditions used in this solution are

$$\frac{a^6}{S_0^4} q_{11}(0) = 0.01, \tag{3.38}$$

$$\frac{a^4}{S_0^3} q_{12}(0) = 5.4 \times 10^{-8}, \tag{3.39}$$

$$\frac{a^2}{S_0^2} q_{22}(0) = 1.3 \times 10^{-5}. \tag{3.40}$$

The numerical solution of the covariance equations is obtained by means of a fifth-order Runge-Kutta algorithm with variable step size. The algorithm computes estimates of the local error, and these are used to automatically adjust the step size. This algorithm is efficient for solving these covariance equations as the time scales of the solutions are dependent on the system parameters, with little known in advance about the form of this dependence. The maximum relative local error is set to 10^{-5}, and the solutions displayed in the following subsection require from 60 to 500 time steps, depending on the caster parameters.

3.4.3 Discussion of Results

The results of the numerical solution of the covariance equations are presented in Figures 3.1, 3.2, and 3.3. The non-dimensionalization chosen permits a study of the effects of a variation in any one of the systems parameters, but the ensuing discussion will concentrate on the dependence on the caster pivot radius ℓ. As can be seen in the figures, for small times ($a^2t/S_0 < 1$), the solution is only weakly dependent on $\gamma = S_0^2/3\ell a^3$. In this range of times, the ground moves beneath the system, which remains stationary in the absolute coordinate system. For larger times, the form taken by the solution is dependent on γ, but it is apparent that very large and small γ define the two limiting response behaviors. For $\gamma \to 0$, the system reaches a steady-state value in both velocity and velocity-displacement covariance while being non-stationary in displacement. If γ is very large, all three statistics grow without bound at constant rates. For intermediate values of γ, the solution moves from the small to large γ limiting solutions, with the transition time depending on the value of γ. The remainder of this subsection is devoted to showing that the lower limit is defined by the Coulomb system, the upper bound by a frictionless system, and the switching time is determined by the caster's displacement variance crossing a threshold, changing the nature of the response.

Due to the $\mathrm{sech}(x/3\ell)$ form of the slip force function, the caster resisting force is small for displacements much larger than 3ℓ. For systems with small ℓ, or large γ, the rms displacement does not have to be large for the effective slip level of the caster to become small. In terms of the covariance equations, $\ell \to 0$ implies through Equation (3.29) that $a_{22} \to 0$ from below. In this case, the covariance equations achieve their highest growth rate. Substitution of $a_{22} = 0$

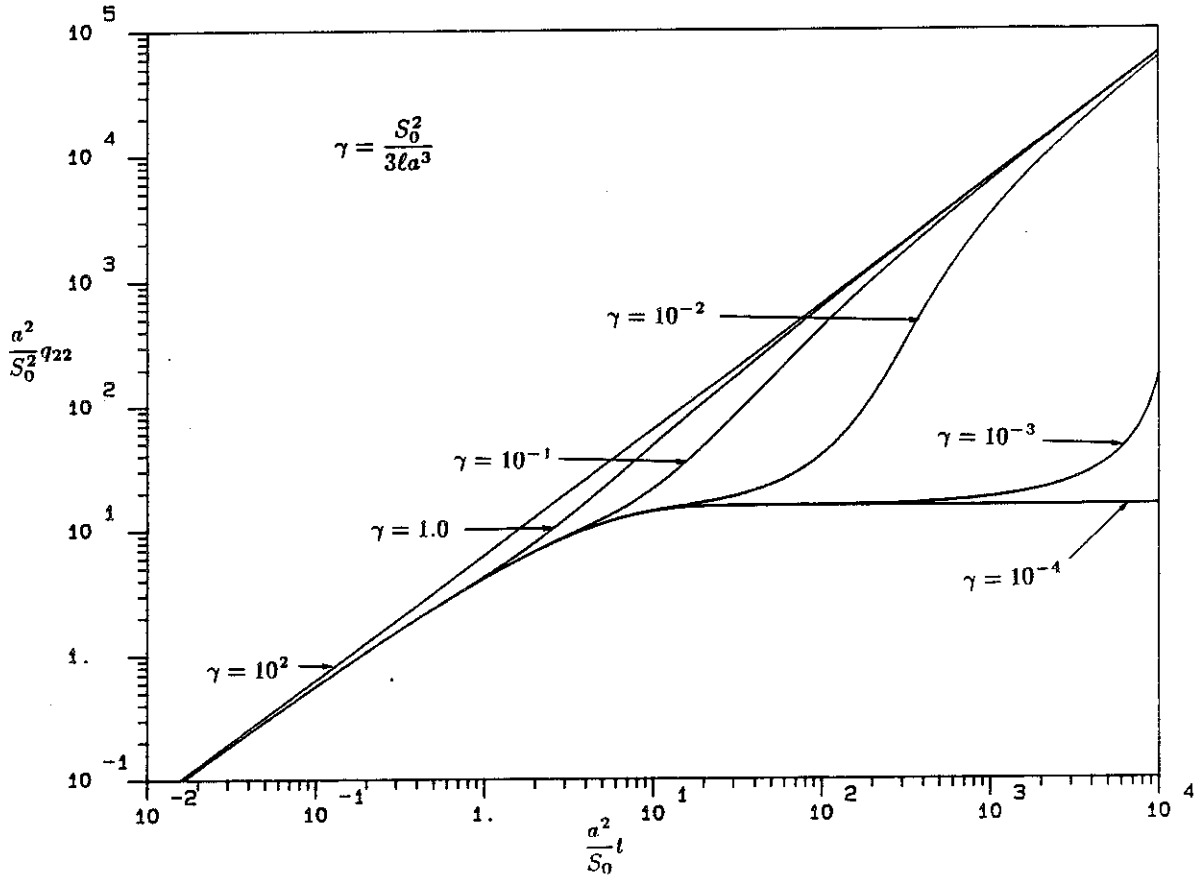

Figure 3.1: Transient velocity variance for caster-mounted system subjected to white noise excitation.

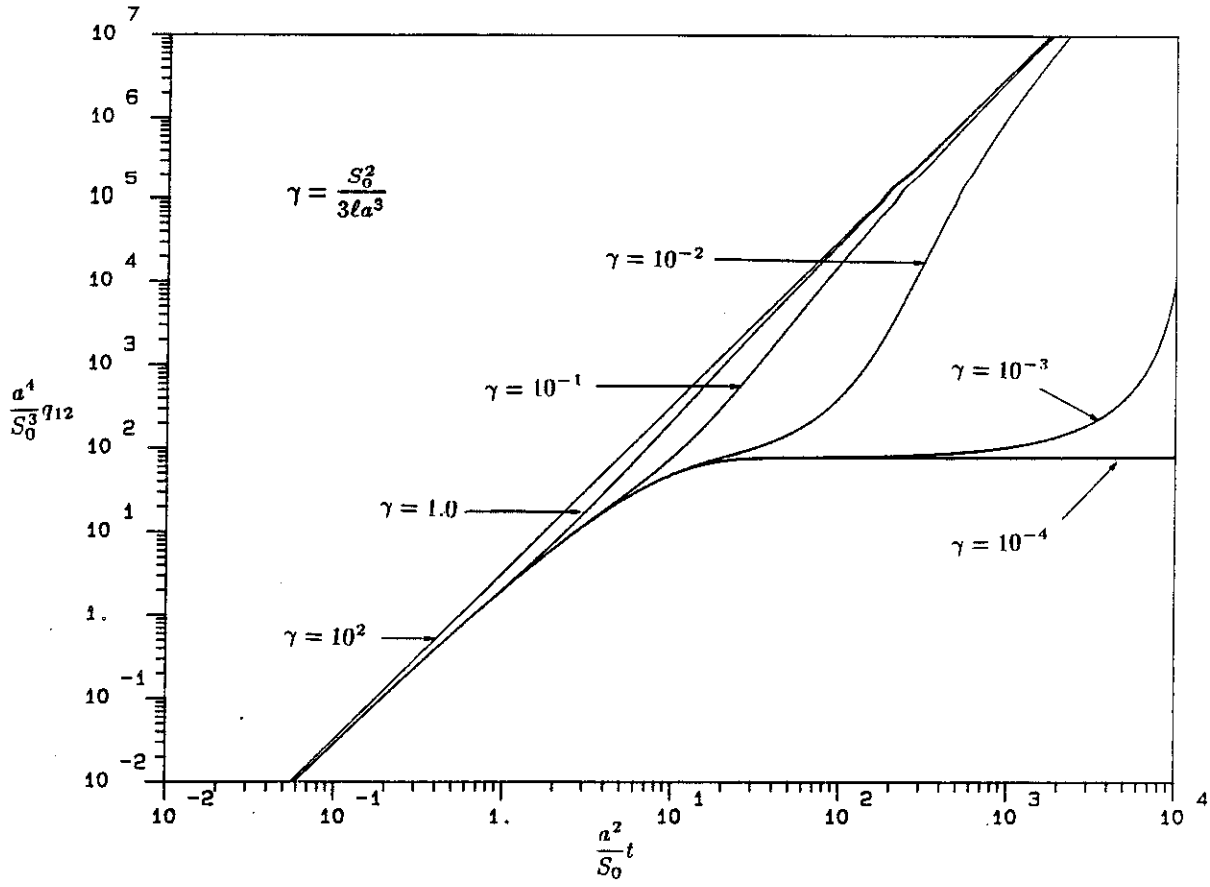

Figure 3.2: Transient velocity-displacement covariance for caster-mounted system subjected to white noise excitation.

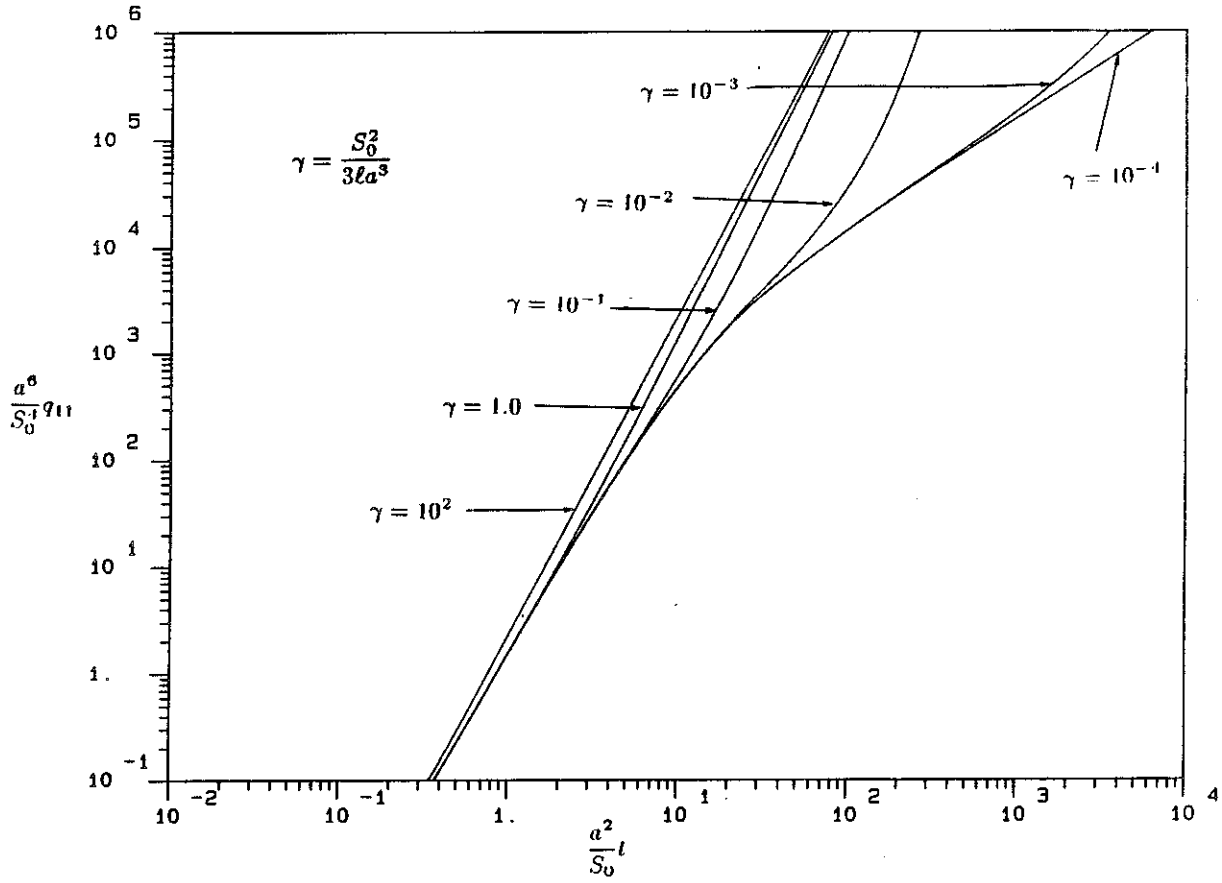

Figure 3.3: Transient displacement variance for caster-mounted system subjected to white noise excitation.

into the covariance Equations (3.32), (3.33), (3.34) and solution, results in

$$q_{22}(t) \equiv E[\dot{x}^2(t)] = 2\pi S_0 t, \tag{3.41}$$

$$q_{12}(t) \equiv E[\dot{x}(t)x(t)] = \pi S_0 t^2, \tag{3.42}$$

$$q_{11}(t) \equiv E[x^2(t)] = \frac{2\pi S_0 t^3}{3}. \tag{3.43}$$

These solutions are exact as the approximations introduced by equivalent linearization all appear in the a_{22} coefficient, which has gone to zero. An equivalent approach is obtained by noting that for a frictionless system the relative measures of the motion equal the negative of the absolute measures. Since the input process is white noise, the absolute input and response statistics for a frictionless system are integrals of the white noise process.

To this point it has been shown that the frictionless system is an upper bound for the caster system response. Recall that this is not only the case for white noise excitation, but also, as shown in Chapter 2, the situation for harmonic input. The subsequent discussion shows that the Coulomb system is a lower bound for the white noise response, as it was in the harmonic excitation.

Letting ℓ go to infinity, or γ to zero, results in the caster resisting force being independent of displacement; i.e. it behaves like a Coulomb block. An asymptotic expansion of (3.29) for large ℓ reveals that

$$\lim_{\ell \to \infty} a_{22} = -a\sqrt{\frac{2}{\pi q_{22}}}. \tag{3.44}$$

This is a lower bound to the value of a_{22}, so the rate of growth of the covariance matrix is minimized when this value is used, providing a lower bound to the caster system response. The solution of the covariance equations using this value of a_{22} correspond to the lower bound curves displayed in Figures 3.1, 3.2,

and 3.3. It can be shown that the value of a_{22} in (3.44) is that of the Coulomb system. Solution of the covariance equations shows that both the velocity variance and velocity-displacement covariance reach steady-state values, but the displacement variance increases proportionally with time for large time. These large time behaviors are given by

$$q_{22} = \frac{\pi^3}{2}\frac{S_0^2}{a^2} \quad \text{for} \quad t > \frac{5S_0}{a^2}, \tag{3.45}$$

$$q_{12} = \frac{\pi^5}{4}\frac{S_0^3}{a^4} \quad \text{for} \quad t > \frac{5S_0}{a^2}, \tag{3.46}$$

$$q_{11} = \frac{\pi^5}{2}\frac{S_0^3}{a^4}t \quad \text{for} \quad t > \frac{5S_0}{a^2}. \tag{3.47}$$

The value of q_{11} in (3.47) is half of that presented by Ahmadi [3], which appears to be in error. For $t < 5S_0/a^2$, the system has not reached stationarity in velocity and the behavior is similar to that of a frictionless system.

The approximation inherent in equivalent linearization is contained in the Coulomb system covariance equations, so they are only an approximate lower bound to the true behavior of the caster systems. Caughey and Dienes [1] have shown that the exact stationary mean-squared velocity is

$$q_{22} = 2\pi^2\frac{S_0^2}{a^2} \quad \text{for} \quad t \to \infty, \tag{3.48}$$

indicating that the equivalent linearization expression given by (3.45) is low by 20%, which is equivalent to an 11% discrepancy in rms values. Using results from [1], Crandall et al. [2] determined that the behavior of the exact large time displacement variance is given by

$$q_{11} \sim 10\pi^3\frac{S_0^3}{a^4}t \quad \text{for} \quad t \to \infty, \tag{3.49}$$

showing that the rate of increase of q_{11} predicted by equivalent linearization in Equation (3.47) is 49% of the exact rate. Since $\dot{q}_{11} = 2q_{12}$, the values of

q_{12} also disagree by the same amount. Consequently, the exact lower bound to the caster responses is somewhat higher than that obtained from equivalent linearization.

As mentioned earlier, the response of the caster-mounted system moves from the lower limit, the Coulomb system response, to that of a frictionless system. An explanation for this transition follows. In Figure 3.3 it is seen that the displacement variance increases with time for all ranges of parameters. Thus, at some time the rms displacement approaches the effective caster pivot radius 3ℓ. As this happens, the effective slip level of the caster system lowers, causing the rms velocity to increase, in turn raising the rate at which the displacement variance increases. This process continues until the displacement variance reaches a level at which the system's effective slip level approaches zero. From this time onward, the system behaves like a frictionless system. The time at which the transition occurs is important, as it determines which of the limiting behaviors describes the caster system motion.

To find the transition time, it is useful to recall the form of a_{22}:

$$a_{22} = -a\sqrt{\frac{2}{q_{22}}}z\exp(z^2)\mathrm{erfc}(z), \quad \text{where } z = \frac{3\ell\sqrt{q_{22}}}{\sqrt{2(q_{11}q_{22} - q_{12}^2)}}. \tag{3.50}$$

For $z \gg 1$, the denominator of z dominates the function, indicating that $\ell \gg \sqrt{q_{11}}$. Thus, the system acts like a Coulomb block. Conversely, for small z the system behaves as if it were frictionless. Arbitrarily setting the transition point at $z = 1$ permits determination of the time t_t at which this occurs. Substituting Equations (3.45), (3.46), and (3.47) for the components of the covariance matrix into $z = 1$ and solving for t_t results in

$$t_t = \frac{S_0}{a^2}\left[\frac{1}{\gamma^2\pi^5} + \frac{\pi^2}{4}\right], \qquad \text{where} \quad \gamma = \frac{S_0^2}{3\ell a^3}, \tag{3.51}$$

subject to the condition that $t_t > 5S_0/a^2$, obtained from the requirement that the caster velocity reach stationarity. For $\gamma > 5 \times 10^{-2}$, t_t is less than $5S_0/a^2$, and the system does not reach velocity stationarity before the transition occurs. Thus, the system acts for all time like a frictionless system. For smaller values of γ, corresponding to larger caster length ℓ, the system transition time predicted by (3.51) agrees with the transition times apparent in the figures. Note that (3.51) indicates that all caster systems with non-zero γ will eventually undergo the transition and behave like a frictionless system, although the transition time can be quite large if γ is small.

3.5 Conclusions

The response of a caster-mounted system to white noise excitation has been examined by means of the generalized equivalent linearization method. The behavior of the elements of the covariance matrix are characterized by two limiting responses: that of the Coulomb system from below, and that of a frictionless system from above. Since the maximum relative response is that of the frictionless system, the relative system motions are bounded from above by the ground motions. For short times, the limiting responses define a narrow band, but as the Coulomb system reaches stationarity in velocity, the range of responses becomes large. It has been demonstrated that the response of a caster system is initially described by the Coulomb system's covariance equations, but as the rms displacement exceeds the caster dimension ℓ, the system response tends to that of the frictionless system. Consequently, all caster-mounted systems will have a non-stationary response in both velocity and displacement when excited by white noise.

Chapter 4

Response of the Coulomb System to Filtered Random Excitation — Equivalent Linearization Approach

4.1 Introduction

This chapter deals with the response to filtered random excitation of systems exhibiting a Coulomb friction resisting force. As was mentioned in Chapter 2, the Coulomb system has been used not only as a model for free-standing equipment and base-isolated structures, but also as a component of more elaborate models such as elasto-plastic and generalized yielding systems. Additionally, it was shown in the previous two chapters that the Coulomb system response is a lower bound to systems with a decaying slip force, such as the caster-mounted system, when the excitation is either harmonic or white noise. Although difficult to prove, it is expected that this lower bound behavior carries over to the more general case of filtered random excitation. Thus, based on the behavior of the Coulomb system to filtered input, the nature of the response of more complex systems can be examined.

In this chapter, the use of the stationary equivalent linearization method

to predict the response to filtered inputs is investigated. This method is widely used and has been used by other authors examining this same problem [4], although with a different excitation spectrum than that presented herein. It was remarked in Chapter 3 that work by Ahmadi [3] shows that both stationary and generalized linearization predict the same small and large time Coulomb system response for white noise input. This agreement is true for both the velocity and the displacement statistics, where the former are stationary while the latter are not. This matching of results from the different linearization methods should also hold for non-white excitation. As the stationary method yields results in a more straightforward manner, this method is used.

In addition to equivalent linearization, simulations are used to obtain estimates of the response statistics. Monte-Carlo simulations are a straightforward, but time-consuming, numerical procedure for determining the response of nonlinear systems such as this one to random excitation. By means of these simulations, it is shown that equivalent linearization correctly determines the non-stationary trends in displacement only when the input has spectral content at zero frequency. For excitation without zero frequency components, it is shown that equivalent linearization predicts stationarity in displacement, while simulations show non-stationarity. An explanation is found in the spectrum of the response velocity, from which it can be deduced that no linearization technique is likely to show the correct trend. The formulation of a technique that determines the correct trend is postponed until the next chapter.

Section 4.2 gives a brief description of previous work in the response of a Coulomb system to filtered excitation. In Section 4.3 the stationary equivalent linearization method is developed and applied to the Coulomb element. The

simulation technique is presented in Section 4.4, and the final section of the chapter compares and discusses the results from the two methods.

4.2 Previous Work

The synopsis of prior work presented in this section is restricted to the response of the Coulomb system with filtered random excitation. For a review of the behavior of this system under white noise, the reader is referred to the second section of the previous chapter.

An analysis of the response to filtered white noise excitation was performed by Constantinou and Tadjbakhsh [4], using the stationary equivalent linearization technique to predict the transient velocity and displacement responses. The spectrum used in their analysis was one proposed by Kanai [7] and Tajimi [8], in which the spectral content of the acceleration is non-zero at zero frequency, rises to a peak as frequency increases and then decays to zero at high frequency. The principal difference between this spectrum and the band-pass filter used in the present study is the spectral content at low frequencies. While the parameters of the band-pass filter considered herein can be adjusted to eliminate content in this range, the Kanai-Tajimi spectrum always has content at zero frequency. It is shown that when the zero frequency content is removed from the input spectrum, the character of the displacement predicted by equivalent linearization changes drastically, and the method is inaccurate when used to determine the response.

A related problem that has received some attention is that of a block on an inclined plane, also formulated as a Coulomb-friction system with non-symmetric sliding force. First proposed by Newmark [20] as a model for failed

portion of an earth dam, it has also been used in studies by Lin [5] and Constantinou, Gazetas, and Tadjbakhsh [21]. The method used by Lin is similar to that used in Chapter 5 of this study, and a discussion of his method is postponed until then. Constantinou et al. used equivalent linearization with a suitable decomposition of the non-zero mean non-stationary input process, to obtain estimates for the mean and standard deviation of the system drift. It is expected that the flaw in equivalent linearization presented in this chapter for Coulomb systems with symmetric sliding forces carries over to the case with unequal sliding force. Thus, their method should be valid only for spectra with zero frequency content.

4.3 Stationary Equivalent Linearization Applied to a Coulomb Element

The stationary equivalent linearization technique is an approximate method useful for predicting the stationary response of nonlinear systems under both white and filtered random excitation. The method is very similar to the generalized equivalent linearization method developed in the previous chapter, with the principal difference being the determination of the response of the equivalent linear system. Instead of permitting the linear parameters to vary with time, as in the generalized equivalent linearization method, the linear parameters are set to constant values determined from the stationary response of the linear system. It is shown in this section that this stationary response is straightforward to calculate, even for an arbitrary input spectrum.

4.3.1 The Method of Stationary Equivalent Linearization for Random Excitation

There are two parts to the Stationary Equivalent Linearization technique. First, the equivalent linear parameters are determined for the approximating system. The method is identical to that in generalized linearization presented in the previous chapter, but some steps are briefly included as the notation is different. Next, the response of this equivalent linear time invariant system system is determined.

4.3.1.1 Determination of the Stationary Linear Parameters

The nonlinear system of interest is of the form

$$\ddot{x} + f(\dot{x}) = -n(t), \tag{4.1}$$

where dots denote derivatives with respect to time, x is the relative displacement, $f(x)$ is the resisting force per unit mass, and $n(t)$ is the ground acceleration, modeled as a Gaussian, mean-zero random process with arbitrary spectral density. Note that this is a first-order equation in velocity, so the only requirement on the use of stationary linearization is that the moments of the velocity reach stationarity. There is no requirement on the displacement response, so non-stationarity in the displacement does not violate assumptions made in using the method.

The above nonlinear system is approximated by the linear viscously damped system

$$\ddot{x} + \zeta_{eq}\dot{x} = -n(t). \tag{4.2}$$

The methods of the previous chapter can be used to show that

$$\zeta_{eq} = E\left[\frac{d}{d\dot{x}} f(\dot{x})\right]. \tag{4.3}$$

4.3.1.2 Stationary Response of the Linearized System

In the previous section, the parameter of the equivalent linear system was determined. The remaining step in the process is to compute the stationary statistics of this auxiliary system.

A well-known result from linear time-invariant system theory [22, p. 120], [23, p. 79] is that when both the excitation and the response are weakly stationary, the response spectral density is the product of the excitation spectral density and the squared magnitude of the system transfer function. Stated mathematically, this becomes

$$S_{\dot{x}\dot{x}}(\omega) = |H_{\dot{x}n}(\omega)|^2 S_{nn}(\omega), \tag{4.4}$$

where $S_{\dot{x}\dot{x}}(\omega)$ and $S_{nn}(\omega)$ are the two-sided input and response velocity spectral densities, respectively, and $H_{\dot{x}n}(\omega)$ is the linear system transfer function.

For the linear system in Equation (4.2), the transfer function is computed from the velocity impulse response

$$h_{\dot{x}n}(t) = e^{-\zeta_{eq} t} u(t), \tag{4.5}$$

where $u(t)$ is the unit step function. The transfer function is then found as

$$\begin{aligned} H_{\dot{x}n}(\omega) &= \int_{-\infty}^{\infty} h_{\dot{x}n}(t) e^{-i\omega t}\, dt \\ &= \frac{1}{\zeta_{eq} + i\omega}. \end{aligned} \tag{4.6}$$

Thus,

$$|H_{\dot{x}n}(\omega)|^2 = \frac{1}{\zeta_{eq}^2 + \omega^2}. \tag{4.7}$$

Substituting this into (4.4) results in

$$S_{\dot{x}\dot{x}}(\omega) = \frac{S_{nn}(\omega)}{\omega^2 + \zeta_{eq}^2}. \tag{4.8}$$

The stationary velocity variance is given by the stationary velocity auto-correlation at zero time difference, which is defined through Parseval's relation as the following integral of the stationary velocity spectral density:

$$\begin{aligned} \sigma_{\dot{x}}^2 &= R_{\dot{x}\dot{x}}(0) \\ &= \int_{-\infty}^{\infty} S_{\dot{x}\dot{x}}(\omega) d\omega \\ &= \int_{-\infty}^{\infty} \frac{S_{nn}(\omega)}{\zeta_{eq}^2 + \omega^2} d\omega. \end{aligned} \tag{4.9}$$

Equations (4.3) and (4.9) form a set of equations, usually implicit, that are solved to obtain the stationary values of the root mean-square velocity $\sigma_{\dot{x}}$ and equivalent damping ζ_{eq}.

The stationary displacement spectral density, when it exists, is given by

$$S_{xx}(\omega) = \frac{1}{\omega^2} S_{\dot{x}\dot{x}}(\omega). \tag{4.10}$$

It is clear from the preceding equation that $S_{\dot{x}\dot{x}}(\omega)$ must be $O(\omega^2)$ as ω tends to zero, for $S_{xx}(\omega)$ to be well behaved. When this is the case,

$$\begin{aligned} \sigma_x^2 &= R_{xx}(0) \\ &= \int_{-\infty}^{\infty} S_{xx}(\omega) d\omega. \end{aligned} \tag{4.11}$$

Substituting (4.10), (4.7), and (4.4) into (4.11) results in

$$\sigma_x^2 = \int_{-\infty}^{\infty} \frac{S_{nn}(\omega)}{\omega^2(\omega^2 + \zeta_{eq}^2)} d\omega. \tag{4.12}$$

In the case where the velocity spectral density $S_{\dot{x}\dot{x}}(\omega)$ is non-zero as ω tends to zero, it has been shown that [2]

$$\sigma_x^2(t) \sim 2\pi S_{\dot{x}\dot{x}}(0)t \text{ as } t \to \infty, \tag{4.13}$$

with $S_{\dot{x}\dot{x}}(0)$ obtained from (4.8). This result is useful for white noise and spectra containing low-pass filtered white noise, as used in [4] for a Kanai-Tajimi input spectrum. It has also been found through simulation that when the zero frequency velocity spectral density is non-zero, this equation gives a good estimate of the divergence of the displacement variance, independent of the form of the input spectrum.

4.3.2 Application of Stationary Equivalent Linearization to the Coulomb Element

The model for the resisting force per unit mass of a Coulomb system given in Chapter 2 is

$$f(x) = a\,\mathrm{sgn}(\dot{x}), \tag{4.14}$$

where

$$a = \mu g. \tag{4.15}$$

The equivalent linear parameter for the Coulomb element is found by substituting (4.14) into (4.3), resulting in

$$\begin{aligned} \zeta_{eq} &= E\left[\frac{d}{d\dot{x}} a\,\mathrm{sgn}(\dot{x})\right] \\ &= E\left[2a\delta(\dot{x})\right], \end{aligned} \tag{4.16}$$

where $\delta(\dot{x})$ is a delta function with unit area. In the previous subsection, it was assumed that $\dot{x}$ was Gaussian, with unknown mean and variance. As the

input process is mean-zero and the resisting force is symmetric, the response also has a zero mean. Thus, the velocity probability density function is

$$p_{\dot{X}}(\dot{x}) = \frac{1}{\sqrt{2\pi}\,\sigma_{\dot{x}}} \exp\left[\frac{-\dot{x}^2}{2\sigma_{\dot{x}}^2}\right]. \tag{4.17}$$

Using this in Equation (4.16) yields

$$\zeta_{eq} = 2a \int_{-\infty}^{\infty} \delta(\dot{x}) p_{\dot{X}}(\dot{x}) d\dot{x} \tag{4.18}$$

$$= \sqrt{\frac{2}{\pi}} \frac{a}{\sigma_{\dot{x}}}. \tag{4.19}$$

Some comments about the above equation are in order. If $\sigma_{\dot{x}}$ increases monotonically until reaching its stationary value, Equation (4.19) shows that ζ_{eq} decreases monotonically. Thus, the equivalent viscous damping is lowest when the system has reached stationarity. This value is precisely that used by the stationary equivalent linearization method and gives conservative predictions for transient velocity statistics when compared to those of the generalized equivalent linearization method, in which ζ_{eq} is permitted to vary in time. Also, with the stationary velocity standard deviation and equivalent damping inversely proportional to each other, large damping is an indicator of small velocity response.

Another expression relating $\sigma_{\dot{x}}$ and ζ_{eq} is obtained from the stationary response of the equivalent linear system. Substituting Equation (4.9) into (4.19) yields

$$\zeta_{eq} = \sqrt{\frac{2}{\pi}}\, a \left[\int_{-\infty}^{\infty} \frac{S_{nn}(\omega)}{\omega^2 + \zeta_{eq}^2} d\omega\right]^{-1/2}. \tag{4.20}$$

The response of the Coulomb element to excitation with a given spectral density $S_{nn}(\omega)$ is determined by solving for the stationary equivalent damping ζ_{eq} using this equation. Substituting this result into a suitably arranged form of

Equation (4.19) gives the stationary velocity standard deviation $\sigma_{\dot{x}}$. In the subsequent subsections, this method is used to study the Coulomb element's response to white noise passed through an ideal band-pass filter.

Before continuing with the solution process, it is shown that Equation (4.20) indicates a limitation to the equivalent linearization method. Note that

$$\int_{-\infty}^{\infty} \frac{S_{nn}(\omega)}{\omega^2 + \zeta_{eq}^2} d\omega \leq \frac{1}{\zeta_{eq}^2} \int_{-\infty}^{\infty} S_{nn}(\omega) d\omega = \left(\frac{\sigma_n}{\zeta_{eq}}\right)^2, \tag{4.21}$$

where σ_n is the excitation standard deviation. The expression on the right side of the previous equation becomes a sharper upper bound as ζ_{eq} becomes large, or, using Equation (4.19), $\sigma_{\dot{x}}$ becomes small. Substitution of (4.21) into (4.20) leads to

$$\frac{\sigma_n}{a} > \sqrt{\frac{2}{\pi}}. \tag{4.22}$$

Consequently, equivalent linearization predicts response velocities when the ratio of the input root mean-squared acceleration to the slip level is greater than $\sqrt{2/\pi}$. Below this, the only physically reasonable solution to (4.20) and (4.19) is infinite viscous damping, which implies zero velocity variance. This breakdown in the equivalent linearization method was also observed by Constantinou and Tadjbakhsh [4] at the same level of rms input to slip level, although they attributed it to the "ground frequency" of the Kanai-Tajimi spectrum, rather than to the low input variance.

A possible explanation for this abrupt cutoff in the equivalent linearization solution is that when $\sigma_n/a \leq \sqrt{2/\pi}$, the majority of the acceleration process is at a level below the slip level of the Coulomb element. Hence, the element does not move for a considerable portion of the process. The assumed Gaussian distribution for the response velocity cannot account for the infinitesimal prob-

ability of being at a particular non-zero velocity as well as the finite probability of zero velocity. Thus, at the critical input rms level the velocity distribution changes from a smooth distribution, allowing non-zero response velocities, to a delta function for which the zero velocity occurs with probability one. Although the true response distribution is unknown, it is expected that an expansion of the exact response in terms of Hermite polynomials, where the Gaussian distribution is the zero-th order polynomial, would show that the "closest" Gaussian distribution is one with zero variance.

4.3.3 Response of a Coulomb Element to Band-Pass Filtered Random Excitation

The spectra of many excitation processes in engineering exhibit behavior that is modeled by Gaussian band-pass filtered white noise. These inputs have small spectral ordinates for both low and high frequencies, and the majority of their energy is within a "band" of frequencies. The spectrum considered herein is produced by the so-called "ideal" band-pass filter, in which the spectral amplitude is a constant value within the pass-band, and zero elsewhere. With this spectrum it is possible to perform a sensitivity analysis on the bandwidth and low frequency content of the excitation. In addition, the sharp falloff in the spectrum is helpful in illustrating reasons that equivalent linerarization fails when used to predict the displacement statistics of the Coulomb element.

The equation of motion for a the Coulomb element is

$$\ddot{x} + a\,\mathrm{sgn}(\dot{x}) = -n(t). \tag{4.23}$$

The assumed ground acceleration process $n(t)$ is Gaussian with mean-zero, standard deviation σ_n. For band-pass filtered excitation, the spectral density

is given by

$$S_{nn}(\omega) = \begin{cases} S_0, & \omega_1 < |\omega| < \omega_2, \\ 0, & \text{elsewhere.} \end{cases} \tag{4.24}$$

From Parseval's relation, the variance of the excitation is given by the integral of the spectral density. Thus,

$$\sigma_n^2 = 2S_0(\omega_2 - \omega_1). \tag{4.25}$$

Letting

$$X = \frac{a^3}{S_0^2}x,\ \tau = \frac{a^2}{S_0}t,\ (\cdot)' = \frac{d}{d\tau}(\cdot) = \frac{a^2}{S_0}\frac{d}{dt}(\cdot) = \frac{a^2}{S_0}(\dot{\cdot}), \tag{4.26}$$

Equation (4.23) becomes

$$X'' + \text{sgn}(X') = -N(\tau), \tag{4.27}$$

where

$$S_{NN}(\Omega) = \begin{cases} 1, & \Omega_1 < |\Omega| < \Omega_2; \\ 0, & \text{elsewhere;} \end{cases} \tag{4.28}$$

$$\Omega = \frac{S_0}{a^2}\omega,\ N(\tau) = \frac{1}{a}n\left(\frac{a^2}{S_0}t\right). \tag{4.29}$$

The variance of this process is given by

$$2\Delta\Omega \equiv 2(\Omega_2 - \Omega_1) = \left(\frac{\sigma_n}{a}\right)^2. \tag{4.30}$$

Note that if this change of variables is performed, the number of independent parameters is reduced from four $(\omega_1, \omega_2, S_0, a)$, to the two groups Ω_1 and Ω_2. The equivalent linear equation corresponding to (4.23) is

$$X'' + Z_{eq}X' = -N(\tau), \tag{4.31}$$

where $Z_{eq} = S_0\zeta_{eq}/a^2$ is the non-dimensional equivalent damping.

The stationary response velocity of the equivalent linear system is obtained with the method of Section 3.3. It is

$$\begin{aligned}\sigma_{X'}^2 &= \int_{-\infty}^{\infty} \frac{S_{NN}(\Omega)}{\Omega^2 + Z_{eq}^2} d\Omega \\ &= 2\int_{\Omega_1}^{\Omega_2} \frac{d\Omega}{\Omega^2 + Z_{eq}^2} \\ &= \frac{2}{Z_{eq}} \arctan\left(\frac{Z_{eq}(\Omega_2 - \Omega_1)}{Z_{eq}^2 - \Omega_1\Omega_2}\right), \end{aligned} \tag{4.32}$$

where

$$\sigma_{X'}^2 = E[\lim_{\tau\to\infty} X^2(\tau)] = \frac{a^2}{S_0^2}\sigma_{\dot{x}}^2. \tag{4.33}$$

The non-dimensional equivalent damping in terms of non-dimensional rms velocity is

$$Z_{eq} = \sqrt{\frac{2}{\pi}}\frac{1}{\sigma_{X'}}. \tag{4.34}$$

Substituting (4.34) into (4.32) results in

$$\frac{1}{Z_{eq}} = \pi \arctan\left(\frac{Z_{eq}(\Omega_2 - \Omega_1)}{Z_{eq}^2 + \Omega_1\Omega_2}\right). \tag{4.35}$$

Since the argument of the arctan term in the previous equation is never negative, $0 \leq \arctan(\cdot) \leq \pi/2$, which implies $0 \leq 1/Z_{eq} \leq \pi^2/2$. Using this in (4.34) yields

$$0 \leq \sigma_{X'} \leq \sqrt{\frac{\pi^3}{2}}. \tag{4.36}$$

It is now shown that the lower limit corresponds to the non-dimensional input variance, $2\Delta\Omega$, being less than $2/\pi$, while the upper limit occurs for white noise input.

The first assertion to be proven is that for $\Delta\Omega < 1/\pi$, the stationary velocity variance is zero. For small arguments, $\arctan(x) \approx x$. Thus, Equation (4.35) becomes

$$\frac{1}{\pi Z_{eq}} = \frac{Z_{eq}(\Omega_2 - \Omega_1)}{Z_{eq}^2 + \Omega_1\Omega_2}, \tag{4.37}$$

provided the right hand side is small. Manipulating this equation to solve for Z_{eq}, gives the result

$$Z_{eq} = \sqrt{\frac{\Omega_1 \Omega_2}{\pi \Delta\Omega - 1}}, \tag{4.38}$$

from which it is seen that real solutions for Z_{eq} exist only if

$$\Delta\Omega > \frac{1}{\pi}. \tag{4.39}$$

Hence, it appears that the method can say nothing for variance levels below this value. This is the same breakdown in the equivalent linearization solution alluded to in Section 4.3, when the ratio of input standard deviation to slip level falls below $\sqrt{2/\pi}$. For the cases where the ratio is too small, the only physically reasonable solution to (4.35), and its approximation (4.37), is that $Z_{eq} \to \infty$. This implies, through Equation (4.34), that the stationary velocity standard deviation $\sigma_{X'}$ is zero. When $\Delta\Omega$ is greater than $1/\pi$, but not too large, then Equation (4.38) is used to determine Z_{eq} provided the right-hand side of (4.37) remains small. It was remarked earlier that the true response does not have zero variance, although the closest Gaussian distribution to the real response distribution is the one with zero standard deviation. In a later section it is shown by means of simulation that the velocity variance is non-zero, but small, indicating that this cutoff exhibited by equivalent linearization is spurious.

Another assertion made is that for white noise input, $\sigma_{X'} = \sqrt{\pi^3/2}$. To model white noise with the band-pass filter, let $\Omega_1 \to 0$ and $\Omega_2 \to \infty$. In this case, Equation (4.35) becomes

$$\frac{1}{\pi Z_{eq}} = \frac{\pi}{2}, \tag{4.40}$$

which upon substitution into (4.34) yields the desired result for $\sigma_{X'}$.

To obtain the stationary velocity standard deviation $\sigma_{X'}$ for general Ω_1 and Ω_2, Equation (4.35) is solved to obtain the equivalent damping Z_{eq}, and this value is substituted into (4.34) to obtain $\sigma_{X'}$. As the former equation is transcendental, an exact solution is not available. A numerical value for Z_{eq} can be obtained by performing numerical iteration on the equation

$$\frac{1}{z_{n+1}} = \pi \arctan\left(\frac{z_n(\Omega_2 - \Omega_1)}{z_n^2 + \Omega_1\Omega_2}\right), \tag{4.41}$$

where

$$\lim_{n\to\infty} z_n = Z_{eq},$$

$$z_0 \gg \frac{2}{\pi^2}.$$

It has been found that practical values for n and z_0 are 50 and 10^6, respectively. The resulting values of Z_{eq} are then substituted into (4.34) to obtain the corresponding rms velocity $\sigma_{X'}$. In cases where $(\Omega_2 - \Omega_1) < 1/\pi$, numerical overflow can occur in iterating on z_n, as the correct solution for this case is $Z_{eq} \to \infty$. Thus, a check is performed in the iteration procedure, and, if an overflow is apparent, z_n is set to an arbitrarily large value.

This procedure has been carried out for values of Ω_1 and $\Delta\Omega$ ranging from zero to two, and the results are displayed in Figure 4.1. In Section 3.4 a comparison is performed between these predictions and simulation results. In the graph it is seen that for $\Delta\Omega < 1/\pi$, the predicted rms response velocity is zero. For slightly larger non-dimensional input bandwidth, the rms velocity increases abruptly, until $\Delta\Omega \approx 2/\pi$. For bandwidths larger than this, $\sigma_{X'}$ is weakly dependent on $\Delta\Omega$ and is more strongly dependent on the non-dimensional low frequency cutoff Ω_1. The peak value of $\sigma_{X'}$ is reached for white noise input $(\Omega_1 \to 0, \Delta\Omega \to \infty)$ and was shown earlier to be $\sqrt{\pi^3/2}$.

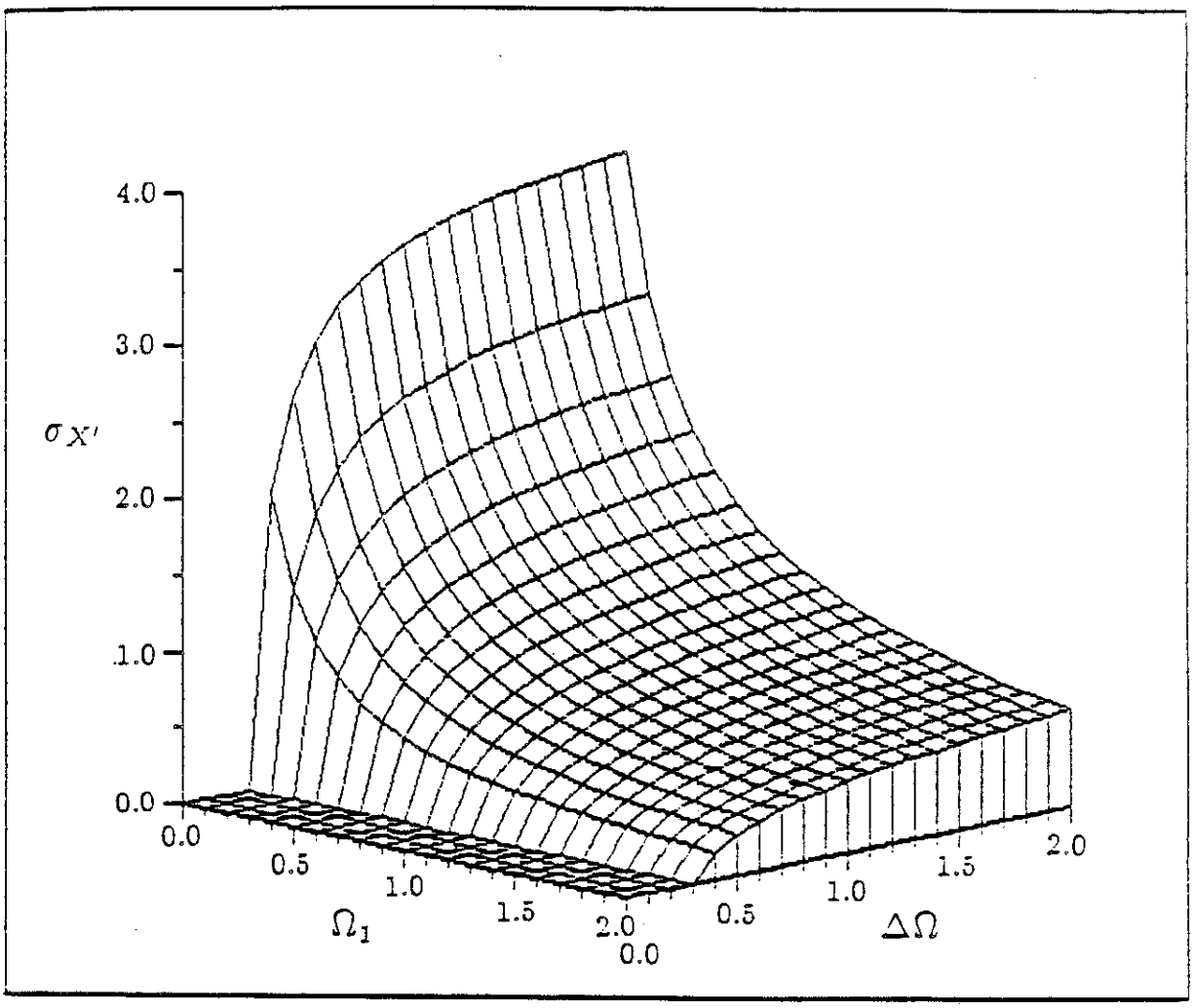

Figure 4.1: Stationary non-dimensional velocity standard deviation $\sigma_{X'}$ as a function of non-dimensional low-pass frequency Ω_1 and non-dimensional bandwidth $\Delta\Omega$. The peak value of $\sigma_{X'}$ in the graph is 3.67, 93% of the equivalent linearization prediction for white noise input.

Since the value of the stationary rms velocity is only weakly dependent on the input bandwidth for excitations with non-dimensional bandwidth $\Delta\Omega$ greater than about $2/\pi$, it is useful to find out the order of this dependence. Asymptotic expansion of (4.35) for large Ω_2 and $\Omega_1 \neq 0$ results in

$$\frac{1}{Z_{eq}} = \pi \arctan \frac{Z_{eq}}{\Omega_1}. \tag{4.42}$$

This equation is also solved iteratively, and after substitution into (4.34), values of $\sigma_{X'}$ are obtained. The results of this procedure are displayed in Figure 3.2. An estimate of the rate of dependence of $\sigma_{X'}$ on Ω_1 is obtained from asymptotic expansions of (4.42) for both large and small ratios of Z_{eq} to Ω_1. When $Z_{eq}/\Omega_1 \gg 1$, this equation implies $Z_{eq} \approx 2/\pi^2$, which through (4.34) gives $\sigma_{X'} \approx \sqrt{\pi^3/2}$, the white noise result derived earlier. For $Z_{eq}/\Omega_1 \ll 1$, $\arctan(Z_{eq}/\Omega_1) \approx Z_{eq}/\Omega_1$, which upon substitution into (4.42) yields

$$Z_{eq}^2 \approx \frac{\Omega_1}{\pi}, \quad \text{for } \Omega_1 \gg \frac{1}{\pi}, \tag{4.43}$$

$$\sigma_{X'} \approx \sqrt{\frac{2}{\Omega_1}}, \quad \text{for } \Omega_1 \gg \frac{1}{\pi}, \tag{4.44}$$

where Equation (4.34) has been used in obtaining the second expression from the first. Hence, for $\Delta\Omega$ large, the dependence of $\sigma_{X'}$ on Ω_1 is initially weak, but as Ω_1 increases, $\sigma_{X'}$ becomes inversely proportional to the square root of Ω_1. Thus, equivalent linearization indicates that the velocity variance is most strongly dependent on the low frequency content of the excitation for inputs whose non-dimensional variance exceeds $4/\pi$. For this reason, it is very important that an input model chosen for use with the Coulomb element accurately represent the low frequency content of the true physical excitation. The high frequency cutoff of the model becomes important only when the non-dimensional bandwidth of the signal is less than $2/\pi$.

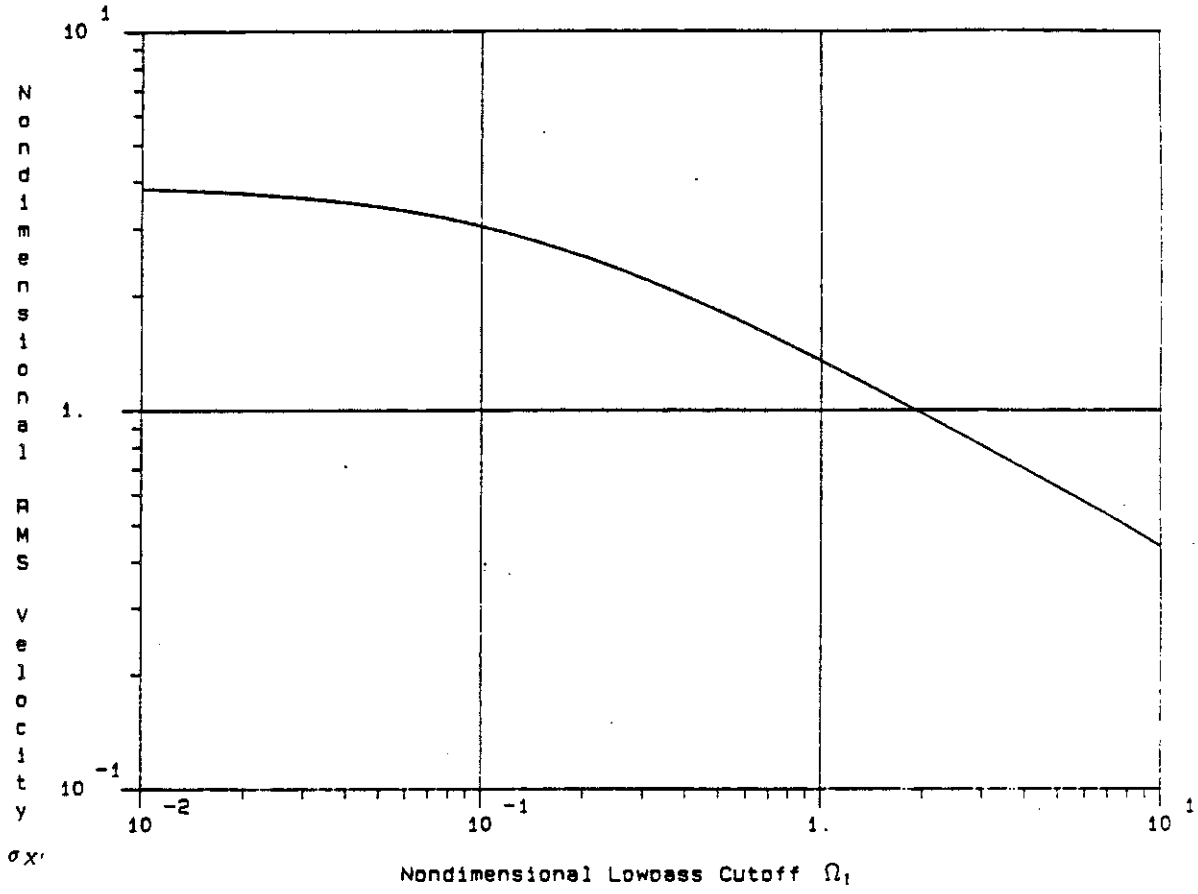

Figure 4.2: Stationary rms velocity $\sigma_{X'}$ as a function of low-pass frequency Ω_1 for $\Omega_2 \to \infty$ using equivalent linearization. All quantities are non-dimensionalized.

An expression for the stationary displacement variance is obtained from Equation (4.12), which after non-dimensionalization and substitution of the ideal band-pass spectrum becomes

$$\begin{aligned}\sigma_X^2 &= \int_{-\infty}^{\infty} \frac{S_{NN}(\Omega)}{\Omega^2(\Omega^2 + Z_{eq}^2)} d\Omega \\ &= \int_{\Omega_1}^{\Omega_2} \frac{2}{\Omega^2(\Omega^2 + Z_{eq}^2)} d\Omega \\ &= \pi\sigma_{X'}^2 \left[\frac{1}{\Omega_1} - \frac{1}{\Omega_2} - \frac{\sigma_{X'}^2}{2}\right], \end{aligned} \tag{4.45}$$

where Equations (4.32) and (4.34) have been used to simplify the results of the integration. The values of Z_{eq} needed in the above expression are obtained from the solution of (4.35). This expression for σ_X is clearly not valid for the case when Ω_1 equals zero. In that case, suitably non-dimensionalized forms of Equations (4.13) and (4.8) predict the long time behavior of the non-stationary displacement variance as

$$\sigma_X^2(t) \sim 2\pi \frac{\tau}{Z_{eq}^2} = \pi^2 \tau \sigma_{X'}^2 \text{ as } \tau \to \infty, \text{ for } \Omega_1 = 0. \tag{4.46}$$

This equivalent linearization prediction that the displacement variance achieves stationarity in all but the $\Omega_1 = 0$ case does not agree with simulations. The discussion of this discrepancy is postponed until the last section of the chapter.

4.4 Simulation studies

The accuracy of the stationary equivalent linearization results is estimated from a comparison with Monte-Carlo simulations of same process. A stationary Gaussian input process with arbitrary spectral density is generated using an inverse fast Fourier transform. This process is then used as excitation to

the system (4.23), which is solved numerically to obtain velocities and displacements. As an interpolation function is used in the solution of the equation of motion, the input spectrum is affected; a proposed correction compensates for these changes. The procedure is repeated until an ensemble is generated, and averages are taken to obtain estimates of the desired statistics. The spectral density of the stationary response velocity is also calculated by means of an FFT, using a Kaiser-Bessel window to improve the spectral resolution.

A stationary time series $n(t)$ with arbitrary spectral density can be generated from [24,25]

$$n(t) = \sum_{k=1}^{N} 2[S_{nn}(\omega_k)\Delta\omega_k]^{1/2}\cos(\omega_k t + \phi_k), \tag{4.47}$$

where $\phi_k (k = 1, 2, \ldots, N)$ are independent identically distributed random variables with a uniform density function on $[0,2\pi]$, and $S_{nn}(\omega_k) = S_{nn}(\omega)|_{\omega=\omega_k}$, with $S_{nn}(\omega)$ being the two-sided spectral density of $n(t)$. If $\Delta\omega_k$ is a constant, then $\omega_k = k\Delta\omega$ and (4.47) simplifies to

$$n(t) = \sum_{k=1}^{N} 2[S_{nn}(k\Delta\omega)\Delta\omega]^{1/2}\cos(kt\Delta\omega + \phi_k). \tag{4.48}$$

When the random process is sampled at discrete times $m\Delta t$, with $\Delta t = \pi/N\Delta\omega$, the previous equation becomes

$$n(m\Delta t) = \sum_{k=1}^{N} 2[S_{nn}(k\Delta\omega)\Delta\omega]^{1/2}\cos\left(\frac{\pi mk}{N} + \phi_k\right), \tag{4.49}$$

which is in the form of a discrete Fourier transform. These series are very efficiently computed using the Fast Fourier Transform (FFT) or inverse FFT algorithms taking advantage of symmetries in the above expression. Yang [25] has remarked that this method should yield variables with accurate Gaussian distributions when $N \geq 500$. For the results presented in this discussion, Hall's

inverse FFT algorithm [26] is used with $N = 512$, producing a time series with 1024 points. The advantages of this method are speed of computation for the time series as well as accurate representation in the time domain of a signal with arbitrary spectral density. Drawbacks to this technique are associated with the discretization of both the time and frequency domains. When the frequency domain is discretized, a periodicity of length $2\pi/\Delta\omega$ is introduced into the time domain signal. This can be overcome by gathering statistics from only the central portion of records. Discretization of the time domain implies that time series values are available only at evenly spaced time intervals. Fortunately, most algorithms used for the numerical solution of ordinary differential equations are perfectly suited for this type of data.

Once the random time series is generated using the previously described method, the next step is to solve the equation of motion

$$\ddot{x} + f(\dot{x}) = -n(t), \tag{4.50}$$

where

$$f(\dot{x}) = \begin{cases} a\,\mathrm{sgn}(\dot{x}), & \dot{x} \neq 0; \\ n(t), & \dot{x} = 0, |n(t)| \leq \mu g, \end{cases}$$

dots denote derivatives with respect to time, x is the relative displacement, a is the slip level, and $n(t)$ is the ground acceleration. Note that the above formulation for $f(\dot{x})$ is different mathematically from that of Coulomb friction in (2.20), although physically the two are equivalent. The particular formulation used here is more convenient for numerical applications. Equation (4.50) can be rewritten as the three separate equations

$$\ddot{x} = x(t) - a, \quad \dot{x} > 0; \tag{4.51}$$

$$\ddot{x} = 0, \qquad \dot{x} = 0, |n(t)| \leq a; \tag{4.52}$$

$$\ddot{x} = n(t) + a, \quad \dot{x} < 0, \tag{4.53}$$

each one corresponding to a different "state" of $\dot{x}$. These equations are easily solved by closed form integration to obtain $\dot{x}(t)$ and $x(t)$ provided the state of $\dot{x}$ does not change. When the solution for $\dot{x}$ indicates a change in state, the solutions must be patched together to ensure continuity in both the relative velocities and displacements.

As was mentioned earlier, the input process used in the simulations provides $n(t)$ at discrete, uniformly spaced times $m\Delta t, m = 1, 2, \ldots, 2N$. Since it is meaningful to obtain x and $\dot{x}$ only at these times, and the system exhibits no memory, the solution can be set up as a discrete process, with the values at time $(m+1)\Delta t$ being determined by the conditions at $m\Delta t$ and the excitations $n(m\Delta t)$ and $n((m+1)\Delta t)$. For the relative velocities and displacements, this can be stated as

$$x((m+1)\Delta t) = p\left[x(m\Delta t), \dot{x}(m\Delta t), n((m+1)\Delta t), n(m\Delta t)\right], \tag{4.54}$$

$$\dot{x}((m+1)\Delta t) = q\left[\dot{x}(m\Delta t), n((m+1)\Delta t), n(m\Delta t)\right], \tag{4.55}$$

where the functions p and q are determined from the solution of (4.53). Note that the expression for $\dot{x}((m+1)\Delta t)$ is independent of the displacement.

A reasonable way to attempt to obtain expressions for p and q would be to use one of the standard numerical solution methods used for solving ordinary differential equations. Unfortunately, the majority of these methods fail when applied to (4.53) because of the abrupt changes in resisting force for a small change in velocity when $\dot{x} \approx 0$ (sometimes referred to as being a "stiff equation") and because of the zero "tangent stiffness" when $\dot{x} \neq 0$. However, a closed form solution of these equations is possible for certain forms of forcing

function $n(t)$.

To solve (4.53) in closed form to obtain relative velocities and displacements for $t \in [m\Delta t, (m+1)\Delta t]$, a continuous extension of $n(t)$ is needed over this range. An interpolation scheme must be chosen to supply this information. Since points are being added to the signal, the spectrum of the interpolated excitation is different from that of the original. A balance must be struck between simplicity in the interpolation, resulting in poor spectral characteristics but ease of solution of equations of motion, and higher-order interpolation for which solution of (4.53) is difficult. For the simulations described herein, linear interpolation is chosen. Thus,

$$n(t) = n(m\Delta t) + \frac{t - m\Delta t}{\Delta t}\left(n((m+1)\Delta t) - n(m\Delta t)\right), \quad m\Delta t \le t \le (m+1)\Delta t. \tag{4.56}$$

The solution of (4.53) with this excitation is straightforward, although many special cases must be considered. Note that the velocity can change sign a maximum of two times within an interval Δt.

It can be shown that the spectrum of a continuous, linearly interpolated signal is given by

$$F_c(l) = F(l) \prod_{k=1}^{\infty} \cos^2\left(\frac{\pi l}{N 2^{k+1}}\right), \tag{4.57}$$

where $F(l)$ is the discrete, periodic spectrum of the discrete, periodic signal $n(m\Delta t)$, and $F_c(l)$ is the discrete spectrum of the interpolated excitation $n(t)$. An illustration of the infinite product on the right-hand side of the previous equation is seen in Figure 4.3. For $|l/N| < .3$, the spectral ordinates of $F(l)$ are reduced by less than 10%, but beyond this the distortion of the desired spectral shape can become quite severe. Although not displayed, the aliased, or periodic, portions of the spectrum of $F(l)$ occurring above the Nyquist frequency

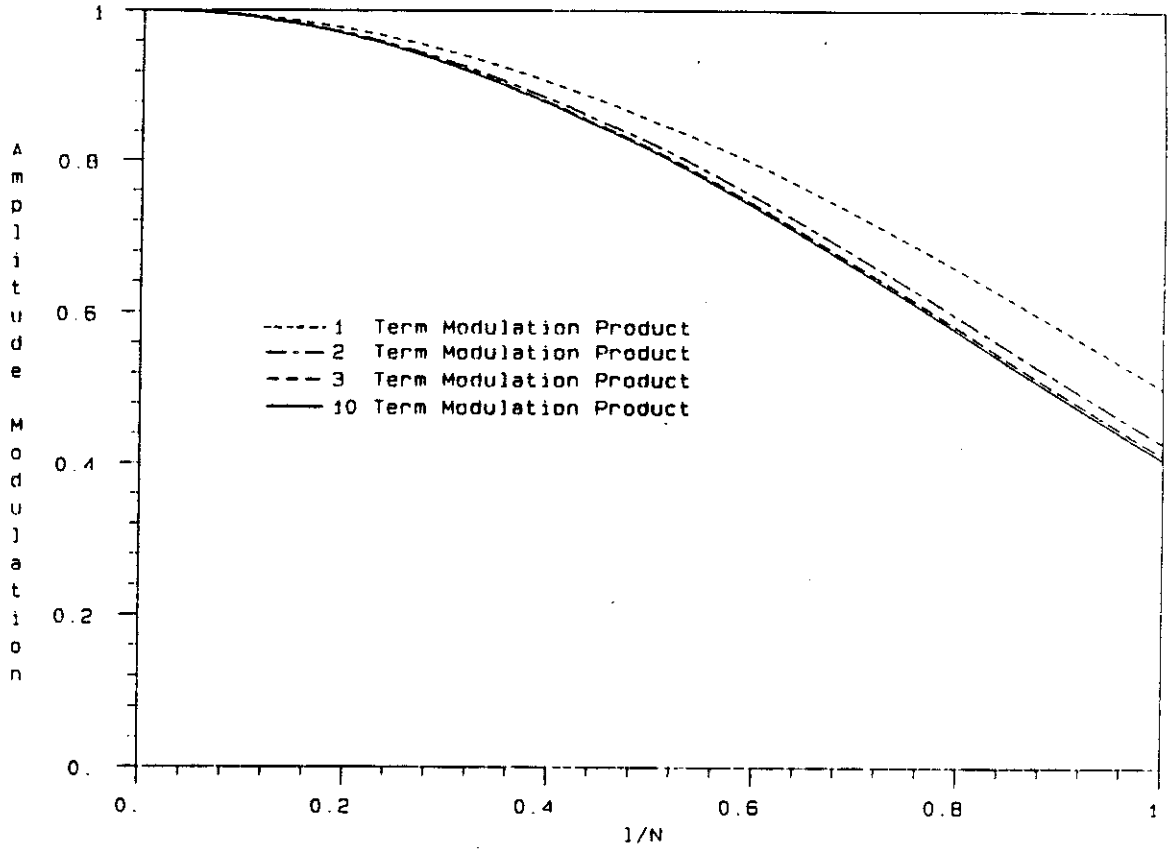

Figure 4.3: Amplitude modulation of the input spectrum caused by linear interpolation. The different curves represent truncated product approximations with varying numbers of terms. The Nyquist frequency is at $l/N = 1.0$.

($|l/N| = 1$) are also modulated, but are of little concern as they do not affect the system of interest. To correct for the reduction of the spectrum in the range $0 \leq |l/N| \leq 1$, $F(l)$ can be multiplied by the reciprocal of the trigonometric product in (4.57), causing the spectrum of the interpolated signal to match the desired spectrum in this range. Thus,

$$F(l) = F_t(l) \left[\prod_{k=1}^{\infty} \cos^2 \left(\frac{\pi l}{N 2^{k+1}} \right) \right]^{-1}, \tag{4.58}$$

where $-N < l \leq N$, and $F_t(l)$ is the target spectrum. This process is the "pre-correction" alluded to earlier. Since $F(l)$ is periodic, each one of its periodic extensions is also affected, but the amplitude of these is reduced by the modulation of (4.57) occurring during interpolation.

This pre-correction procedure is applied to the spectra used in the simulations. Although seemingly cumbersome, the input power spectrum is multiplied only once by the product in Equation (4.58). Also, the use of a 10-term truncated product results in values accurate to five significant figures when compared to a 100-term truncation, indicating that 10 is a sufficiently large number of terms to represent the infinite product.

The methods described to this point are sufficient to obtain time series for the response velocities and displacements. A brief overview of how these data is used to generate ensemble statistics now follows. The statistics estimated are the response velocity and displacement variances and covariance, and the input acceleration variance, which are computed using

$$E\left[y_i(t)y_j(t) - E[y_i(t)]E[y_j(t)]\right] = E[y_i(t)y_j(t)] - E[y_i(t)]E[y_j(t)], \tag{4.59}$$

where

$$E[f(y(t))] \approx \frac{1}{N_E} \sum_{p=1}^{N_E} f_p(y(t)), \tag{4.60}$$

and y represents either acceleration, velocity or displacement, $f_p(y(t))$ is a sample from a single simulation, and N_E is the number of records in an ensemble. This estimator is unbiased, and it can be shown that [27]

$$E[f(y)] = \frac{1}{N_E}\sum_{p=1}^{N_E} f_p(y) \pm \frac{\sigma_{f(x)}}{\sqrt{N_E}}. \tag{4.61}$$

In the simulations, 1000 records are used in an ensemble, which can be seen by the above equation to give a good estimate of the true values, provided $\sigma_{f(x)}$ is small. The sums are determined by keeping a running average, updated after each simulation, and the times kept are the sampling times $m\Delta t$.

Stationary estimates of the input covariance, velocity variance, and covariance of velocity and displacement are obtained by taking timewise averages of the ensemble statistics. As zero initial conditions are used for both velocity and displacement, the response process is initially non-stationary. It is also found that the final portion of the records are non-stationary due to the periodicity inherent in using FFT's to generate the input signal. For these reasons, only the central 512 of the 1024 points in the velocity record are used in obtaining an estimate of the velocity variance; a check is also made to ensure stationary of the velocity response process.

In addition to generating the response velocity and displacement, there is also interest in determining the spectral content of the stationary portion of the velocity response. The spectral resolution is improved if the central 512 points of the velocity record are multiplied by a Kaiser-Bessel window of the form

$$W(n) = \alpha \frac{I_0\left[\beta\sqrt{1-(2n/N)^2}\right]}{I_0(\beta)}, \tag{4.62}$$

where α is a numerically determined coefficient that normalizes the rms value of the window to one, β is the time-bandwidth product, I_0 is the modified

Bessel function of order zero, and $n - 512 = -N/2, \ldots, -1, 0, 1, \ldots, N/2$. The parameter β is set to 8.0, since it has been shown that this lowers the first Fourier amplitude side lobe below 70 dB., equivalent to 140 dB. or 10^{-7} in the spectral density. The tradeoff for these low side lobes is an increase in the width of the main lobe. The spectral density of the record is then found from a forward FFT using Hall's algorithm [26] on the windowed segment of the record. The squared magnitude of the spectrum is then computed, and this quantity is divided by $4\pi N\Delta t$ to obtain the spectral density for a single record. An estimate of the stationary velocity spectral density is then found by taking an average of the densities across the ensemble.

4.5 Comparison of Stationary Equivalent Linearization and Simulation Results for Ideal Band-Pass Filtered Input

In this section, the simulation methods described in the preceding subsection are used to check the accuracy of the stationary equivalent linearization predictions. Three measures of the response are used in this comparison: the stationary velocity standard deviation, the stationary velocity spectral density, and the displacement variance. It is shown that the agreement is reasonably good for rms velocity, but differences in the low frequency content of the velocity spectral density cause the displacement variance in the simulations to be always non-stationary. This is contrary to the equivalent linearization prediction of stationarity for all excitations with $\Omega_1 \neq 0$. The discussion begins with a detailed comparison of results from these two methods for a particular set of

input parameters, followed by a comparison of the rms velocity results over a broad range of input parameters.

A comparison is performed between the simulation statistics of the Coulomb element response and those predicted by equivalent linearization, as well as simulations performed on a linear system using the viscous damping value computed by stationary equivalent linearization. The equations of motion for the linear system simulation are solved using the fourth order Runge-Kutta method. This linear simulation is useful not only for determining the effects of a finite ensemble size, but also in establishing the accuracy of the method used to generate the band-limited excitation.

The case that is studied in detail has input parameters $\Delta\Omega = \Omega_1 = 20/\pi^2 \approx 2.02$. This input is broadband, and, as can be seen in Figure 4.1, has a value of $\Delta\Omega$ well above the critical bandwidth of equivalent linearization. Another important feature of this input is the lack of spectral content near $\Omega = 0$. This will be useful during the discussion of differences between the velocity spectral densities of the linear and Coulomb systems.

A comparison of the rms velocity for the Coulomb and linear system simulation methods as well as the stationary equivalent linearization predictions is found in Figure 4.4. Both of the equivalent linear systems are within 10% of the Coulomb element simulation once stationarity is reached. The fluctuations exhibited by the simulations are caused by two aspects of the random input. The overshoot at the beginning of the record is caused by the periodicity of the input records, while the oscillations occurring in the rest of the record are due to the sharp low frequency cutoff of the band-pass filter. Stationarity is reached within a short time compared with the length of the record, so the use of fixed

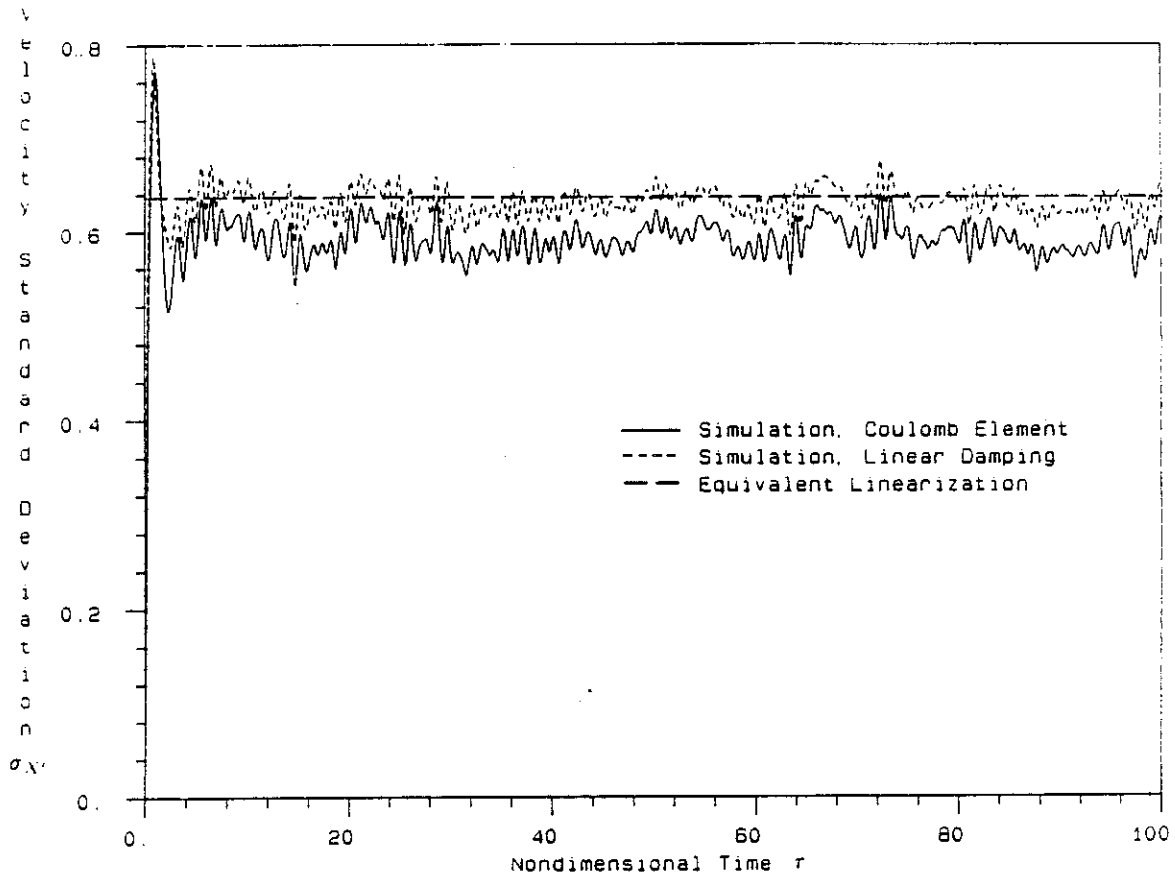

Figure 4.4: Comparison of response velocity standard deviation for simulations of Coulomb element and equivalent linear systems, along with stationary equivalent linearization results. For this case $\Delta\Omega = \Omega_1 = 20/\pi^2$, $\Delta\tau = 0.1$, and the ensemble size is 1000.

linear parameters is acceptable. In fact, the fixed linear parameters used in the linear simulation even do a good job of predicting the initial non-stationary response.

Figure 4.5 presents the stationary velocity spectral densities for the Coulomb and linear system simulations along with the equivalent linearization prediction. The latter result is obtained from a non-dimensionalized form of Equation (4.8). On a linear scale, all three responses appear limited to the input frequency range. The linear and nonlinear simulation responses are similar within this range, and it seems that the differences are due more to discrepancies in the rms velocity than to the shapes of the power spectra of the different systems. The agreement between the two linear systems is not as good as in the rms velocity. A possible reason for this discrepancy is that the simulation spectral densities are computed from data that may not be mean-zero, while the equivalent linearization has a zero mean. Since the spectral density is a measure of the mean-squared statistics, the use of a non-zero mean signal increases the spectral density.

On the logarithmic plot of Figure 4.5, it can be seen that outside the frequency range of the input, the response of the linear systems is practically zero, as it should be, but the nonlinear Coulomb element exhibits small but finite response in this range. The apparent response of the linear system simulation outside the input band is due to the use of a finite length record, which causes the appearance of side lobes in the frequency domain. As was mentioned earlier, the use of a Kaiser-Bessel window in the time domain has the effect of making the side lobe amplitude 10^{-7} times that of the main lobe. A drawback to the window is that the main lobe of the signal is widened. Both

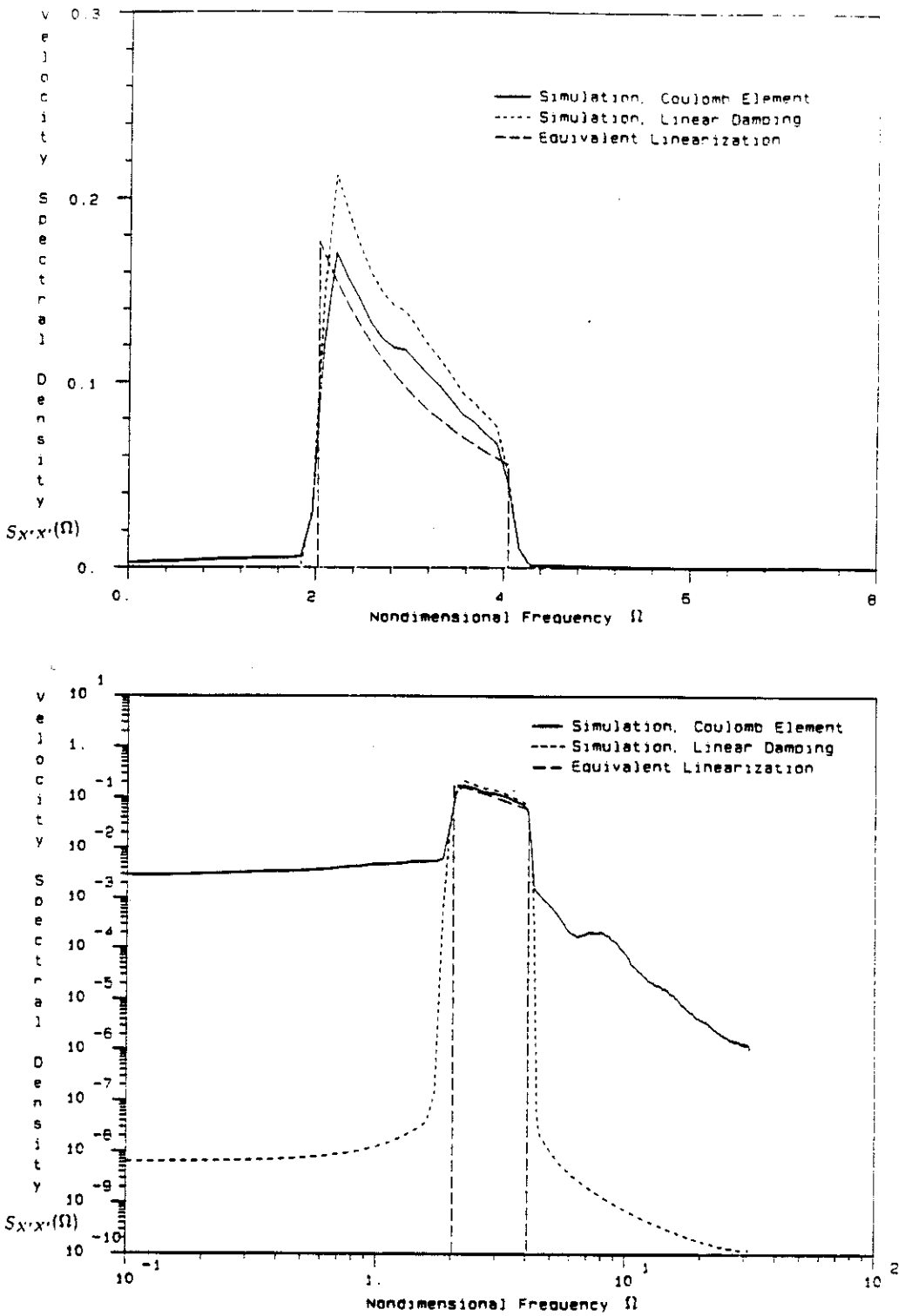

Figure 4.5: Stationary velocity spectral densities from simulations of Coulomb and equivalent linear systems, and analytical stationary equivalent linearization; linear scale (top), and logarithmic scale (bottom). For this case $\Delta\Omega = \Omega_1 = 20/\pi^2$, $\Delta\tau = 0.1$, and the ensemble size is 1000.

these effects are apparent when a comparison is performed between the linear simulation and the equivalent linearization prediction in the logarithmically scaled portion of Figure 4.5. The Coulomb element response is far above the side lobe level, indicating that a velocity response in these frequency ranges is truly present in the stationary signal. It can be seen that this non-zero spectral content is present at zero frequency. Hence, the displacement is non-stationary, and its rate of growth is given approximately by

$$\sigma_X^2(t) \sim 2\pi\tau S_{X'X'}(0) \text{ as } \tau \to \infty. \tag{4.63}$$

Since the linear system shows no response in this frequency range, the displacement response is expected to be stationary.

The results of the simulation displacement response for Coulomb element and the equivalent linear system are shown in Figure 4.6 The linear system achieves stationarity quite rapidly, but the nonlinear system does not reach stationarity within the span of the record. Thus, the prediction of equivalent linearization that the displacement response is stationary if $\Omega_1 \neq 0$ is incorrect. The unbounded increase in displacement variance for the Coulomb element indicates that the system drifts, and that as time increases the expected position of the system is known with decreasing accuracy. This non-stationary behavior is not unique to the parameters of this simulation, and has been observed in all simulations of the response of the Coulomb element to band-pass filtered excitation.

The accuracy of the equivalent linearization method can be studied further by means of simulations performed with varying $\Delta\Omega$ and Ω_1. Two series of simulations are presented herein: in the first, $\Delta\Omega$ is held constant while Ω_1 is varied, and in the second the opposite situation is considered. This is equiv-

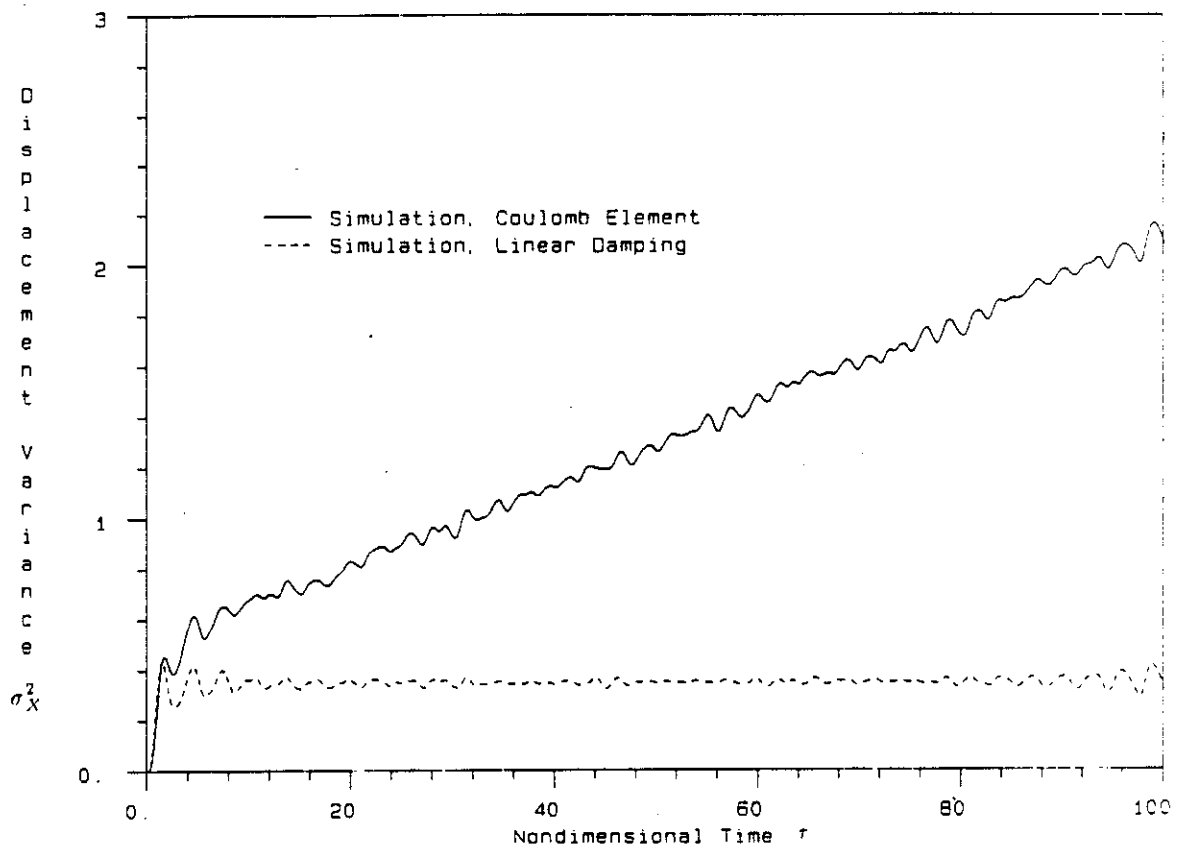

Figure 4.6: Comparison of displacement variance for simulations of Coulomb element and equivalent linear systems. For this case $\Delta\Omega = \Omega_1 = 20/\pi^2$, $\Delta\tau = 0.1$, and the ensemble size is 1000.

alent to checking the accuracy of the method in two perpendicular slices across Figure 4.1. A comparison between the methods is made only in the stationary value of rms velocity, as the displacement behavior predicted by equivalent linearization is universally incorrect.

Before the results are presented, a few comments on the efficiency of the two methods are in order. To generate the 400 points plotted in Figure 4.1 using the equivalent linearization procedure requires approximately 1 minute on an IBM PC-AT. One simulation, resulting in a single data point, uses about 3 hours of computing time on the same machine. Thus, the equivalent linearization method is significantly more efficient, while simulations are a valuable tool in estimating accuracy.

A comparison of the predicted rms velocity by equivalent linearization and simulations is presented in Figure 4.7, where the value of $\Delta\Omega$ has been set to $20/\pi^2$. It is seen that the accuracy of the approximate method is better than 20% in all cases, and within 10% in most. The results of the same comparison for Ω_1 held fixed, while $\Delta\Omega$ is varied, is given in Figure 4.8. For $\Delta\Omega \leq 1/\pi$, the equivalent linearization prediction of zero response velocity is not accurate, as demonstrated by the two simulations in this range with non-zero response. As the input variance is increased above the critical level, the equivalent linearization method is shown to be better than 20% accurate in predicting the rms velocity.

In this chapter it has been shown that while equivalent linearization is accurate in predicting the velocity response of a Coulomb element for most ranges of input parameters, it cannot capture the non-stationary nature of the displacement response when the excitation spectrum has no content at

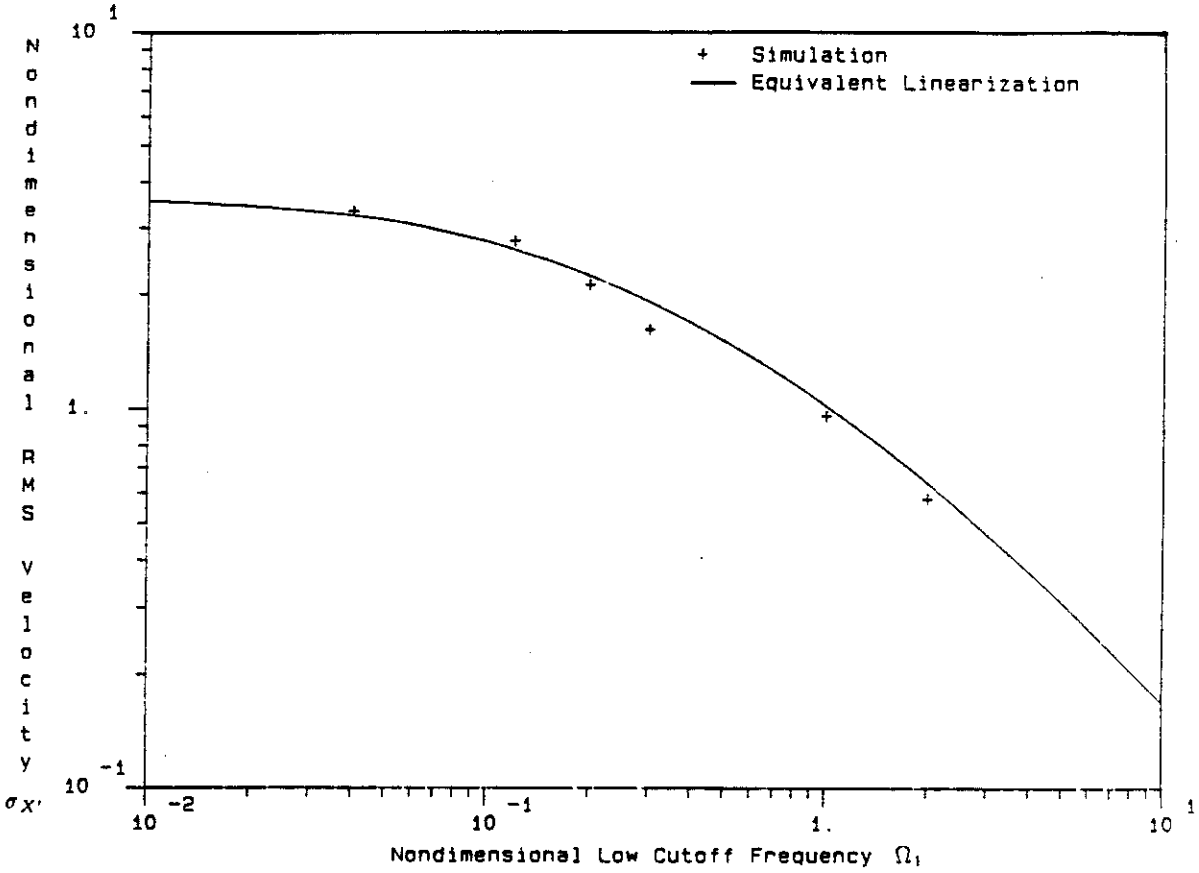

Figure 4.7: Comparison of rms velocities using equivalent linearization and simulations for fixed $\Delta\Omega$. The data presented is for $\Delta\Omega = 20/\pi^2$, and the ensemble size is 1000 for the simulations.

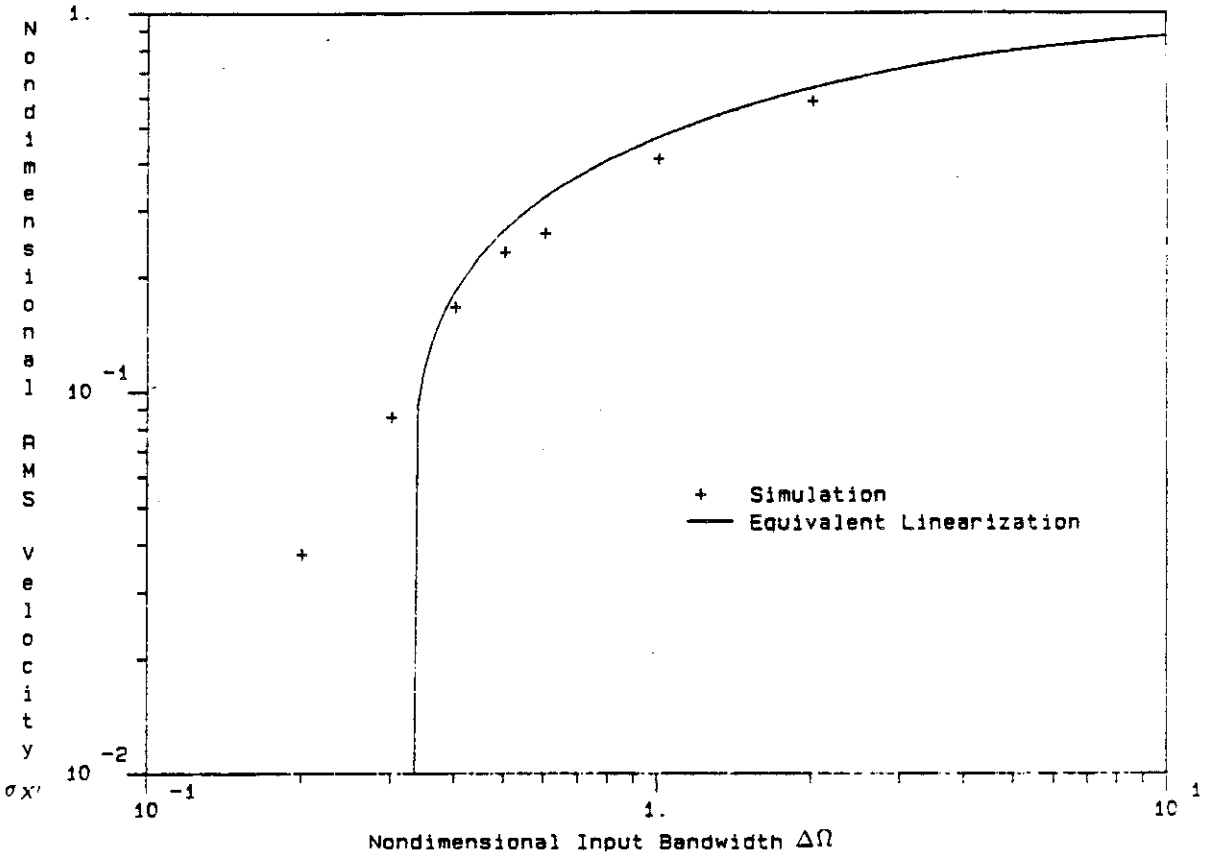

Figure 4.8: Comparison of rms velocities using equivalent linearization and simulations for fixed Ω_1. The data presented is for $\Omega_1 = 20/\pi^2$, and the ensemble size is 1000 for the simulations.

zero frequency. It is also shown that the system's velocity response is most sensitive to low frequency content, with the same behavior expected for the displacement. Although a discussion of the nature of the spectral content of an earthquake is postponed until the next chapter, one important feature is the lack of zero frequency content. Thus, neither of the equivalent linearization technique described thus far can be used to estimate displacement variance for seismic excitation. In the next chapter, a different approximate method is developed and is shown to give good estimates of both the rms velocity and rate of increase for the rms displacement.

Chapter 5

Response of the Coulomb System to Filtered Random Excitation — Poisson Process Approximate Approach

5.1 Introduction

In the previous chapter it was shown that the equivalent linearization method was inadequate for predicting displacement statistics for the simple Coulomb system with band-pass filtered excitation. An alternate method is proposed in this chapter. This method, to be called the Poisson process method, is shown to be accurate in predicting response statistics for both velocity and displacement.

The chapter begins with an illustration of the differences in the response of a linear viscously damped system and a Coulomb block when excited by a symmetric rectangular pulse. These differences in response are exploited to develop a random process consisting of pulses with this shape, but with random amplitude and random starting times. If superposition is assumed to hold, the response process can be calculated as a sum of responses to the individual pulses. If the overlaps in the input pulses are taken into account, estimates that are accurate over a larger parameter range are obtained. As in

the previous chapter, the accuracy of the approximate method is determined by comparison with simulation results. The simulation techniques are described in Section 5.5, and in Section 5.6 simulation results are compared with those predicted by the Poisson process approach. In the final section the response of stick-slip systems to seismic excitation is considered, using a Poisson process model for earthquakes.

5.2 An Illustration of Differences in Response for Coulomb and Linear Systems

In Chapter 4 it was shown that the displacement response of a Coulomb element and an equivalent linear system have a fundamentally different character. The linear system displays bounded variance, while the Coulomb damper's variance increases linearly with time once the velocity reaches stationarity. In this section, the response of the two systems to a particular type of loading is examined to further illustrate differences in response. The insight gained through this example is useful in formulating an approximate method developed later in the chapter.

The equation of motion for the Coulomb element is

$$\ddot{x} + a\,\mathrm{sgn}(\dot{x}) = -n(t), \tag{5.1}$$

while that the viscously damped linear system is

$$\ddot{x} + \zeta_{eq}\dot{x} = -n(t). \tag{5.2}$$

The excitation $n(t)$ applied in this example is

$$n(t) = \begin{cases} b, & \text{if } 0 < t < \Delta t; \\ -b, & \text{if } \Delta t < t < 2\Delta t; \\ 0, & \text{elsewhere.} \end{cases} \tag{5.3}$$

The Fourier spectrum of the input pulse is obtained through the transformation

$$\hat{n}(\omega) = \int_{-\infty}^{\infty} n(t) e^{i\omega t}\, dt, \tag{5.4}$$

where $i = \sqrt{-1}$. Substituting (5.3) into (5.4) one obtains

$$\hat{n}(\omega) = -\frac{ib}{4\pi\omega}\left[1 - 2e^{-i\omega\Delta t} + e^{-2i\omega\Delta t}\right], \tag{5.5}$$

which is used to obtain the Fourier Amplitude Spectrum of the pulse

$$|\hat{n}(\omega)| = \frac{|b|}{2\pi\omega}\left[4\sin^2\frac{\omega\Delta t}{2} - \sin^2\omega\Delta t\right]^{\frac{1}{2}}. \tag{5.6}$$

From the above expression it is observed that for low frequencies the pulse amplitude spectrum increases linearly with frequency, while for high frequency it is bounded from above by an envelope that decreases inversely with frequency.

The relative velocity of the response of a Coulomb element can be solved in closed form, and for $|b| > a$ is given by

$$v(t) = \begin{cases} -(|b| - a)\mathrm{sgn}(b)\, t, & 0 < t < \Delta t; \\ [-(|b| - a)\Delta t + (|b| + a)(t - \Delta t)]\mathrm{sgn}(b), & \Delta t < t < 2\Delta t\left(\frac{|b|}{|b|+a}\right); \\ (|b| - a)\left[t - 2\Delta t\left(\frac{|b|}{|b|+a}\right)\right]\mathrm{sgn}(b), & 2\Delta t\left(\frac{|b|}{|b|+a}\right) < t < 2\Delta t; \\ \left[2\Delta t(|b| - a)\left(\frac{a}{|b|+a}\right) - a(t - 2\Delta t)\right]\mathrm{sgn}(b), & 2\Delta t < t < 4\Delta t\left(\frac{|b|}{|b|+a}\right); \\ 0, & \text{elsewhere.} \end{cases} \tag{5.7}$$

Note that the maximum duration of the velocity response is $4\Delta t$, occurring for $|b| \gg a$. The relative displacement is obtained by integrating the expression

for the relative velocity. As the result is a complicated algebraic expression, only the final displacement is presented. This is:

$$\Delta x = -a\,\Delta t^2 \mathrm{sgn}(b)\left[\frac{(\beta-1)\beta}{\beta+1}\left(1-\frac{2}{\beta+1}\right)\right], \quad \text{for } t > 4\Delta t\left(\frac{\beta}{\beta+1}\right), \beta > 1, \tag{5.8}$$

where

$$\beta = \frac{|b|}{a}. \tag{5.9}$$

This final displacement offset Δx is non-zero for all input amplitudes that exceed the slip level of the Coulomb element. If $|b| < a$, the response velocity and displacement are both be identically zero.

The linear system response is obtained from the convolution of the input with the impulse response of the system. Thus,

$$v(t) = -\int_0^t h_v(t-\theta)\, n(\theta)\, d\theta, \tag{5.10}$$

$$d(t) = -\int_0^t h_d(t-\theta)\, n(\theta)\, d\theta, \tag{5.11}$$

where

$$h_v(\theta) = e^{-\zeta_{eq}\theta}\, u(\theta), \tag{5.12}$$

$$h_d(\theta) = \frac{1}{\zeta_{eq}}(1-e^{-\zeta_{eq}\theta})\, u(\theta); \tag{5.13}$$

v and d are the relative velocity and displacement, respectively, and $u(\theta)$ is the unit step-function. The relative velocity response to the symmetric rectangular pulse is found by manipulation of these expressions to be

$$v(t) = \begin{cases} -\frac{b}{\zeta_{eq}}\left[1-e^{-\zeta_{eq}t}\right], & 0 < t < \Delta t; \\ \frac{b}{\zeta_{eq}}\left[1-2e^{-\zeta_{eq}(t-\Delta t)}+e^{-\zeta_{eq}t}\right], & \Delta t < t < 2\Delta t; \\ \frac{b}{\zeta_{eq}}e^{-\zeta_{eq}t}\left[1-e^{\zeta_{eq}\Delta t}\right]^2, & t > 2\Delta t. \end{cases} \tag{5.14}$$

The relative displacement is given by

$$d(t) = \begin{cases} -\frac{b}{\zeta_{eq}}\left[t - \frac{1}{\zeta_{eq}}\left(1 - e^{-\zeta_{eq}t}\right)\right], & 0 < t < \Delta t; \\ \frac{b}{\zeta_{eq}}\left[t - 2\Delta t + \frac{1}{\zeta_{eq}}\left(2e^{-\zeta_{eq}(t-\Delta t)} - e^{-\zeta_{eq}t} - 1\right)\right], & \Delta t < t < 2\Delta t; \\ -\frac{b}{\zeta_{eq}^2}e^{-\zeta_{eq}t}\left[1 - e^{-\zeta_{eq}\Delta t}\right]^2, & t > 2\Delta t. \end{cases} \quad (5.15)$$

Note that for $t \gg 2\Delta t$, the displacement goes to zero for all values of ζ_{eq}.

Plots of the excitation in the time and frequency domains, and the response velocity and displacement for both the linear and Coulomb systems are presented in Figures 5.1, 5.2, and 5.3. For the case displayed in these figures, $\Delta t = 1.0, a = 1.0, b = 1.5$, and ζ_{eq} has been adjusted so that both systems exhibit the same rms velocity. The linear and Coulomb system velocity responses shown in the latter figure are similar in shape, although the Coulomb block's response is not mean-zero, while the linear system's is. When the displacement responses of the two systems are compared, the shapes are again quite similar with one notable exception: the Coulomb element exhibits a permanent offset, while the linear system does not.

These differences between systems are consistent with those discussed in Chapter 4, although the input spectra used are not identical. Since the input pulse's spectrum is proportional to frequency for low frequencies, the velocity spectrum of the linear system should exhibit the same trend, which implies that the velocity has a zero mean because it has no content for zero frequency. Thus, the displacement exhibits no offset for times which are large compared with the duration of the excitation.

It can be shown that the Fourier amplitude spectrum for the Coulomb element's velocity does not go to zero for zero frequency, the same trend exhibited in the previous chapter by the Coulomb system under band-limited excitation. Consequently, the displacement response to an input pulse input

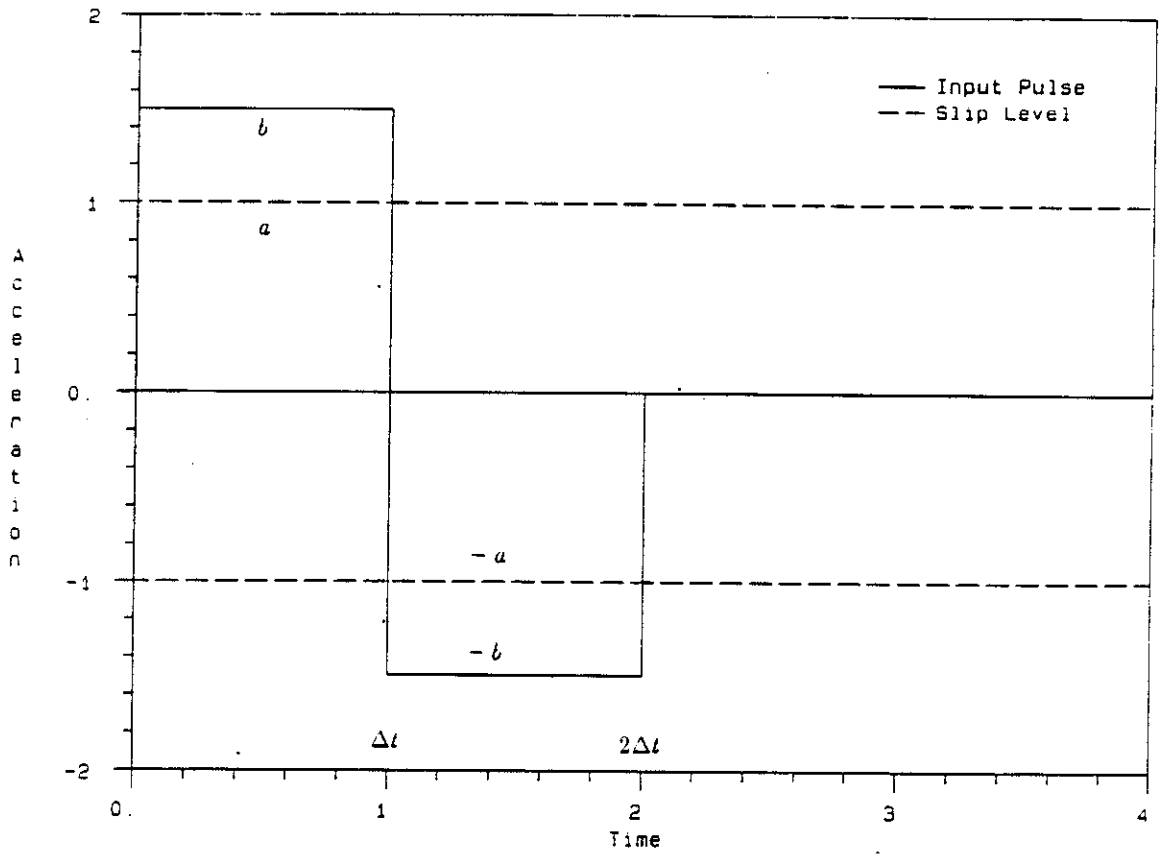

Figure 5.1: Input acceleration pulse $n(t)$ and slip level a used in the example. The parameter values are $a = 1.0$, $b = 1.5$, and $\Delta t = 1.0$.

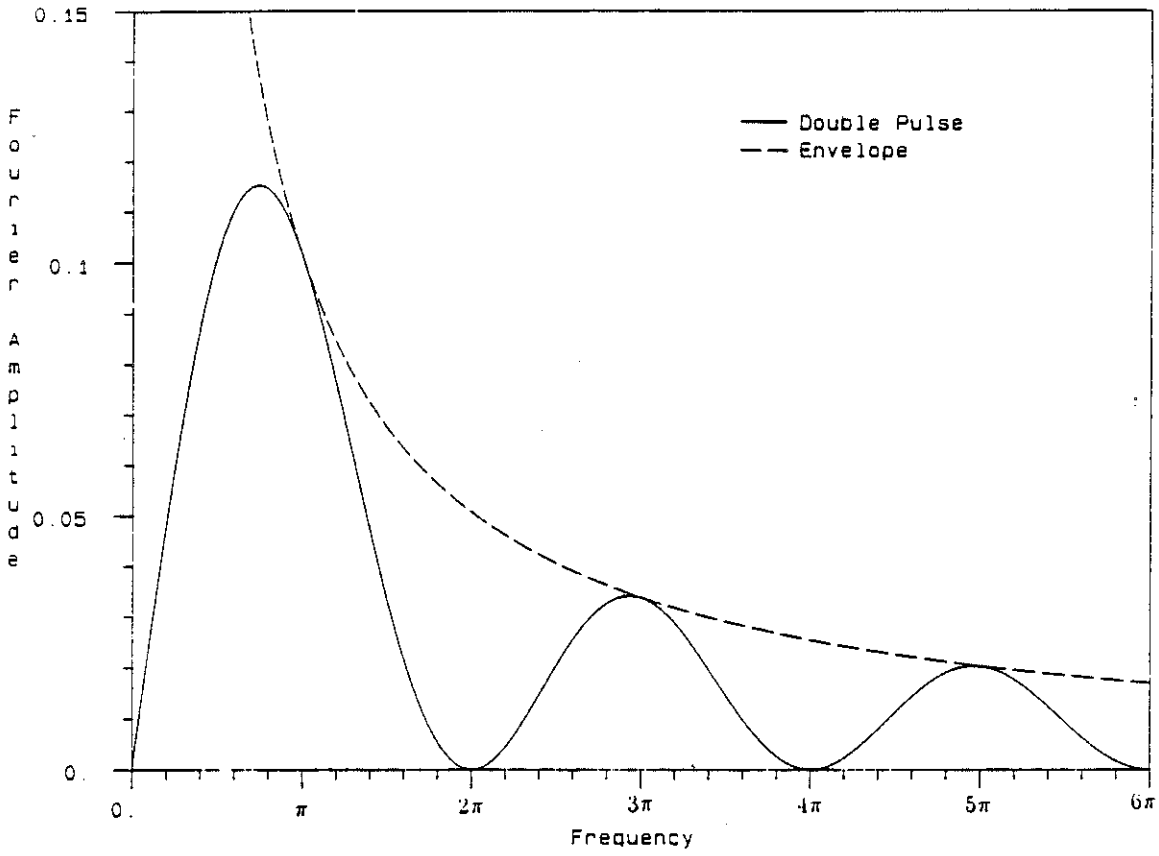

Figure 5.2: Fourier amplitude for the pulse used in the example, along with an envelope that decays inversely with frequency. The parameter values are $a = 1.0$, $b = 1.5$, and $\Delta t = 1.0$.

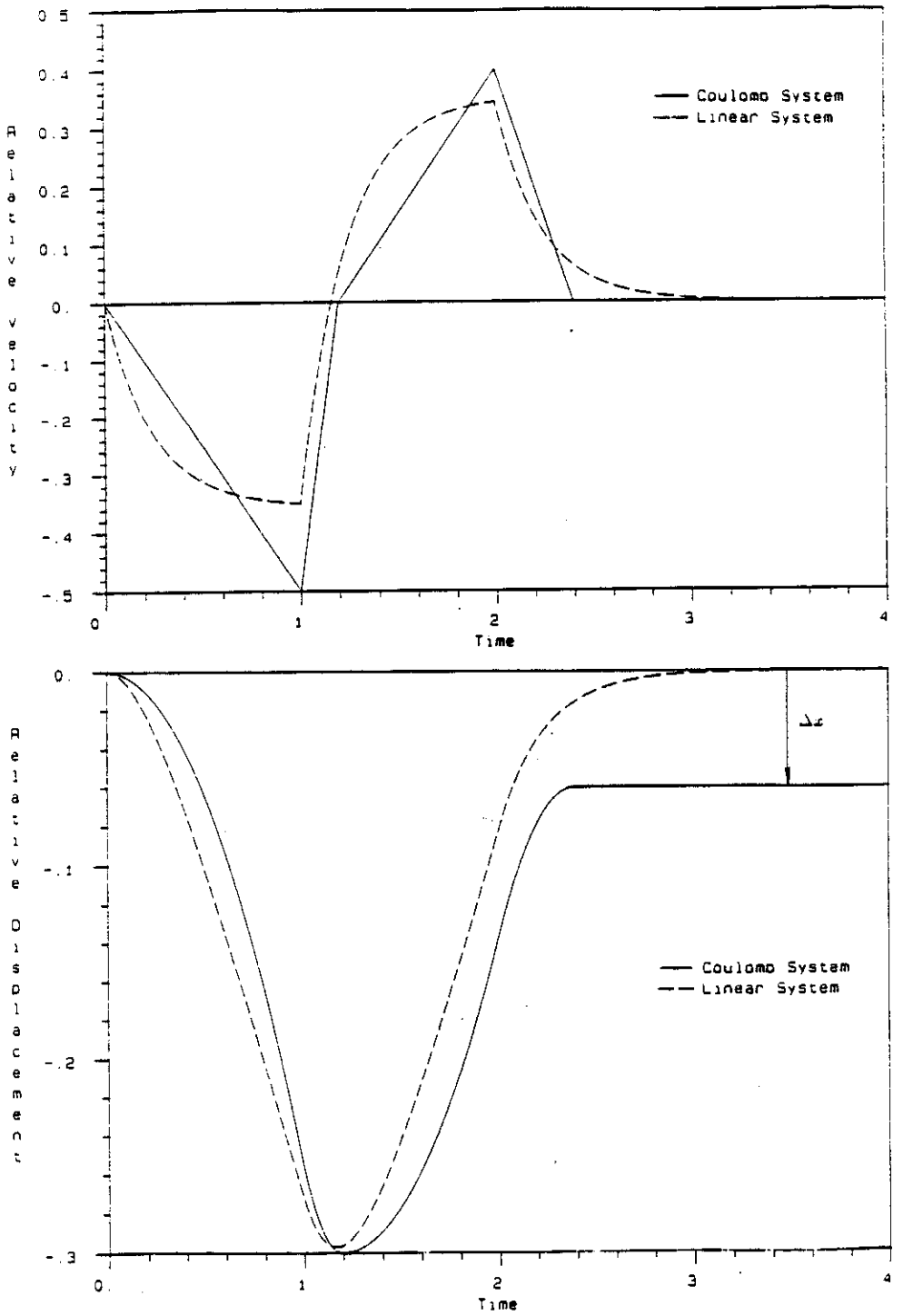

Figure 5.3: Response relative velocity (top) and relative displacement (bottom) for Coulomb and linear systems subjected to single input pulse. Parameter values are $a = 1.0$, $b = 1.5$, $\Delta t = 1.0$, with ζ_{eq} adjusted so that both systems have the same rms velocity. Note that the Coulomb system exhibits a non-zero final offset in the relative displacement, while the linear one does not.

has a final offset, and the Fourier transform of the displacement does not exist. This is analogous to the displacement's not having a stationary spectral density. Since the response to a single symmetric rectangular pulse exhibits many of the features not captured by the equivalent linearization method of the previous chapter, it is used to construct an approximate method where the input is characterized as a sum of pulses. The remainder of this chapter is devoted to developing and using this technique.

5.3 A Poisson Process Approximate Method

In the previous section it was shown that by examining the response to a *single symmetric rectangular pulse* many of the differences between a linear and Coulomb system's response could be examined. A random process with a prescribed power spectrum is generated from a suitably arranged sum of input pulses. This process is used as an input to the Coulomb system, and an approximate method is employed in determining the response statistics of the stick-slip system.

The method used herein is related to that used by J. S. Lin [5] to determine the response of a Coulomb block on an inclined plane. To obtain the mean and variance of the system's drift, Lin used a mean-zero set of rectangular pulses with random amplitude occurring at *evenly* spaced times. Since the angle of the slope was assumed to be moderate, the model considered only sliding in the downhill direction. An empirical fit to simulations was then used to determine relations between the drift and seismic parameters. The Coulomb system in the present study is placed on a flat surface, so the method must account for bidirectional motion. The Poisson process used herein consists of

random amplitude pulses occurring at *random* times, making the relation between time and frequency domain representations of the process more direct than Lin's process. In addition, estimates of the mean and variance are obtained analytically, with simulations being used for determining their accuracy.

Y. K. Lin [22, pp. 87–94] has shown that a rather general class of random processes can be generated using a sum of random amplitude pulses beginning at randomly spaced times. A subclass of these processes can be written in the form

$$n(t) = \sum_{k=1}^{M(t)} b_k w(t - \tau_k), \tag{5.16}$$

where $M(t)$ is a counting process, b_k are identically distributed random variables, and $w(t-\tau_k)$ is a deterministic function describing the pulse shape commencing at a random time τ_k. If the counting process $M(t)$ is a Poisson process with stationary increments and arrival rate λ, then the following hold:

$$E[M(t)] = \lambda t, \tag{5.17}$$

$$E[n(t)] = \lambda E[b] \int_{-\infty}^{\infty} w(u)\, du, \tag{5.18}$$

$$E[n^2(t)] = \lambda E[b^2] \int_{-\infty}^{\infty} w^2(u)\, du, \tag{5.19}$$

$$S_{nn}(\omega) = 2\pi\lambda E[b^2]\, |\hat{w}(\omega)|^2 + (E[n])^2\, \delta(\omega), \tag{5.20}$$

where $S_{nn}(\omega)$ is the spectral density of the process, and $\hat{w}(\omega)$ is the Fourier spectrum of the deterministic pulse shape. Hence, the power spectrum of the overall process is determined from the statistics of the pulse amplitude and the Fourier amplitude spectrum of the deterministic pulse shape. Alternately, from the process spectral density, the deterministic pulse shape can be determined to within a constant. Since the time domain representation of the pulse is

zero for $t < \tau_k$, a Hilbert transform can be used to obtain the missing phase information needed to determine $w(t)$ from $|\hat{w}(\omega)|$. It should be emphasized that all parameters of a pulse process are not uniquely determined by the overall spectral density. This will be important in the final section of this chapter where a pulse process is used to simulate earthquake motions.

An approximate method for finding the response of a nonlinear system to a Poisson process is constructed by assuming that superposition is valid for this problem. The accuracy of this assumption must be verified by independent means; in the case of the Coulomb element, a set of simulations is used to establish the range of parameters for which the method appears to be accurate. The response process is then be made up of a sum of the responses to the individual pulses. Letting $y(t)$ represent any of the response parameters, one obtains from the superposition assumption that

$$y(t) \approx \sum_{k=1}^{M(t)} z(t - \tau_k, b_k), \tag{5.21}$$

where $z(t - \tau_k, b_k)$ is the response to a single pulse $b_k w(t - \tau_k)$. For a nonlinear system the response pulse shape is dependent on the amplitude of the input. Hence, the response process generally cannot be separated into a deterministic shape multiplied by the pulse amplitude.

The mean of the response process is given by

$$E[y(t)] \approx E\left[\sum_{k=1}^{M(t)} z(t - \tau_k, b_k)\right] \tag{5.22}$$

$$= E[M(t)]\, E[z(t, b)], \tag{5.23}$$

where the stationarity of the process and lack of correlation in pulse arrival times have been used to simplify the first expression. The second expectation

operator in the previous equation must be evaluated with respect to both time and pulse amplitude. Thus,

$$E[z(t,b)] = \frac{1}{t}\int_0^t \int_{-\infty}^{\infty} z(t,b)p(b)\,db\,dt, \tag{5.24}$$

where $p(b)$ is the probability density function of pulse amplitudes. Substitution of this expression along with (5.17) into (5.23) yields an approximation for the response process mean

$$\begin{aligned} E[y(t)] &\approx \lambda t \frac{1}{t}\int_0^t \int_{-\infty}^{\infty} z(t,b)p(b)\,db\,dt \\ &= \lambda \int_0^t \left[\int_{-\infty}^{\infty} z(t,b)p(b)\,db\right] dt. \end{aligned} \tag{5.25}$$

To determine the variance of the response variable $y(t)$ a similar procedure results in

$$\begin{aligned} E[y^2(t)] &\approx E\left[\sum_{k=1}^{M(t)}\sum_{j=1}^{M(t)} z(t-\tau_k,b_k)z(t-\tau_j,b_j)\right] \\ &= E\left[\sum_{k=1}^{M(t)} z^2(t-\tau_k,b_k)\right], \end{aligned} \tag{5.26}$$

where the independence of the pulses was used in the last simplification. Stationarity of the pulse process leads to

$$E[y^2(t)] \approx E[M(t)]\,E[z^2(t,b)]. \tag{5.27}$$

Performing expectations over both time and pulse amplitude in the last equation and substitution into (5.17) yield

$$E[y^2(t)] \approx \lambda \int_{-\infty}^{\infty} \left[\int_0^t z^2(t,b)\,dt\right] p(b)\,db. \tag{5.28}$$

In principle it should be possible to determine approximately all moments of the response process by continuing along similar lines of reasoning. These in

turn can be used in a series to determine a characteristic function whose Fourier transform is the approximate probability density function of the response variable. The approximations are valid for both stationary and non-stationary response statistics.

The previous results are now used to obtain estimates of the response of a Coulomb element to a series of symmetric rectangular pulses. The deterministic form of the pulse is given by

$$w(t-\tau_k) = \begin{cases} 1, & \tau_k < t < \tau_k + \Delta t; \\ -1, & \tau_k + \Delta t < t < \tau_k + 2\Delta t; \\ 0, & \text{elsewhere,} \end{cases} \tag{5.29}$$

while the amplitude of the pulses is set by the random variable b_k. For the ensuing discussion, b_k will be taken to be Gaussian with mean zero and standard deviation σ_b, with probability density function

$$p(b) = \frac{1}{\sqrt{2\pi}\,\sigma_b} \exp\left(\frac{b^2}{2\sigma_b^2}\right). \tag{5.30}$$

The approximate velocity response process for a Coulomb element is given by

$$\dot{x}(t) \approx \sum_{k=1}^{M(t)} v(t-\tau_k, b_k), \tag{5.31}$$

where $v(t-\tau_k, b_k)$ is the exact velocity response of a Coulomb element to a single acceleration pulse given by Equation (5.7). The velocity response can be shown to be mean-zero for mean-zero pulse amplitude by substituting (5.31), and (5.7) in (5.25).

To approximately determine the velocity variance, the integral over time of the squared velocity response to a single pulse is needed. It was remarked in Section 5.2 that the maximum duration of a velocity pulse is $4\Delta t$, so for

times larger than this, the integral of the velocity squared will be a constant. Performing this integration gives

$$\int_0^t v^2(t,b)\,dt = \frac{2a^2\,\Delta t^3}{3}\frac{(\beta-1)^2\beta}{(\beta+1)}\left[1+\frac{4}{(\beta+1)^2}\right], \quad t > 4\Delta t, \tag{5.32}$$

where

$$\beta = \frac{|b|}{a}. \tag{5.33}$$

The resulting approximate stationary velocity variance is obtained by using (5.32), and (5.30) in (5.28), to yield

$$\begin{aligned} E[\dot{x}^2(t)] &\approx \lambda\int_{-\infty}^{\infty} p(b)\left[\int_0^t v^2(t,b)dt\right]db, \quad t > 4\Delta t \\ &= \frac{\lambda a^2\,\Delta t^3}{\sigma_B}h(\sigma_B), \end{aligned} \tag{5.34}$$

where

$$h(\sigma_B) = \frac{2}{3}\sqrt{\frac{2}{\pi}}\int_1^{\infty}\frac{(\beta-1)^2\beta}{\beta+1}\left[1+\frac{4}{(\beta+1)^2}\right]\exp\left(\frac{-\beta^2}{2\sigma_B^2}\right)d\beta, \tag{5.35}$$

$$\sigma_B = \frac{\sigma_b}{a}. \tag{5.36}$$

The function $h(\sigma_B)$ can be evaluated numerically using trapezoidal integration. From the expression for $E[\dot{x}^2]$ it can be seen that the velocity will be weakly stationary for $t > 4\Delta t$. This predicted stationary value is compared with simulation results in a later section.

The approximate displacement response is given by the series

$$x(t) \approx \sum_{k=1}^{M(t)} d(t-\tau_k, b_k). \tag{5.37}$$

For times much larger that $4\Delta t$, the values of the integrals of response displacement and displacement squared are dominated by contributions of the

final displacement offset. Thus,

$$\int_0^t d(t,b)\,dt \;\approx\; t\,\Delta x(b), \qquad t \gg 4\Delta t, \tag{5.38}$$

$$\int_0^t d^2(t,b)\,dt \;\approx\; t\,\Delta x^2(b), \qquad t \gg 4\Delta t, \tag{5.39}$$

where Δx is found in Equation (5.8). If the first of these equations is used with (5.8), (5.30) and (5.25), it can be shown that the large time mean will be zero for mean-zero input.

The large time displacement variance is found by substituting (5.39), (5.8) and (5.30) into (5.28), yielding

$$\begin{aligned} E[x^2(t)] \;&\approx\; t\,\lambda \int_{-\infty}^{\infty} p(b)\,\Delta x^2(b)\,db, \qquad t \gg 4\Delta t \\ &=\; t\,\frac{\lambda a^2\,\Delta t^4}{\sigma_B}\,g(\sigma_B), \end{aligned} \tag{5.40}$$

where

$$g(\sigma_B) = \sqrt{\frac{2}{\pi}} \int_1^{\infty} \left[\frac{(\beta-1)\beta}{\beta+1}\left(1-\frac{2}{\beta+1}\right)\right]^2 \exp\left(\frac{-\beta^2}{2\sigma_B^2}\right) d\beta, \tag{5.41}$$

which is evaluated numerically. From the above equation for the displacement variance, it can be seen that this quantity increases linearly for large time. This behavior was exhibited by the simulations in the last chapter, although the random processes used are different. Later in this chapter a comparison will be made between the predicted slope of the displacement variance and the value found through simulations performed using a Poisson pulse process.

Rms values for the absolute ground velocity and displacement are obtained by using a similar procedure. The variance of the absolute excitation velocity is given by

$$E[\dot{x}_g^2(t)] = \lambda \int_{-\infty}^{\infty} p(b) \left[\int_0^t v^2(t,b)dt\right] db, \quad t > 2\Delta t, \tag{5.42}$$

where $\dot{x}_g$ is the ground velocity, and

$$\int_0^t v^2(t,b)\,dt = \frac{2\Delta t^3 b^2}{3}, \quad t > 2\Delta t. \tag{5.43}$$

Substituting (5.43) into (5.42), and performing the integration results in

$$\sigma_{\dot{x}g}^2 \equiv E[\dot{x}^2(t)] = \frac{2\lambda\Delta t^3}{3}\sigma_b^2. \tag{5.44}$$

From (5.19), it can be shown that the variance of the input process is given by

$$\sigma_n^2 = 2\lambda\Delta t\sigma_b^2, \tag{5.45}$$

which, upon substitution into (5.44) yields

$$\sigma_{\dot{x}g} = \frac{\sigma_n\Delta t}{\sqrt{3}}. \tag{5.46}$$

The absolute ground displacement variance is obtained from

$$E[x_g^2] = \lambda t\int_{-\infty}^{\infty} p(b)\Delta x^2(b)\,db, \tag{5.47}$$

where x_g is the absolute ground displacement, and Δx is the absolute displacement of each pulse, given by

$$\Delta x = b\Delta t^2. \tag{5.48}$$

Thus,

$$\sigma_{xg}^2(t) \equiv E[x_g^2(t)] = \frac{\sigma_n^2\Delta t^3}{2}t. \tag{5.49}$$

Consequently, the displacement variance of the input motions grows linearly with time.

The expressions for the rms absolute ground velocity and displacement are exact. These values can be used to determine the accuracy of the approximate Poisson pulse methods by observing the case for which the slip level goes to zero. When the system is frictionless, the absolute measures of the input

should equal the relative response measures, with discrepancies being an indication of error in the approximate method. This comparison is performed in the last section of this chapter, although the approximate method used is a refinement on the previously developed method. The remainder of this section is devoted to improvements on the Poisson pulse method.

The Coulomb element acts as a thresholding system: if the excitation is below the slip level, the system does not move. Individually, a collection of pulses with amplitude standard deviation below the slip level only occasionally causes the system to slip. However, when these pulses are assembled into a Poisson process, overlaps between the pulses will produce additional crossings of the threshold. Based upon this argument, for processes with rms pulse amplitude below the slip level, the accuracy of the approximate method can be improved if the overlaps are considered. Since a model that creates composite pulses out of overlapping pulses can be very complicated, a process is developed to accounts for overlaps in a simple manner.

This method, to be called the "overlap series method," accounts only for overlaps occurring during the first half of the pulse. If the starting times of two or more pulses are within Δt of the starting time of the first pulse, then the starting times are all shifted to correspond to that of the first pulse. The amplitude of the resulting pulse is the sum of the amplitudes of the individual pulses. Any overlaps occurring for times greater than Δt are ignored, and the response is computed with the pulses operating individually. Due to the use of identical, mean-zero, Gaussian distributions for the pulse amplitudes, the standard deviation for the overlapping pulse is given by

$$\sigma_{b(m)} = \sqrt{m+1}\,\sigma_b, \tag{5.50}$$

where m is the number of pulses overlapping the first. The combined pulse is simply treated as an individual pulse with larger variance. The probability of overlaps occurring is determined by the arrival time process. As the interarrival times are independent, Poisson distributed, the probability of exactly m arrivals occurring within an interval t is

$$P(m,t) = \frac{(\lambda t)^m}{m!} e^{-\lambda t}. \tag{5.51}$$

The response to this input process is the sum over the number of overlaps of the response to processes with the overlapping pulse variance, multiplied by the probability of the number of overlaps occurring. This can be stated mathematically as

$$E[y_{ovl}^2(t)] \approx \sum_{m=0}^{\infty} P(m,\Delta t) E[y^2(t,\sigma_{b(m)})], \tag{5.52}$$

with the expectation operation on the right being the response computed earlier in this section. Substitution of (5.50) and (5.51) into the previous equation results in

$$E[y_{ovl}^2(t)] \approx e^{-\lambda\,\Delta t} \sum_{m=0}^{\infty} \frac{(\lambda\,\Delta t)^m}{m!} E[y^2(t), \sqrt{m+1}\,\sigma_b]. \tag{5.53}$$

The velocity variance is found by substituting Equation (5.34) into the previous equation, producing

$$\sigma_{\dot{x}}^2 \approx e^{-\lambda\,\Delta t} \left(\frac{\lambda a^2 \Delta t^3}{\sigma_B}\right) \sum_{m=0}^{\infty} \frac{(\lambda\,\Delta t)^m}{m!\sqrt{m+1}} h(\sqrt{m+1}\,\sigma_B), \tag{5.54}$$

with $h(\cdot)$ computed using Equation (5.35). Likewise, the displacement variance is given by

$$E[x^2(t)] = t\, e^{-\lambda\,\Delta t} \left(\frac{\lambda a^2 \Delta t^4}{\sigma_B}\right) \sum_{m=0}^{\infty} \frac{(\lambda\,\Delta t)^m}{m!\sqrt{m+1}} g(\sqrt{m+1}\,\sigma_B), \tag{5.55}$$

where (5.40) has been replaced in (5.53), and $g(\cdot)$ is found from (5.41).

If the slip level is more than three times the standard deviation of the pulse amplitudes, it is possible to construct a different process accounting for overlaps in both the first and second half of the pulse. As the method is rather involved, and this thesis is primarily concerned with processes having good likelihood of causing motion of the Coulomb element, the details of the method are not carried further.

5.4 Simulation Techniques

The accuracy of the approximate method developed in the previous section is estimated by comparison with a series of simulations. The simulation process consists of two parts: the generation of the pulse input process, and the solution of the equation of motion for the Coulomb element. This section deals chiefly with the former, as the latter was discussed in some detail in the previous chapter.

The first step in the creation of the input process is the determination of the random arrival times of the pulses. The arrival times constitute a Poisson process, so the inter-arrival times are exponentially distributed. Variates with this distribution are generated through the transformation [28, pp. 452–3]

$$T = -\frac{1}{\lambda} \ln R, \tag{5.56}$$

where T is the desired exponential variate, λ is the arrival rate of the process, and R is a uniformly distributed random number on [0,1]. The process begins at an arbitrarily selected starting time, and inter-arrival times are generated until the total duration of the process has reached a desired length. In order to randomize the time of the first pulse, the starting time is set to $-10/\lambda$, with

pulses occurring before zero being ignored. The resulting starting times are a portion of a stationary process for $t > 0$, but the pulse process is not, since pulses starting during $-2\Delta t < t < 0$ are ignored but are required for the overall process to be a portion of a stationary record. However, the system reaches stationarity in velocity more rapidly when excited by this non-stationary process than if the process were stationary. Thus, it is advantageous to use this particular form of an initially non-stationary input process when stationary response statistics are required.

Associated with each pulse arrival time is a Gaussian distributed pulse amplitude. These are generated using the Box-Muller transformation [28, pp. 453–4]

$$N_1 = \sigma_b \left(-2 \ln R_1\right)^{1/2} \cos(2\pi R_2), \tag{5.57}$$

$$N_2 = \sigma_b \left(-2 \ln R_1\right)^{1/2} \sin(2\pi R_2), \tag{5.58}$$

where N_1 and N_2 are independent Gaussian distributed with mean zero, and standard deviation σ_b, and R_1 and R_2 are independent uniformly distributed on [0,1]. Once the arrival times and amplitudes are determined, a table is assembled with these, as well as the times at which the pulses change value, which, in the case of symmetric rectangular pulses, occur at the arrival times plus Δt and $2\Delta t$. Each of the pulses can be produced by summing step-functions, so the next step is to produce a list of step-function amplitudes and starting times from the previous table. These step-functions are then sorted into ascending time order using a hash sort routine. As response statistics must be taken at a consistent set of times for all records in the ensemble, sampling times are added in chronological order to the list as step-functions with zero amplitude. This method avoids having to use a complicated algorithm to extract response

data from the randomly timed response record. Repeated times are eliminated, and an absolute acceleration record is produced by summing the step-function amplitudes.

The acceleration record is then used as an input to the Coulomb element. In Chapter 4, a method was described to exactly solve the stick-slip system's equations of motion under piecewise linear input. The pulse process consists of piecewise constant inputs with varying length, permitting the use of the same algorithm. The system equation is solved to obtain the response velocity and displacement, and values of these at the sampling times are used to obtain response statistics. Ensemble statistics useful for comparisons with the approximate method predictions are the stationary velocity variance and the stationary velocity-displacement covariance, the latter being used to determine the slope of the divergence of the displacement variance through the relation

$$\frac{d}{dt}E[x^2(t)] = 2E[x(t)\dot{x}(t)]. \tag{5.59}$$

Thus, a positive stationary value of $E[x(t)\dot{x}(t)]$ indicates linear increase in the displacement variance. Overall values for the stationary statistics are found by taking timewise averages of the ensemble statistics using data from the central half of the record.

5.5 Comparison of Poisson Pulse Process and Simulation Results

When a dimensional analysis is performed on the Coulomb system with Poisson process excitation, it can be shown that the four natural parameters of the problem $(\lambda, \Delta t, \sigma_b, a)$ can be collected into two dimensionless groups. The

groups chosen for use in this section are $\lambda\,\Delta t$, which can be considered a measure of the pulse spacing, and $\sigma_B = \sigma_b/a$, the ratio of the rms pulse amplitude to the slip level. Simulations are performed using the methods of the previous section and are used to determine the parameter ranges for which the approximate methods are accurate. Ensemble sizes of 1000 are used, with the programs requiring from 3 to 6 hours to complete on a PC-AT. The response statistics used in the comparisons are the rms velocity and the rate of increase of the velocity variance. The two approximate methods checked against simulations are the simple Poisson process, in which overlaps are not taken into account, and the overlap series method. The data for the no-overlap method are obtained from Equations (5.34) and (5.40), while that for the overlap series are from (5.54) and (5.55).

As was mentioned earlier, $\lambda\,\Delta t$ is an indicator of the pulse spacing. For $\lambda\,\Delta t = 0.5$, the pulse duration is equal to the reciprocal of the arrival rate, and a large number of overlaps are likely to occur. Smaller values of $\lambda\,\Delta t$ ensure more time, on the average, between the pulses.

In Figure 5.4 results for the stationary rms velocity and the displacement variance rate are plotted for simulations and for the approximate methods, for the case where the rms amplitude of the acceleration pulses is one third of the slip level. With this low input level, less than 0.3% of the pulses individually exceed the slip level. Thus, overlaps in the pulses may be a large contributor to the response statistics. This is indeed the case, as the two approximate methods disagree by large amounts, with the difference between predictions increasing as $\lambda\,\Delta t$ increases. The overlap series method does a very good job of predicting the stationary rms velocity, but its predictions for the displacement

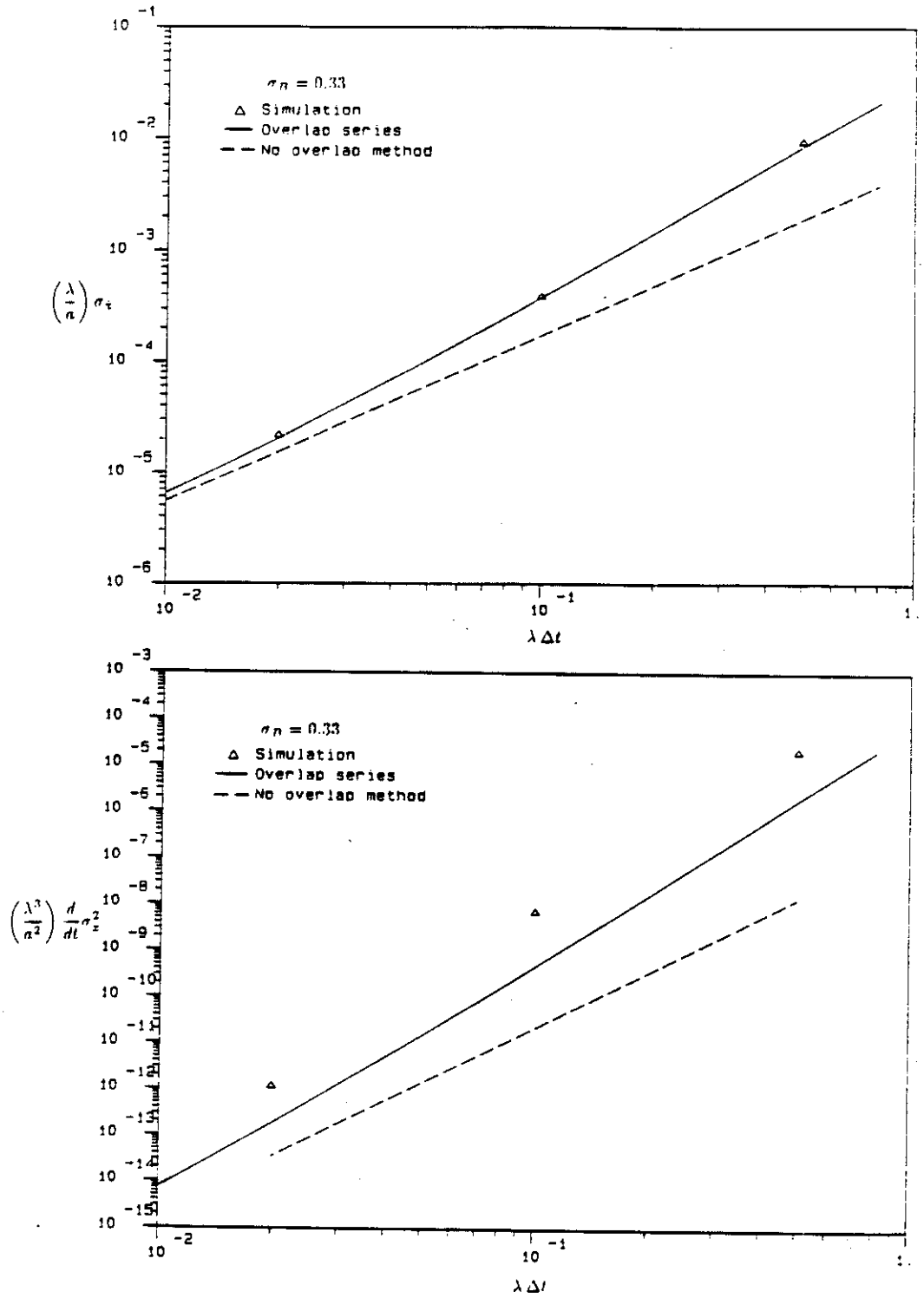

Figure 5.4: Comparison of simulation results with approximate method predictions of stationary rms velocity (top) and rate of increase of displacement variance (bottom). The ratio of rms acceleration pulse amplitude to slip level is 1:3, and the ensemble size is 1000.

variance rate are off by an order of magnitude. Although these errors are large in relative terms, use of parameter values realistic for earthquakes indicate that both the predicted and actual displacements are small in absolute terms. The no-overlap method is half of the simulation result for rms velocity when $\lambda\,\Delta t$ small, with the error increasing to almost an order of magnitude for large $\lambda\,\Delta t$. In displacement rate, the no-overlap method is in error by one to two orders of magnitude.

As σ_B, the ratio of rms pulse amplitude to slip level, is increased, more of the pulses individually exceed the slip level, so the effect of overlaps diminishes. Figure 5.5 exhibits a comparison of simulations with approximate methods for $\sigma_B = 1.0$. Both approximate methods do a reasonable job of predicting rms velocity, with the maximum error for the overlap series method being on the order of 10%, while the no-overlap method is in error by up to 30%. The displacement variance rate error is on the order of 50% for the overlap series, while the no-overlap method is off by up to an order of magnitude for large $\lambda\,\Delta t$.

At $\sigma_B = 5.0$, the majority of the pulses individually exceed the slip level, and overlaps have a negligible effect. The simulation points and approximate method curves are plotted in Figure 5.6, and it is seen that errors in both methods in both velocity and displacement are below 20% over the range tested.

As can be seen by this comparison, the overlap series method is superior in accuracy to the no-overlap method. The penalty in computational time and programming effort is slight, as the expressions evaluated are easily implemented numerically. The overlap method appears to be an accurate pre-

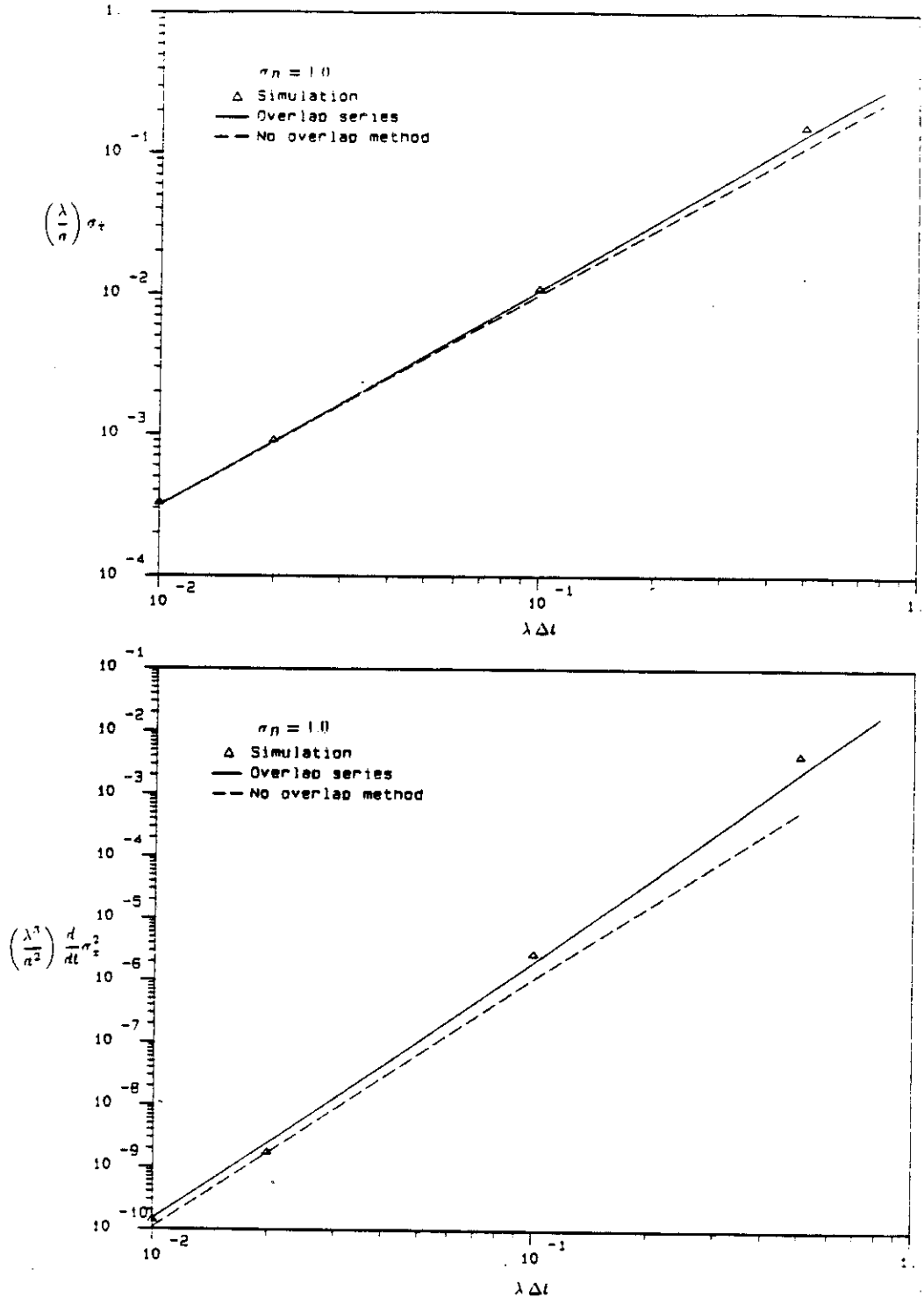

Figure 5.5: Comparison of simulation results with approximate method predictions of stationary rms velocity (top) and rate of increase of displacement variance (bottom). The ratio of rms acceleration pulse amplitude to slip level is 1:1, and the ensemble size is 1000.

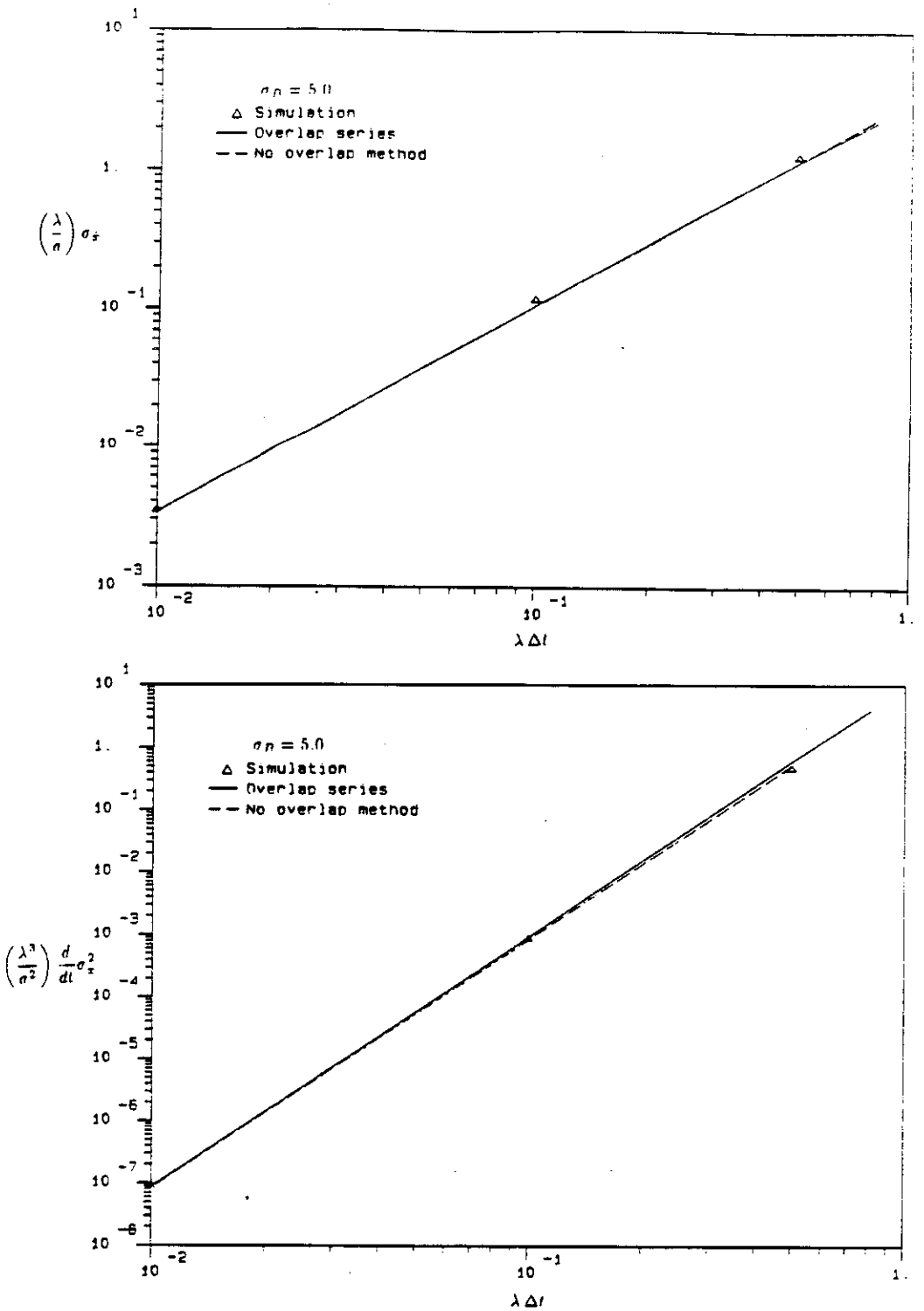

Figure 5.6: Comparison of simulation results with approximate method predictions of stationary rms velocity (top) and rate of increase of displacement variance (bottom). The ratio of rms acceleration pulse amplitude to slip level is 5:1, and the ensemble size is 1000.

dictor of rms displacement for $\lambda\,\Delta t$ below 1.0. The displacement variance rate is within 50% for $\sigma_B \geq 1/3$ and for $\lambda\,\Delta t < 1.0$.

In the next section, values are assigned to the input parameters to correspond to the motions expected during earthquakes. The overlap series method is then used to predict final rms displacements for these seismic motions as a function of the Coulomb system coefficient of friction.

5.6 Response of Stick-Slip System to Earthquake-Like Motions

The motion of the Coulomb system under seismic excitation is studied by means of the overlap series method. The study is comprised of two parts. First, the parameters of the model must be chosen so that a reasonable emulation of earthquake motions is performed. The second step is to use these parameters in the overlap series method to predict the displacement variance rate. This rate, along with the duration of the strong shaking, is useful for predicting a displacement rms value at the end of the earthquake. The section closes with a discussion of factors not considered in the model that could affect the system response.

Before using the Poisson pulse methods to model earthquakes, a check must be performed to determine whether the acceleration pulse process is a suitable representation of the strong motion portion of a seismic event. The first aspect to be examined is the ability of the process to replicate the spectrum of an earthquake. Although there is no consensus on the part of seismologists and earthquake engineers on an equation for the acceleration spectrum, a number of proposed models [29,30,31] characterize the far-field spectrum as increasing

with the square of frequency for low frequency, and decaying as the inverse of frequency squared or higher power for high frequency. The low frequency behavior of these models is a consequence of the assumption that the earthquake can be modeled as a release of energy by a series of double couples arranged along a dislocation surface. The near-field spectrum for such an arrangement increases linearly with frequency for low frequency, while decaying as ω^{-2} or faster for large ω.

Since the strongest seismic motions are generally experienced in locations in the near field of an earthquake, the most useful spectrum for predicting ground motions likely to cause system sliding is the near-field one. In Section 5.2 it was remarked that the form of the acceleration spectrum for a model consisting of a set of Poisson distributed pulses is given by a constant times the spectrum of a single pulse. A symmetric pulse of the form given in Equation (5.3) increases at the proper rate to model the near-field spectrum, but the high frequency fall-off rate is not as high as that required by the near-field model. This deficiency is not serious when the model is used as an input to the stick-slip system, since, as was shown in Chapter 4, this system is most sensitive to the low frequency content of the excitation. Thus, the pulse has much of the spectral character of the near-field accelerations, and a process consisting of symmetric pulses with a deterministic shape given by (5.29) should constitute a reasonable approximation to an earthquake when used as input to a Coulomb element.

The three parameters that determine a given pulse process are $\lambda, \Delta t$, and σ_b, if the pulse amplitude distribution is taken to be mean-zero, Gaussian. The value for Δt can be determined from the center frequency of the seismic

spectrum, and the relation between these is given by

$$\Delta t = \frac{\pi}{\omega_c}, \tag{5.60}$$

where ω_c is the center frequency in radians per second. The value for this center frequency may not be immediately apparent from the spectrum of a given earthquake, but may be determined by performing a curve-fitting using a spectrum of the form (5.6) with undetermined coefficients. A similar procedure has been used by Lai [32] in determining the coefficients for a Kanai-Tajimi spectrum for an ensemble of earthquake records.

Another parameter that has been used to characterize various earthquakes is the rms acceleration for the strong motion [33,32]. Substitution of (5.29) into (5.19) results in the variance of the pulse process being given by

$$E[n^2] = 2\lambda\,\Delta t\,\sigma_i^2. \tag{5.61}$$

One way to specify this rms value is, using Parseval's relation, to use the area beneath the earthquake spectral density. The previous two relations are the only constraints on the pulse process obtained from the earthquake spectrum. Consequently, the three process parameters cannot be uniquely determined from the spectrum.

A third constraint that can be applied to the variables is determined from the nature of the strong motion. As was mentioned in the preceding section, the group $\lambda\,\Delta t$ determines the spacing of the pulses. During an earthquake, the excitation has no gaps, so $\lambda\,\Delta t$ should be chosen to produce closely spaced pulses. However, if $\lambda\,\Delta t$ is very large, the approximate method loses accuracy. A compromise between these two requirements is obtained by letting $\lambda\,\Delta t = 0.5$, for which it has been shown that the overlap series method is

Size	Dist.†	σ_n (cm/s^2)	$2\pi\omega_c$ (Hz.)	t_d (s)	σ_b (cm/s^2)	λ (s^{-1})	Δt (s)	$\sigma_{\dot{x}g}$ (cm/s)	$\sigma_{xg}(t_d)$ (cm)
Great	VNF	250	3	60	250	3	1/6	24	93
Great	NF	100	2.5	60	100	2.5	1/5	12	49
Mod.	VNF	200	4	15	200	4	1/8	14	24
Mod.	NF	50	3	15	50	3	1/6	4.8	9.3

† VNF: Very-Near-Field (0–20 km)
NF: Near-Field (20–50 km)

Table 5.1: Event parameters used in study of response of stick-slip systems to seismic excitation. The values of the rms absolute ground velocity $\sigma_{\dot{x}g}$ and final displacement $\sigma_{xg}(t_d)$ are computed from the other input parameters using Equations (5.46) and (5.49), respectively.

reasonably accurate for $\sigma_B \geq 1/3$. Another benefit of using this value of $\lambda\,\Delta t$ is that the peak acceleration is usually between 3 and 4 times the rms value, agreeing with the general behavior of an earthquake.

A number of studies have been performed [32,33,34] attempting to correlate parameters such as center frequency, rms acceleration, and strong motion duration to earthquake features such as epicentral distance, distance to fault rupture, local magnitude, peak ground acceleration, and soil conditions. These investigations point out trends, but the correlations exhibit much scatter, diminishing the predictive value of the regression equations. Instead of using these models to determine a general response equation, four sets of parameters with values consistent with certain types of seismic records are proposed. These parameter sets are listed in Table 5.1 along with the Poisson process parameters they induce. Although near-field records do not exist for a "great" earthquake,

the values used in this study are consistent with the expected motions for this size event.

The response statistic of greatest importance for design purposes is the maximum expected displacement. Although the overlap process method cannot predict this value, it can be used to obtain an estimate for the rms displacement at the end of the record, from which other methods can be used to estimate a maximum response. The non-stationarity present in earthquake records is incorporated into the Poisson process model by initiating the process at zero time, and stopping it at t_d, the record duration. The rms final displacement is $(E[x^2(t_d)])^{1/2}$, where Equation (5.55) is used to obtain the overlap series estimate for the displacement variance. This resulting rms displacement determined by substituting parameters from Table 5.1 into this equation are displayed as a function of coefficient of friction in Figure 5.7. The salient features of Figure 5.7 are now discussed. The great earthquake, very-near-field model predicts an rms ground displacement close to one meter, which is not unreasonable if one considers that fault offsets during this size events are on the order of several meters. This is in good agreement with the value shown in the Figure 5.7 for the coefficient of friction approaching zero. The same agreement is true for the great earthquake, near-field case, although the final displacements are on the order of half a meter. For the moderate earthquake, the overlap series method overestimates the absolute ground displacement by about 50% for both the near- and very-near-field models. For increasing coefficients of friction, all curves decrease monotonically, but at different rates. It can be seen that the great earthquake produces large displacements over a much larger range of coefficients of friction than the moderate event does.

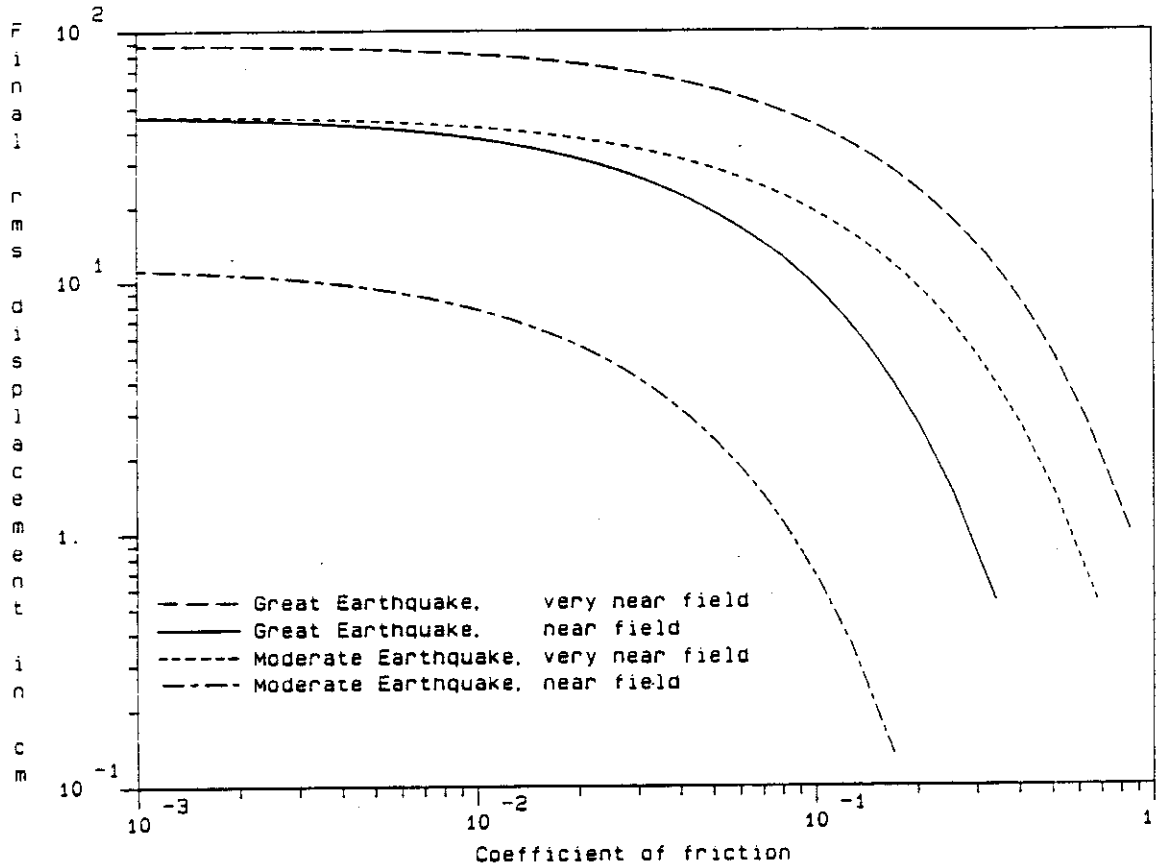

Figure 5.7: Final rms displacement as a function of Coulomb element coefficient of friction using the overlap series method. The parameters used in the model are found in Table 5.1.

The range where σ_B is small and the errors in the overlap series method become large relative to the simulation results is at high coefficients of friction, where the rms displacements are below 1 cm. In this range, the maximum error in displacement rate is about an order of magnitude, producing a factor of three error in rms displacement. As the predicted displacements are small, the absolute error should not be of much concern.

Measurements performed on computer equipment mounted on pads or boots on a smooth floor indicate that coefficients of static friction for this type of systems range from 0.3 to 0.7 [35]. The kinematic coefficient, the one used in determining a Coulomb friction model, is generally between one-half and one-third of the static one, possibly even lower if the surfaces are very clean. Thus, the coefficient of friction for a Coulomb model of computer equipment on a smooth floor is probably in the 0.1 to 0.3 range. For these values, the very-near-field response to a moderate earthquake is in the tens of centimeters, which is generally consistent with the observed behavior for such systems. However, there have been some reports of post-seismic drift on the order of a meter. The remainder of this section is devoted to a qualitative discussion of characteristics of real systems that may affect the scale of the motion, causing it to deviate from the estimates given herein.

If the equipment is mounted inside a building, the structure behaves as a filter by amplifying the motions at certain frequencies. The effect seen by the Coulomb element is an increase in both the rms acceleration and the duration of the strong shaking, both of which increase the displacement response. In addition, if the structure is large, the center frequency of the process may be lowered, producing larger displacement offset rates. However, the reduction in

bandwidth of the spectrum may reduce the displacement offset expected for a given rms input.

A true earthquake is not simply a one-dimensional process, but a three-dimensional random process. The vertical acceleration produces a variation in the normal force, causing the slip level to increase and decrease randomly. The effective slip force is most likely below the value for one-dimensional excitation, producing larger displacements than those predicted by the model. Since the friction force acts vectorially, the horizontal slip level in a particular direction for a horizontal two-dimensional excitation is given by

$$f(t) = -\mu g \cos\theta(t), \tag{5.62}$$

where $f(t)$ is the desired slip level, and $\theta(t)$ is the instantaneous angle between the axis of interest and the applied force. Since $|\cos\theta(t)| \leq 1$, the perceived slip force for two-dimensional motion is on the average lower than that for one-dimensional motion. Consequently, if horizontal excitation were to be added in a direction orthogonal to the already considered one-dimensional process, the resulting relative displacements would most likely increase in the direction of interest.

In freestanding equipment, the center of gravity is sometimes high when compared to the length of the system's base. Consequently, the equipment may rock and "walk" during an earthquake. This type of motion can contribute to large displacements for high coefficient of friction and low width-to-height ratio systems.

Another possible source of error in the predicted motion is the assumption that the pulse amplitudes are mean-zero. It may be entirely possible that for a given earthquake and site, the first portion of the pulses would be more

likely to be of one sign than another. The overall process would still be mean-zero because the pulses are symmetric, but the Coulomb element would undergo a non-zero mean response, increasing the estimated displacement. A related but different problem is that of a system resting on an inclined plane. In this case, the Coulomb force is not symmetric, and the system response again has a non-zero mean.

As can be seen, a one-dimensional model that accounts for friction in a simple manner does not account for all effects present in real freestanding objects. A complete understanding of the motion of these systems would require an investigation of these conditions. Nonetheless, the Poisson process models are valuable tools in obtaining order of magnitude estimates for permanent offsets from sliding during earthquakes.

Although this Poisson process technique has not been applied to the caster-mounted system, it is possible to speculate on the outcome based upon results in Chapters 2 and 3. In these chapters it is shown that for both harmonic and white noise excitation, upper and lower bounds for the caster response are determined by the frictionless and Coulomb system, respectively. If the same holds true for this excitation, then the results in Figure 5.7 can be used to bound the caster system response.

Chapter 6

Summary and Conclusions

In this thesis the response of frictional systems with both constant and displacement-dependent force has been examined for deterministic and random excitation. The response to harmonic excitation is examined in Chapter 2. When the method of slowly varying parameters is used, it is observed that the Coulomb, or constant force, system is a lower bound to the caster-mounted system response; the latter system's frictional force is displacement dependent. An upper bound is given by the displacement amplitude of the input motion. All solutions for the response amplitude of the Coulomb system as a function of frequency are stable. The caster-mounted system exhibits unstable regions of response, but only for small input amplitudes.

The use of centering devices has been proposed previously for reducing the drift of frictional systems. It is shown in the second chapter that the centering mechanism shifts the peak response frequency for both the Coulomb and caster-mounted systems. The response amplitude is shown to increase for many input frequencies, the opposite effect from that sought. Another drawback to the use of centering devices is that the response is no longer bounded from above by the ground displacement. Thus, it is more difficult to predict the peak steady-state response amplitude.

The third chapter is devoted to the examination of the response of the caster system to white noise excitation. By means of the equivalent linearization method, it is shown that the response is characterized by two limiting behaviors. The lower limit is the Coulomb system, which achieves steady-state in both the velocity variance, and the velocity-displacement covariance, but remains non-stationary in displacement. From above, the response is bounded by the absolute input motion, which diverges in both velocity and displacement. The nature of the caster response is shown to change from the lower to the upper bound behaviors, with the transition time being a clearly defined function of the system and excitation parameters.

Spectra more representative of earthquakes are obtained by filtering white noise. Chapter 4 contains an equivalent linearization study of the response of the Coulomb system to band-pass filtered excitation. The results are compared with simulations, and it is shown that velocity is accurately predicted in most cases, but the displacement trends are erroneous when the input contains no zero frequency spectral content. An explanation is found in the velocity spectrum of the response, where it is seen that the linear system response is limited to the band of input frequencies, while the nonlinear Coulomb system response extends outside this band, reaching all the way to zero frequency. This zero frequency response then causes the displacement variance to increase linearly with time. It appears that no linearization method is capable of capturing this behavior.

In Chapter 5, an approximate method able to represent this response is developed. When the input is described in terms of a Poisson process, the method computes the overall response as a superposition of responses to in-

dividual pulses. If overlapping in the input pulses is considered, the method agrees closely with simulation results. Estimates for final rms displacements as a function of coefficient of friction are computed by using parameters representative of certain seismic events. Although no precise estimates for the caster system are computed with the method, lower and upper bounds may be found in the Coulomb system response and the absolute ground motion, respectively.

References

[1] Caughey, T. K. and Dienes, J. K., "Analysis of a Nonlinear First-Order System with a White Noise Input," *Journal of Applied Physics*, vol. 32, pp. 2476–2479, Nov. 1961.

[2] Crandall, S. H., Lee, S. S., and Williams, Jr., J. H., "Accumulated Slip of a Friction-Controlled Mass Excited by Earthquake Motions," *Journal of Applied Mechanics*, pp. 1094–1098, Dec. 1974.

[3] Ahmadi, G., "Stochastic Earthquake Response of Structures on Sliding Foundation," *International Journal of Engineering Science*, vol. 21, no. 2, pp. 93–102, 1983.

[4] Constantinou, M. C. and Tadjbakhsh, I. G., "Response of a Sliding Structure to Filtered Random Excitation," *Journal of Structural Mechaincs*, vol. 12, no. 3, pp. 401–418, 1984.

[5] Lin, J. S., *Probabilistic Evaluation of the Seismically-Induced Permanent Displacements in Earth Dams.* Ph. D. thesis, Massachusetts Institute of Technology, Feb. 1982.

[6] Bergman, L. A. and Spencer, Jr., B. F., "First Passage of a Sliding Rigid Structure on a Frictional Foundation," *Earthquake Engineering and Structural Dynamics*, vol. 13, pp. 281–291, 1985.

[7] Kanai, K., "Semi-Empirical Formula for the Seismic Characteristics of the Ground," *Bulletin of the Seismological Society of America*, vol. 35, 1957.

[8] Tajimi, H., "A Statistical Method of Determining the Maximum Response of a Building Structure During an Earthquake," in *Proceedings of the 2nd World Conference on Earthquake Engineering, Vol. 11*, 1960.

[9] Nayfeh, A. H., *Perturbation Methods.* John Wiley, 1973.

[10] Minorski, N., *Nonlinear Oscillations.* D. VanNostrand Co., Inc., 1962.

[11] "Dynamic Testing of Caster Cups—Phase II," May 1984. Tridis Engineers, San Marino, CA, Report No. SP124.

[12] Asano, K. and Iwan, W. D., "An Alternative Approach to the Random Response of Bilinear Hysteretic Systems," *Earthquake Engineering and Structural Dynamics*, vol. 12, pp. 229–236, 1984.

[13] Iwan, W. D., "A Distributed-Element Model for Hysteresis and Its Steady-State Dynamic Response," *Journal of Applied Mechanics*, vol. 33, no. 4, pp. 893–900, 1966.

[14] Cifuentes, A. O., *System Identification of Hysteretic Structures.* Ph. D. thesis, California Institute of Technology, Sept. 1984.

[15] Iwan, W. D. and Mason, Jr., A. B., "Equivalent Linearization for Systems Subjected to Non-Stationary Random Excitation," *International Journal of Non-Linear Mechanics*, vol. 15, pp. 71–82, 1980.

[16] Caughey, T. K., "Response of Nonlinear Systems to Random Excitation," 1953. Lecture Note, California Institute of Technology, 1954.

[17] Booten, R. C., "The Analysis of Nonlinear Control Systems with Random Inputs," in *Proceedings of the Symposium of Non-linear Circuit Analysis*, Polytechinc Inst. Brooklyn, New York, 1953. Vol. 2.

[18] Iwan, W. D. and Patula, E. J., "The Merit of Different Error Minimization Criteria in Approximate Analysis," *Journal of Applied Mechanics*, pp. 257–262, Mar. 1972.

[19] Atalik, T. S. and Utku, S., "Stochastic Linearization of Multi-Degree-of-Freedom Non-linear Systems," *Earthquake Engineering and Structural Dynamics*, vol. 4, pp. 411–420, 1976.

[20] Newmark, N. M., "Effects of Earthquakes on Dams and Embankments," *Géotechnique*, vol. 15, pp. 139–160, 1965.

[21] Constantinou, M. C., Gazetas, G., and Tadjbakhsh, I., "Stochastic Seismic Sliding of Rigid Mass Supported Through Non-Symmetric Friction," *Earthquake Engineering and Structural Dynamics*, vol. 12, pp. 777–793, 1984.

[22] Lin, Y. K., *Probabilistic Theory of Structural Dynamics.* McGraw-Hill, Inc., New York, 1967.

[23] Bendat, J. S., *Engineering Applications of Correlation and Spectral Analysis.* John Wiley and Sons, New York, 1980.

[24] Shinozuka, M. and Jan, C. M., "Digital Simulation of Random Processes and Its Applications," *Journal of Sound and Vibration*, vol. 25, no. 1, pp. 111–128, 1972.

[25] Yang, J. N., "On the Normality and Accuracy of Simulated Random Processes," *Journal of Sound and Vibration*, vol. 26, no. 3, pp. 417–428, 1973.

[26] Hall, J. F., "An FFT Algorithm for Structural Dynamics," *Earthquake Engineering and Structural Dynamics*, vol. 10, pp. 797–811, 1982.

[27] Caughey, T. K., "Advanced Dynamics," 1984. Lecture Notes, California Institute of Technology.

[28] Dahlquist, G., Björk, Å., and Anderson, N., *Numerical Methods*. Prentice-Hall, Inc., Englewood Cliffs, NJ, 1974.

[29] Boore, D. M., "Stochastic Simulation of High-Frequency Ground Motions Based on Seismological Models of the Radiated Spectra," *Bulletin of the Seismological Society of America*, vol. 73, pp. 1865–1894, Dec. 1983.

[30] Brune, J. N., "Tectonic Stress and the Spectra of Seismic Shear Waves from Earthquakes," *Journal of Geophysical Research*, vol. 75, pp. 4997–5002, Sept. 1970.

[31] Luco, J. E., "On Strong Ground Motion Estimates Based on Models of the Radiated Spectra," *Bulletin of the Seismological Society of America*, vol. 75, pp. 641–649, June 1985.

[32] Lai, S. P., "Statistical Characterization of Strong Ground Motions Using Power Spectral Density Function," *Bulletin of the Seismological Society of America*, vol. 72, pp. 259–274, Feb. 1982.

[33] McCann, Jr., M. W., "Rms Acceleration and Duration of Strong Ground Motion," Tech. Rep. 46, J. A. Blume Earthquake Engineering Center, Stanford University, Oct. 1980.

[34] Vanmarke, E. H. and Lai, S. P., "Strong Motion Duration of Earthquakes," Tech. Rep. R77–16, MIT Department of Civil Engineering, July 1977.

[35] Gates, W. E. and Scawthorn, C., "Mitigation of Earthquake Effects on Data Processing Equipment," ASCE Conference, 1982. Las Vegas, Nevada, Preprint No. 82-056.

Appendix A

Equations of Motion for a Caster

A caster is a pivoting wheel on which mobile objects such as data-processing and hospital equipment are routinely mounted. In this appendix, the force-displacement relation is found for the rectilinear motion of a caster. The first part of the derivation consists of finding the resisting force as a function of the caster's angle. Next, a kinematic relation is found relating the linear position with the angle of the caster. This kinematic relation is then used with the resisting force relation to determine a force-displacement relation for motion along a straight line.

A number of assumptions are made in deriving the equations of motion, and some are discussed below. The caster is assumed massless, as its mass generally is much smaller than that of the equipment it supports. Consequently, the equations of motion can be derived quasistatically. The only energy loss mechanism is frictional due to slipping of the caster on the floor as it pivots. Losses due to rolling and bearing friction are ignored. The wheel and the ground on which it rests are assumed rigid, and the load is assumed to be uniformly distributed along the line of contact between the wheel and the ground. The resisting force is the sum of the frictional forces on the infinitesimal elements that constitute the line of contact. Each one of the contact line elements applies

a force in the direction opposing its relative velocity, with magnitude equal to the coefficient of friction multiplied by the load per unit length of contact.

A.1 Resisting Force as a Function of Angle

The configuration of the caster used in the ensuing discussion can be seen in Figure A.1. The caster is oriented at an angle θ from the x-axis. The coordinate system used for the caster consists of an axis s along the direction in which the caster rolls freely and an axis n normal to this axis. All coordinate systems have origins at the point O, the center about which the caster pivots. The horizontal distance between O and the wheel axis is ℓ, and the wheel axis lies directly above the line of contact. The point A is at the center of the line of contact, and B is a general point along the line of contact, both points being on the wheel. The wheel has radius r and width w.

The components of the velocity of B in terms of the velocity of A and the caster rotation rate $\dot{\theta}$ are

$$v_{Bs} = v_{As} - n\dot{\theta}, \tag{A.1}$$

$$v_{Bn} = v_{An}. \tag{A.2}$$

The components of the frictional force along the line of contact are given by

$$f_{Bn} = -\frac{\mu N}{w}\frac{v_{Bn}}{|v_B|}, \tag{A.3}$$

$$f_{Bs} = -\frac{\mu N}{w}\frac{v_{Bs}}{|v_B|}, \tag{A.4}$$

where

$$|v_B| = \sqrt{v_{Bn}^2 + v_{Bs}^2}, \tag{A.5}$$

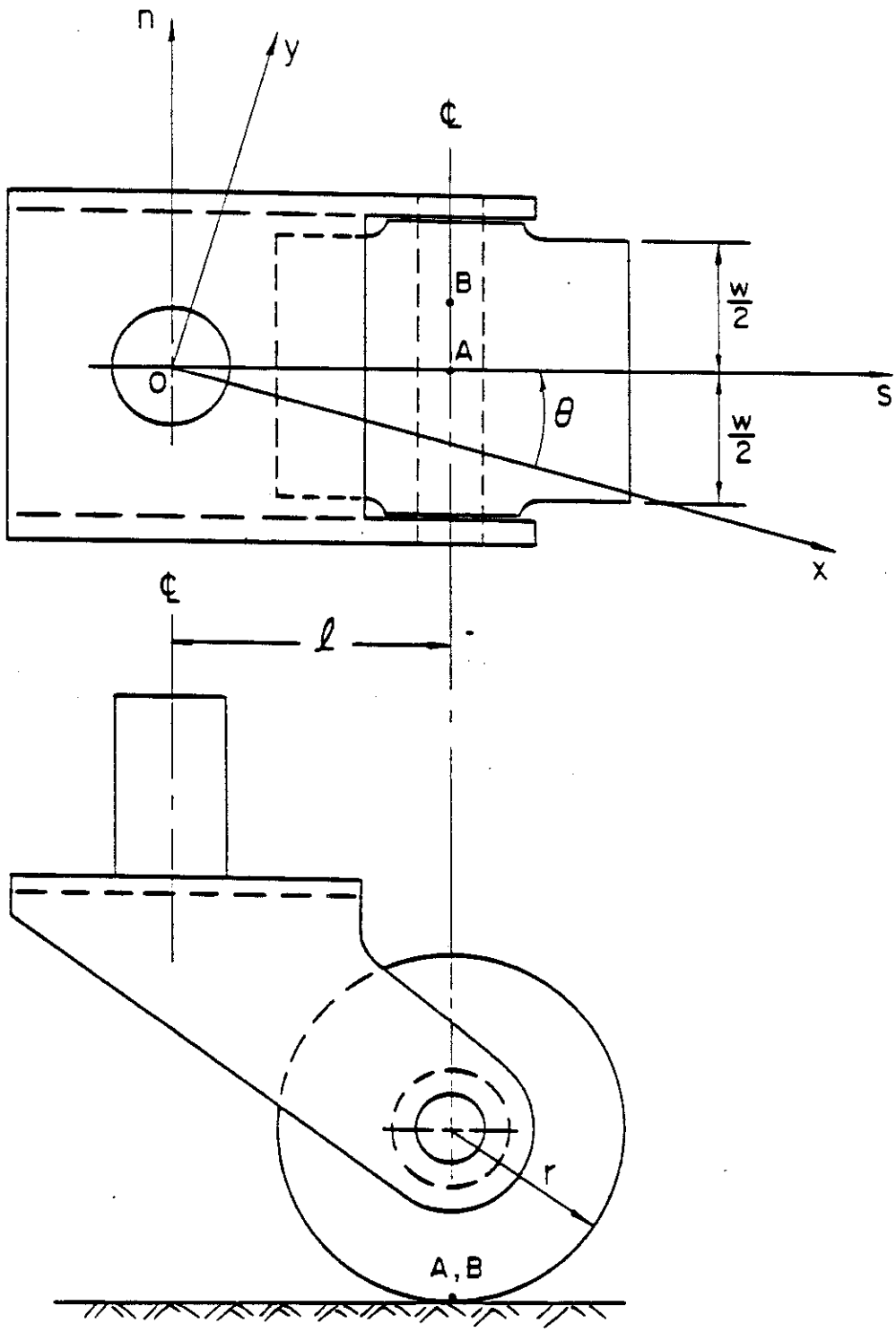

Figure A.1: Caster configuration used in the equations of motion.

and μ is the coefficient of friction, N is the load on the caster, and w is the wheel width.

Due to the assumption of no rolling friction and no energy losses in the wheel bearings, the net force in the s, or rolling, direction is zero. Thus,

$$F_s = \int_{-w/2}^{w/2} f_{Bs}\, dn = 0. \tag{A.6}$$

The force in the n direction, which is not yet known, is given by

$$F_n = \int_{-w/2}^{w/2} f_{Bn}\, dn. \tag{A.7}$$

The goal in this section is to determine this force F_n. The net moment at the thrust bearing at O is zero, leading to the expression

$$M_O = F_n \ell - \int_{-w/2}^{w/2} f_{Bs} n\, dn = 0. \tag{A.8}$$

Substitution of Equations (A.4) and (A.1) into (A.6), integration, and manipulation, leads to the condition

$$v_{As} = 0. \tag{A.9}$$

Thus, the relative velocity of the wheel midline in the rolling direction is zero. Replacement of (A.3) and (A.2) in (A.7) and integration results in

$$F_n = -\frac{\mu N \beta}{2} \ln\left[\frac{\sqrt{1+\beta^2}+1}{\sqrt{1+\beta^2}-1}\right], \tag{A.10}$$

where

$$\beta = \pm\frac{2v_{An}}{w\dot{\theta}}. \tag{A.11}$$

Integration of (A.8) and substitution of the expression for F_n given above results in the condition

$$\frac{\mu N}{2}\left(\frac{w\beta^2}{4} - \beta\ell\right) \ln\left[\frac{\sqrt{1+\beta^2}+1}{\sqrt{1+\beta^2}-1}\right] = 0. \tag{A.12}$$

Since the expression in brackets never equals one, the only solution to the above equation is

$$\beta = \frac{4\ell}{w}, \tag{A.13}$$

which leads to

$$v_{An} = \pm 2\ell\dot{\theta}. \tag{A.14}$$

Substitution of (A.13) into the expression for F_n given by (A.10) yields an expression for the normalized lateral force

$$\frac{F_n}{\mu N} = s\left(\frac{\ell}{w}\right), \tag{A.15}$$

with

$$s(\gamma) = 2\gamma \ln\left[\frac{\sqrt{1+(4\gamma)^2}+1}{\sqrt{1+(4\gamma)^2}-1}\right]. \tag{A.16}$$

Thus, the normalized lateral force is only a function of ℓ/w, the ratio of caster pivot radius to wheel width.

The relationship between lateral force and caster geometry given by Equation (A.15) is plotted in Figure A.2. It is seen in the figure that for $\ell/w < 0.1$, the lateral force F_n is a small fraction of the total available frictional force μN. For $\ell/w > 0.3$, the lateral force is over 90% of the available frictional force. Casters used for mounting data-processing equipment typically have ℓ/w between 0.5 and 2, so the lateral force is almost equal to the available frictional force μN in these applications.

A.2 Kinematics of the Caster Motion

Since the caster-mounted equipment is herein assumed to move in a straight line, only the one-dimensional kinematics is derived in this section. If the caster

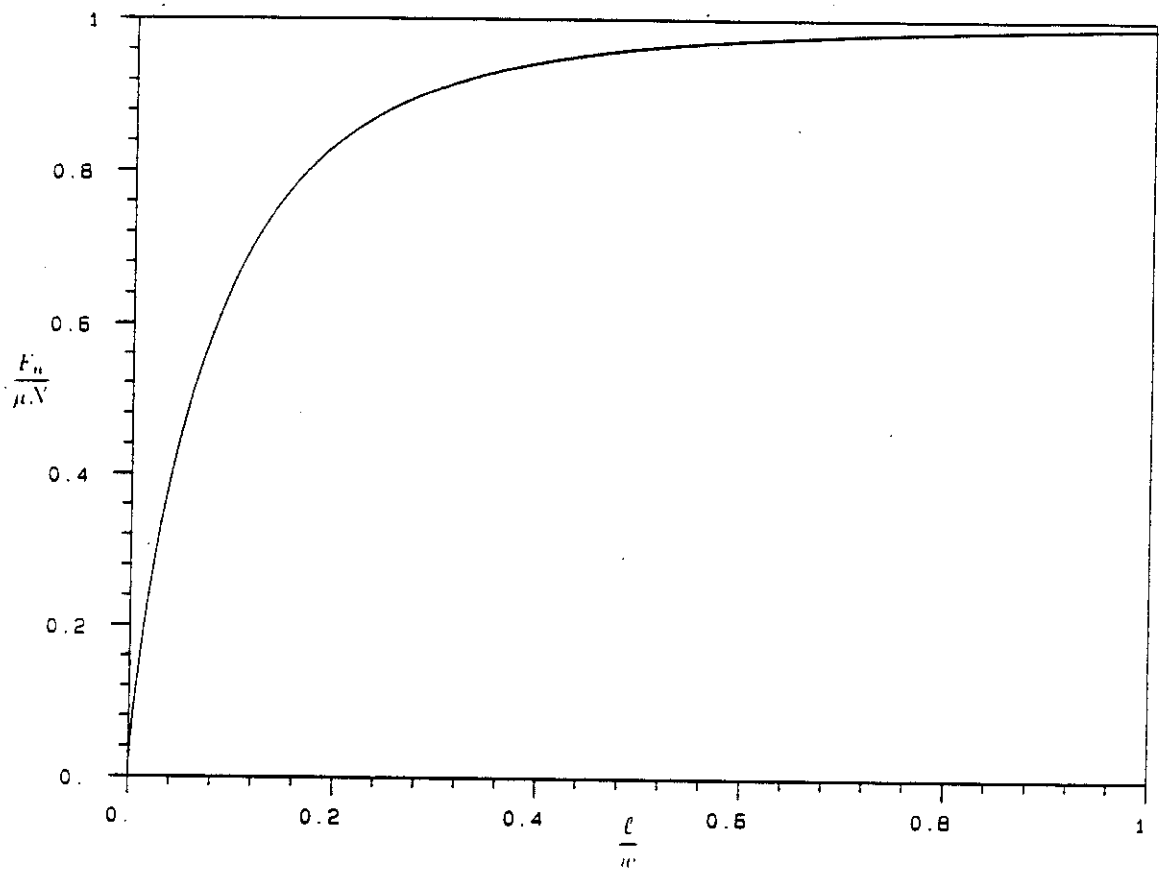

Figure A.2: Normalized lateral caster force as a function of caster geometry

support point O is displaces along the x-axis with velocity $\dot{x}$, then the lateral velocity of the point A on the wheel is given by

$$v_{An} = -\dot{x}\sin\theta + \ell\dot{\theta}. \tag{A.17}$$

In the previous section, it was shown that the condition for zero moment at O led to

$$v_{An} = \pm 2\ell\dot{\theta}. \tag{A.18}$$

Manipulation of the previous expressions for v_{An} yields the two equations

$$\dot{\theta} = -\frac{\dot{x}}{\ell}\sin\theta, \tag{A.19}$$

$$\dot{\theta} = \frac{\dot{x}}{3\ell}\sin\theta. \tag{A.20}$$

The first of these can be eliminated on physical grounds, so the remainder of the analysis considers only the second relation. Solution of this equation with the initial conditions $x_0 = 0$ and $\theta_0 = \pi/2$ results in

$$\frac{x}{3\ell} = \ln\tan\left(\frac{\theta}{2}\right). \tag{A.21}$$

The initial condition on θ indicates that in the zero position, the caster rolling axis is perpendicular to the direction of support motion. Solution of (A.21) to obtain θ as a function of x yields

$$\theta = 2\arctan\left(e^{x/3\ell}\right). \tag{A.22}$$

This kinematic relation gives the caster orientation as a function of the location of the support point and will prove to be useful in the next section.

Note that when $\theta \approx 0$ or $\theta \approx \pi$, Equation (A.21) indicates that a small change in the angle causes a very large change in x. Thus, when the wheel is

directly ahead of, or behind, the pivot point, a small perturbation can cause the apparent position of the caster to change by a large amount. This sensitivity causes the motion to not be reversible if the displacements are sufficient to cause the wheel angle to approach π. However, for $|x| < 3\ell$, the angles remain reasonably insensitive to perturbation, and the motion is reversible.

A.3 Force-Displacement Relation for Rectilinear Caster Motion

The force in the x direction that must be applied at the support point O to move the caster is given by

$$F_x = F_n \sin\theta \, \mathrm{sgn}\dot{\theta}, \tag{A.23}$$

where F_n is given by (A.15). Using (A.22) in (A.23) and the use of transcendental function identities leads to

$$F_x = -F_n \, \mathrm{sgn}(\dot{x}) \, \mathrm{sech}\left(\frac{x}{3\ell}\right). \tag{A.24}$$

It was remarked in an earlier section that for casters used with data processing and hospital equipment

$$F_n \approx \mu N. \tag{A.25}$$

If the weight of the caster-mounted equipment is evenly distributed among four casters, then for each caster

$$N = \frac{\mu m g}{4}, \tag{A.26}$$

where m is the mass of the equipment. Thus, the force of each caster per unit mass of equipment is

$$\frac{F_x}{m} = -\frac{\mu g}{4} \, \mathrm{sgn}(\dot{x}) \, \mathrm{sech}\left(\frac{x}{3\ell}\right). \tag{A.27}$$

While excitations considered in the thesis are one-dimensional in the absolute coordinate system, it is unknown beforehand whether the response measured in the relative coordinate system is also one-dimensional. When the caster initial angles are symmetrically arranged about the direction of excitation, the forces in the perpendicular direction cancel, and the relative motion is one-dimensional. For the more general case where the initial positions of the casters are arbitrary, possibly random, the situation is more complex. If the weight of the object supported by the casters is large compared with the frictional forces, then the absolute motions are small compared to the relative ones, and the relative motion is predominantly one-dimensional. For frictional forces on the order of the system weight, a more careful analysis beyond the scope of this study must be performed. Any two-dimensionality of the motion causes a perturbation in the effective angle of the caster, in turn producing a non-reversible motion for large excursions.

CALIFORNIA INSTITUTE OF TECHNOLOGY

Reports Published

by

Earthquake Engineering Research Laboratory*
Dynamic Laboratory
Disaster Research Center

Note: Numbers in parenthesis are Accession Numbers assigned by the National Technical Information Service; these reports may be ordered from the National Technical Information Service, 5285 Port Royal Road, Springfield, Virginia, 22161. Accession Numbers should be quoted on orders for reports (PB --- ---). Reports without this information either have not been submitted to NTIS or the information was not available at the time of printing. An N/A in parenthesis indicates that the report is no longer available at Caltech.

1. Alford, J.L., G.W. Housner and R.R. Martel, "Spectrum Analysis of Strong-Motion Earthquake," 1951. (Revised August 1964). (N/A)

2. Housner, G.W., "Intensity of Ground Motion During Strong Earthquakes," 1952. (N/A)

3. Hudson, D.E., J.L. Alford and G.W. Housner, "Response of a Structure to an Explosive Generated Ground Shock," 1952. (N/A)

4. Housner, G.W., "Analysis of the Taft Accelerogram of the Earthquake of 21 July 1952." (N/A)

5. Housner, G.W., "A Dislocation Theory of Earthquakes," 1953. (N/A)

6. Caughey, T.K., and D.E. Hudson, "An Electric Analog Type Response Spectrum," 1954. (N/A)

7. Hudson, D.E., and G.W. Housner, "Vibration Tests of a Steel-Frame Building," 1954. (N/A)

8. Housner, G.W., "Earthquake Pressures on Fluid Containers," 1954. (N/A)

9. Hudson, D.E., "The Wilmot Survey Type Strong-Motion Earthquake Recorder," 1958. (N/A)

10. Hudson, D.E., and W.D. Iwan, "The Wilmot Survey Type Strong-Motion Earthquake Recorder, Part II," 1960. (N/A)

---

* To order directly by phone the number is 703-487-4650.

11. Caughey, T.K., D.E. Hudson, and R.V. Powell, "The CIT Mark II Electric Analog Type Response Spectrum Analyzer for Earthquake Excitation Studies," 1960. (N/A)

12. Keightley, W.O., G.W. Housner and D.E. Hudson, "Vibration Tests of the Encino Dam Intake Tower," 1961. (N/A)

13. Merchant, Howard Carl, "Mode Superposition Methods Applied to Linear Mechanical Systems Under Earthquake Type Excitation," 1961. (N/A)

14. Iwan, Wilfred D., "The Dynamic Response of Bilinear Hysteretic Systems," 1961. (N/A)

15. Hudson, D.E., "A New Vibration Exciter for Dynamic Test of Full-Scale Structures," 1961. (N/A)

16. Hudson, D.E., "Synchronized Vibration Generators for Dynamic Tests of Full-Scale Structures," 1962. (N/A)

17. Jennings, Paul C., "Velocity Spectra of the Mexican Earthquakes of 11 May and 19 May 1962," 1962. (N/A)

18. Jennings, Paul C., "Response of Simple Yielding Structures to Earthquake Excitation," 1963. (N/A)

19. Keightley, Willard O., "Vibration Tests of Structures," 1963. (N/A)

20. Caughey, T.K., and M.E.J. O'Kelly, "General Theory of Vibration of Damped Linear Dynamic Systems," 1963. (N/A)

21. O'Kelly, M.E.J., "Vibration of Viscously Damped Linear Dynamic Systems," 1964. (N/A)

22. Nielsen, N. Norby, "Dynamic Response of Miltistory Buildings," 1964. (N/A)

23. Tso, Wai Keung, "Dynamics of Thin-Walled Beams of Open Section," 1964. (N/A)

24. Keightley, Willard O., "A Dynamic Investigation of Bouquet Canyon Dam," 1964. (N/A)

25. Malhotra, R.K., "Free and Forced Oscillations of a Class of Self-Excited Oscillators," 1964.

26. Hanson, Robert D., "Post-Elastic Response of Mild Steel Structures," 1965.

27. Masri, Sami F., "Analytical and Experimental Studies of Impact Dampers," 1965.

28. Hanson, Robert D., "Static and Dynamic Tests of a Full-Scale Steel-Frame Structures," 1965.

29. Cronin, Donald L., "Response of Linear, Viscous Damped Systems to Excitations Having Time-Varying Frequecy," 1965.

30. Hu, Paul Yu-fei, "Analytical and Experimental Studies of Random Vibration," 1965.

31. Crede, Charles E., "Research on Failure of Equipment when Subject to Vibration," 1965.

32. Lutes, Loren D., "Numerical Response Characteristics of a Uniform Beam Carrying One Discrete Load," 1965. (N/A)

33. Rocke, Richard D., "Transmission Matrices and Lumped Parameter Models for Continuous Systems," 1966. (N/A)

34. Brady, Arthur Gerald, "Studies of Response to Earthquake Ground Motion," 1966. (N/A)

35. Atkinson, John D., "Spectral Density of First Order Piecewise Linear Systems Excited by White Noise," 1967. (N/A)

36. Dickerson, John R., "Stability of Parametrically Excited Differential Equations," 1967. (N/A)

37. Giberson, Melbourne F., "The Response of Nonlinear Multi-Story Structures Subjected to Earthquake Excitation," 1967. (N/A)

38. Hallanger, Lawrence W., "The Dynamic Stability of an Unbalanced Mass Exciter," 1967.

39. Husid, Raul, "Gravity Effects on the Earthquake Response of Yielding Structures," 1967. (N/A)

40. Kuroiwa, Julio H., "Vibration Test of a Multistory Building," 1967. (N/A)

41. Lutes, Loren Daniel, "Stationary Random Response of Bilinear Hysteretic Systems," 1967.

42. Nigam, Navin C., "Inelastic Interactions in the Dynamic Response of Structures," 1967.

43. Nigam, Navin C. and Paul C. Jennings, "Digital Calculation of Response Spectra from Strong-Motion Earthquake Records," 1968.

44. Spencer, Richard A., "The Nonlinear Response of Some Multistory Reinforced and Prestressed Concrete Structures Subjected to Earthquake Excitation," 1968. (N/A)

45. Jennings, P.C., G.W. Housner and N.C. Tsai, "Simulated Earthquake Motions," 1968.

46. "Strong-Motion Instrumental Data on the Borrego Mountain Earthquake of 9 April 1968," (USGS and EERL Joint Report), 1968.

47. Peters, Rex B., "Strong Motion Accelerograph Evaluation," 1969.

48. Heitner, Kenneth L., "A Mathematical Model for Callculation of the Run-Up of Tsunamis," 1969.

49. Trifunac, Mihailo D., "Investigation of Strong Earthquake Ground Motion," 1969. (N/A)

50. Tsai, Nien Chien, "Influence of Local Geology on Earthquake Ground Motion," 1969. (N/A)

51. Trifunac, Mihailo D., "Wind and Microtremor Induced Vibrations of a Twenty-Two Steel Frame Building," EERL 70-01, 1970.

52. Yang, I-Min, "Stationary Random Response of Multidegree-of-Freedom Systems," DYNL-100, June 1970. (N/A)

53. Patula, Edward John, "Equivalent Differential Equations for Nonlinear Dynamic Systems," DYNL-101, June 1970.

54. Prelewicz, Daniel Adam, "Range of Validity of the Method of Averaging," DYNL-102, 1970.

55 Trifunac, M.D., "On the Statistics and Possible Triggering Mechanism of Earthquakes in Southern California," EERL 70-03, July 1970.

56. Heitner, Kenneth Leon, "Additional Investigations on a Mathematical Model for Calculation of Run-Up of Tsunamis," July 1970.

57. Trifunac, Mihailo D., "Ambient Vibration Tests of a Thirty-Nine Story Steel Frame Building," EERL 70-02, July 1970.

58. Trifunac, Mihailo D. and D.E. Hudson, "Laboratory Evaluations and Instrument Corrections of Strong-Motion Accelerographs," EERL 70-04, August 1970. (N/A)

59. Trifunac, Mihailo D., "Response Envelope Spectrum and Interpretation of Strong Earthquake Groun Motion," EERL 70-06, August 1970.

60. Keightley, W.O., "A Strong-Motion Accelerograph Array with Telephone Line Interconnections," EERL 70-05, September 1970.

61. Trifunac, Mihailo D., "Low Frequency Digitization Errors and a New Method for Zero Baseline Correction of Strong-Motion Accelerograms," EERL 70-07, September 1970.

62. Vijayaraghavan, A., "Free and Forced Oscillations in a Class of Piecewise-Linear Dynamic Systems," DYNL-103, January 1971.

63. Jennings, Paul C., R.B. Mathiesen and J. Brent Hoerner, "Forced Vibrations of a 22-Story Steel Frame Building," EERL 71-01, February 1971. (N/A) (PB 205 161)

64. Jennings, Paul C., "Engineering Features of the San Fernando Earthquake of February 9, 1971," EERL 71-02, June 1971. (PB 202 550)

65. Bielak, Jacobo, "Earthquake Response of Building-Foundation Systems," EERL 71-04, June 1971. (N/A) (PB 205 305)

66. Adu, Randolph Ademola, "Response and Failure of Structures Under Stationary Random Excitation," EERL 71-03, June 1971. (N/A) (PB 205 304)

67. Skattum, Knut Sverre, "Dynamic Analysis of Coupled Shear Walls and Sandwich Beams," EERL 71-06, June 1971. (N/A) (PB 205 267)

68. Hoerner, John Brent, "Model Coupling and Earthquake Response of Tall Buildings," EERL 71-07, June 1971. (N/A) (PB 207 635)

69. Stahl, Karl John, "Dynamic Response of Circular Plates Subjected to Moving Massive Loads," DYNL-104, June 1971. (N/A)

70. Trifunac, M.D., F.E. Udwadia and A.G. Brady, "High Frequency Errors and Instrument Corrections of Strong-Motion Accelerograms," EERL 71-05, 1971. (PB 205 369)

71. Furuike, D.M., "Dynamic Response of Hysteretic Systems With Application to a System Containing Limited Slip," DYNL-105, September 1971. (N/A)

72. Hudson, D.E. (Editor), "Strong-Motion Instrumental Data on the San Fernando Earthquake of February 9, 1971," (Seismological Field Survey, NOAA, C.I.T. Joint Report), September 1971. (PB 204 198)

73. Jennings, Paul C. and Jacobo Bielak, "Dynamics of Building-Soil Interaction," EERL 72-01, April 1972. (PB 209 666)

74. Kim, Byung-Koo, "Piesewise Linear Dynamic Systems with Time Delays," DYNL-106, April 1972.

75. Viano, David Charles, "Wave Propagation in a Symmetrically Layered Elastic Plate," DYNL-107, May 1972.

76. Whitney, Albert W., "On Insurance Settlements Incident to the 1906 San Francisco Fire," DRC 72-01, August 1972. (PB 213 256)

77. Udwadia, F.E., "Investigation of Earthquake and Microtremor Ground Motions," EERL 72-02, September 1972. (PB 212 853)

78. Wood, John H., "Analysis of the Earthquake Response of a Nine-Story Steel Frame Building During the San Fernando Earthquake," EERL 72-04, October 1972. (PB 215 823)

79. Jennings, Paul C., "Rapid Calculation of Selected Fourier Spectrum Ordinates," EERL 72-05, November 1972.

80. "Research Papers Submitted to Fifth World Conference on Earthquake Engineering, Rome, Italy, 25-29 June 1973," EERL 73-02, March 1973. (PB 220 431)

81. Udwadia, F.E., and M.D. Trifunac, "The Fourier Transform, Response Spectra and Their Relationship Through the Statistics of Oscillator Response," EERL 73-01, April 1973. (PB 220 458)

82. Housner, George W., "Earthquake-Resistant Design of High-Rise Buildings," DRC 73-01, July 1973. (N/A)

83. "Earthquake and Insurance," Earthquake Research Affiliates Conference, 2-3 April, 1973, DRC 73-02, July 1973. (PB 223 033)

84. Wood, John H., "Earthquake-Induced Soil Pressures on Structures," EERL 73-05, August 1973. (N/A)

85. Crouse, Charles B., "Engineering Studies of the San Fernando Earthquake," EERL 73-04, March 1973. (N/A)

86. Irvine, H.Max, "The Veracruz Earthquake of 28 August 1973," EERL 73-06, October 1973.

87. Iemura, H. and P.C. Jennings, "Hysteretic Response of a Nine-Story Reinforced Concrete Building During the San Fernando Earthquake," EERL 73-07, October 1973.

88. Trifunac, M.D. and V. Lee, "Routine Computer Processing of Strong-Motion Accelerograms," EERL 73-03, October 1973. (N/A) (PB 226 047/AS)

89. Moeller, Thomas Lee, "The Dynamics of a Spinning Elastic Disk with Massive Load," DYNL 73-01, October 1973.

90. Blevins, Robert D., "Flow Induced Vibration of Bluff Structures," DYNL 74-01, February 1974.

91. Irvine, H. Max, "Studies in the Statics and Dynamics of Simple Cable Systems," DYNL-108, January 1974.

92. Jephcott, D.K. and D.E. Hudson, "The Performance of Public School Plants During the San Fernando Earthquake," EERL 74-01, September 1974. (PB 240 000/AS)

93. Wong, Hung Leung, "Dynamic Soil-Structure Interaction," EERL 75-01, May 1975. (N/A) (PB 247 233/AS)

94. Foutch, D.A., G.W. Housner, and P.C. Jennings, "Dynamic Responses of Six Multistory Buildings During the San Fernando Earthquake," EERL 75-02, October 1975. (PB 248 144/AS)

95. Miller, Richard Keith, "The Steady-State Response of Multidegree-of-Freedom Systems with a Spatially Localized Nonlinearity," EERL 75-03, October 1975. (PB 252 459/AS)

96. Abdel-Ghaffar, Ahmed Mansour, "Dynamic Analyses of Suspension Bridge Structures," EERL 76-01, May 1976. (PB 258 744/AS)

97. Foutch, Douglas A., "A Study of the Vibrational Characteristics of Two Multistory Buildings," EERL 76-03, September 1976. (PB 260 874/AS)

98. "Strong Motion Earthquake Accelerograms Index Volume," Earthquake Engineering Research Laboratory, EERL 76-02, August 1976. (PB 260 929/AS)

99. Spanos, P-T.D., "Linearization Techniques for Non-Linear Dynamical Systems," EERL 76-04, September 1976. (PB 266 083/AS)

100. Edwards, Dean Barton, "Time Domain Analysis of Switching Regulators," DYNL 77-01, March 1977.

101. Abdel-Ghaffar, Ahmed Mansour, "Studies of the Effect of Differential Motions of Two Foundations upon the Response of the Superstructure of a Bridge," EERL 77-02, January 1977. (PB 271 095/AS)

102. Gates, Nathan C., "The Earthquake Response of Deteriorating Systems," EERL 77-03, March 1977. (PB 271 090/AS)

103. Daly, W., W. Judd and R. Meade, "Evaluation of Seismicity at U.S. Reservoirs," USCOLD, Committee on Earthquakes, May 1977. (PB 270 036/AS)

104. Abdel-Ghaffer, A.M. and G.W. Housner, "An Analysis of the Dynamic Characteristics of a Suspension Bridge by Ambient Vibration Measurements," EERL 77-01, January 1977. (PB 275 063/AS)

105. Housner, G.W. and P.C. Jennings, "Earthquake Design Criteria for Structures," EERL 77-06, November 1977. (PB 276 502/AS)

106. Morrison, P., R. Maley, G. Brady, R. Porcella, "Earthquake Recordings on or Near Dams," USCOLD, Committee on Earthquakes, November 1977. (PB 285 867/AS)

107. Abdel-Ghaffar, A.M., "Engineering Data and Analyses of the Whittier, California Earthquake of January 1, 1976," EERL 77-05, November 1977. (PB 283 750/AS)

108. Beck, James L., "Determining Models of Structures from Earthquake Records," EERL 78-01, June 1978. (PB 288 806/AS)

109. Psycharis, Ioannis, "The Salonica(Thessaloniki) Earthquake of June 20, 1978," EERL 78-03, October 1978. (PB 290 120/AS)

110. Abdel-Ghaffar, A.M. and R.F. Scott, "An Investigation of the Dynamic Characteristics of an Earth Dam," EERL 78-02, August 1978. (PB 288 878/AS)

111. Mason, Alfred B., Jr., "Some Observations on the Random Response of Linear and Nonlinear Dynamical Systems," EERL 79-01, January 1979. (PB 290 808/AS)

112. Helmberger, D.V. and P.C. Jennings (Organizers), "Strong Ground Motion: N.S.F. Seminar-Workshop," SL-EERL 79-02, February 1978.

113. Lee, David M., Paul C. Jennings and George W. Housner, "A Selection of Important Strong Motion Earthquake Records," EERL 80-01, January 1980. (PB 80 169196)

114. McVerry, Graeme H., "Frequency Domain Identification of Structural Models from Earthquake Records," EERL 79-02, October 1979. (PB-80-194301)

115. Abdel-Ghaffar A.M., R.F.Scott and M.J.Craig, "Full-Scall Experimental Investigation of a Modern Earth Dam," EERL 80-02, February 1980. (PB-81-123788)

116. Rutenberg, Avigdor, Paul C. Jennings and George W. Housner, "The Response of Veterans Hospital Building 41 in the San Fernando Earthquake," EERL 80-03, May 1980. (PB-82-201377)

117. Haroun, Medhat Ahmed, "Dynamic Analyses of Liquid Storage Tanks," EERL 80-04, February 1980. (PB-81-123275)

118. Liu, Wing Kam, "Development of Finite Element Procedures for Fluid-Structure Interaction," EERL 80-06, August 1980. (PB 184078)

119. Yoder, Paul Jerome, "A Strain-Space Plasticity Theory and Numerical Implementation," EERL 80-07, August 1980. (PB-82-201682)

120. Krousgrill, Charles Morton, Jr., "A Linearization Technique for the Dynamic Response of Nonlinear Continua," EERL 80-08, September 1980. (PB-82-201823)

121. Cohen, Martin, "Silent Boundary Methods for Transient Wave Analysis," EERL 80-09, September 1980. (PB-82-201831)

122. Hall, Shawn A., "Vortex-Induced Vibrations of Structures," EERL 81-01, January 1981. (PB-82-201849)

123. Psycharis, Ioannis N., "Dynamic Behavior of Rocking Structures Allowed to Uplift," EERL 81-02, August 1981. (PB-82-212945)

124. Shih, Choon-Foo, "Failure of Liquid Storage Tanks Due to Earthquake Excitation," EERL 81-04, May 1981. (PB-82-215013)

125. Lin, Albert Niu, "Experimental Observations of the Effect of Foundation Embedment on Structural Response," EERL 82-01, May 1982. (PB-84-163252)

126. Botelho, Dirceau L.R., "An Empirical Model for Vortex-Induced Vibrations," EERL 82-02, August 1982. (PB-84-161157)

127. Ortiz, L. Alexander, "Dynamic Centrifuge Testing of Cantilever Retaining Walls," SML 82-02, August 1982. (PB-84-162312)

128. Iwan, W.D., Editor, "Proceedings of the U.S. National Workshop on Strong-Motion Earthquake Instrumentation, April 12-14, 1981, Santa Barbara, California," California Institute of Technology, Pasadena, California, 1981.

129. Rashed, Ahmed, "Dynamic Analysis of Fluid-Structure Systems," EERL 82-03, July 1982. (PB-84-162916)

130. National Academy Press, "Earthquake Engineering Research-1982."

131. National Academy Press, "Earthquake Engineering Research-1982, Overview and Recommendations."

132. Jain, Sudhir Kumar, "Analytical Models for the Dynamics of Buildings," EERL 83-02, May 1983. (PB-84-161009)

133. Huang, Moh-Jiann, "Investigation of Local Geology Effects on Strong Earthquake Ground Motions," EERL 83-03, July 1983. (PB-84-161488)

134. Mcverry, G.H. and J.L. Beck, "Structural Identification of JPL Building 180 Using Optimally Synchronized Earthquake Records." EERL 83-01, August 1983. (PB-84-162833)

135. Bardet, J.P., "Application of Plasticity Theory to Soil Behavior: A New Sand Model," SML 83-01, September 1983. (PB-84-162304)

136. Wilson, John C., "Analysis of the Observed Earthquake Response of a Multiple Span Bridge," EERL 84-01, May 1984. (PB-85-240505/AS)

137. Hushmand, Behnam, "Experimental Studies of Dynamic Response of Foundations," SML 83-02, November 1983. (PB-86-115383/A)

138. Cifuentes, Arturo O., "System Identification of Hysteretic Structures," EERL 84-04, 1984. (PB-240489/AS14)

139. Smith, Kenneth Scott, "Stochastic Analysis of the Seismic Response of Secondary Systems," EERL 85-01, November 1984. (PB-85-240497/AS)

140. Maragakis, Emmanuel, "A Model for the Rigid Body Motions of Skew Bridges," EERL 85-02, December 1984. (PB-85-248433/AS)

141. Jeong, Garrett Duane, "Cumulative Damage of Structures Subjected to Response Spectrum Consistent Random Process," EERL 85-03, January 1985. (PB-86-100809)

142. Chelvakumar, Kasivisvanathan, "A Simple Strain-Space Plasticity Model for Clays," EERL 85-05, 1985. PB-

143. Pak, Ronald Y.S., "Dynamic Response of a Patially Embedded Bar Under Transverse Excitations," EERL 85-04, May 1985. PB-

144. Tan, Thiam-Soon, "Two Phase Soil Study: A. Finite Strain Consolidation, B. Centrifuge Scaling Considerations," SML 85-01, August 1985. PB-

145. Iwan, Wilfred D., Michael A. Moser and Chia-Yen Peng, "Strong-Motion Earthquake Measurement Using a Digital Accelerograph," EERL 84-02, April 1984.

146. Beck, R.T. and J.L. Beck, "Comparison Between Transfer Function and Modal Minimization Methods for System Identification," EERL ~~84-02~~ 85-06, April 1984.

147. Jones, Nicholas Patrick, "Flow-Induced Vibration of Long Structures," DYNL 86-01, May 1986. PB-

148. Peek, Ralf, "Analysis of Unanchored Liquid Storage Tanks Under Seismic Loads," EERL 86-01, April 1986. PB-

Strong-Motion Earthquake Accelerograms
Digitized and Plotted Data

Uncorrected Accelerograms

Volume I

Part	Report No.	NTIS Accession No.
A	EERL 70-20	PB 287 847
B	EERL 70-21	PB 196 823
C	EERL 71-20	PB 204 364
D	EERL 71-21	PB 208 529
E	EERL 71-22	PB 209 749
F	EERL 71-23	PB 210 619
G	EERL 72-20	PB 211 357
H	EERL 72-21	PB 211 781
I	EERL 72-22	PB 213 422
J	EERL 72-23	PB 213 423
K	EERL 72-24	PB 213 424
L	EERL 72-25	PB 215 639
M	EERL 72-26	PB 220 554
N	EERL 72-27	PB 223 023
O	EERL 73-20	PB 222 417
P	EERL 73-21	PB 227 481/AS
Q	EERL 73-22	PB 232 315/AS
R	EERL 73-23	PB 239 585/AS
S	EERL 73-24	PB 241 551/AS
T	EERL 73-25	PB 241 943/AS
U	EERL 73-26	PB 242 262/AS
V	EERL 73-27	PB 243 483/AS
W	EERL 73-28	PB 243 497/AS
X	EERL 73-29	PB 243 594/AS
Y	EERL 73-30	PB 242 947/AS

Strong-Motion Earthquake Accelerograms
Digitized and Plotted Data

Corrected Accelerograms and Integrated
Ground Velocity and Displacement Curves

Volume II

Part	Report No.	NTIS Accession No.
A	EERL 71-50	PB 208 283
B	EERL 72-50	PB 220 161
C	EERL 72-51	PB 220 162
D	EERL 72-52	PB 220 836
E	EERL 73-50	PB 223 024
F	EERL 73-51	PB 224 977/9AS
G	EERL 73-52	PB 229 239/AS
H	EERL 74-50	PB 231 225/AS
I	EERL 74-51	PB 232 316/AS
J,K	EERL 74-52	PB 233 257/AS
L,M	EERL 74-53	PB 237 174/AS
N	EERL 74-54	PB 236 399/AS
O,P	EERL 74-55	PB 239 586/AS
Q,R	EERL 74-56	PB 239 587/AS
S	EERL 74-57	PB 241 552/AS
T	EERL 75-50	PB 242 433/AS
U	EERL 75-51	PB 242 949/AS
V	EERL 75-52	PB 242 948/AS
W,Y	EERL 75-53	PB 243 719

Analyses of Strong-Motion Earthquake Accelerograms
Response Spectra

Volume III

Part	Report No.	NTIS Accession No.
A	EERL 72-80	PB 212 602
B	EERL 73-80	PB 221 256
C	EERL 73-81	PB 223 025
D	EERL 73-82	PB 227 469/AS
E	EERL 73-83	PB 227 470/AS
F	EERL 73-84	PB 227 471/AS
G	EERL 73-85	PB 231 223/AS
H	EERL 74-80	PB 231 319/AS
I	EERL 74-81	PB 232 326/AS
J,K,L	EERL 74-82	PB 236 110/AS
M,N	EERL 74-83	PB 236 400/AS
O,P	EERL 74-84	PB 238 102/AS
Q,R	EERL 74-85	PB 240 688/AS
S	EERL 74-86	PB 241 553/AS
T	EERL 75-80	PB 243 698/AS
U	EERL 75-81	PB 242 950/AS
V	EERL 75-82	PB 242 951/AS
W,Y	EERL 75-83	PB 243 492/AS

Analyses of Strong-Motion Earthquake Accelerograms
Fourier Amplitude Spectra

Volume IV

Part	Report No.	NTIS Accession No.
A	EERL 72-100	PB 212 603
B	EERL 73-100	PB 220 837
C	EERL 73-101	PB 222 514
D	EERL 73-102	PB 222 969/AS
E	EERL 73-103	PB 229 240/AS
F	EERL 73-104	PB 229 241/AS
G	EERL 73-105	PB 231 224/AS
H	EERL 74-100	PB 232 327/AS
I	EERL 74-101	PB 232 328/AS
J,K,L,M	EERL 74-102	PB 236 111/AS
N,O,P	EERL 74-103	PB 238 447/AS
Q,R,S	EERL 74-104	PB 241 554/AS
T,U	EERL 75-100	PB 243 493/AS
V,W,Y	EERL 75-101	PB 243 494/AS
Index Volume	EERL 76-02	PB 260 929/AS